Observer based control of an magnetorheological damper

by

Mehmet Ali Eroglu

Thesis submitted for degree of Doctor of Philosophy

June 2013

Department of Mechanical Engineering

Supervisor: Dr N. D. Sims

sun and earth

SUMMARY

Magnetorheological (MR) fluids enable the rapid and continuous alteration of flow resistance via the application of a magnetic field. This unique characteristic can be utilised to build semi-active dampers for a wide variety of vibration control systems, including structural, automotive, and bridge applications. However, the non-linear behaviour of smart fluid dampers makes the objective of achieving a desired control force very difficult. Most of the control algorithms proposed to overcome this problem require the measurement of both the MR damper force and the states of the system, which increases the complexity of the system. In this thesis, this problem is overcome by developing a non-linear observer.

A further aim of this thesis is to investigate the effective control techniques for broadband excited observer-based MR vibration systems. Through an extensive series of numerical and experimental investigations, the general single-degree-of-freedom and tuned mass damper problems are presented. In an experimental case study, the hardware-in-the-loop-simulation method is adopted, which provides an excellent means to bridge the gap between theory and practice when the behaviour of a specific component is complex. Here, the vibration absorber with controllable MR damper is physically tested, whilst the remainder of the structure is simulated in real-time. The results demonstrate that the chosen control strategy can provide significant performance benefits when compared to more commonly used strategies and equivalent passive systems.

ACKNOWLEDGEMENTS

Praises to Allah and peace be upon the beloved final Prophet Muhammad. Thank to Allah to be always with me to give the guidance and mercy along my life. From His help and blessing to give me strength and taught me patience to complete the thesis. I would like to express my deepest appreciation to my supervisor Dr Neil D Sims, for his strong encouragement, help, advice, expertise and rich ideas in supervising with patience and understanding from the start to the end of my PhD study.

My thanks go to M. Rennison, C. Grigson, and J. Booth for their technical support of the rig facility. I would also like to thank my officemates and departmental staff for their support and good friendship. I express my gratefulness for my PhD studentship sponsored by the Ministry of Education of Turkey , which made this research possible.

I show my deepest thanks to my parents, my entire family, for their moral support which has made me feel stronger and inspired. I have no worries to move forward as there is no greater support and encouragement besides all of you.

Contents

NOMENCLATURE

A	System state matrix
B	Feedback gain
B	Input matrix
c_a	Absorber damping coefficient
$c_{a,opt}$	Optimal absorber damping coefficient
c_p	Viscous damping
c_s	Structural damping coefficient
C	Output matrix
C_{post}	Post yield damping coefficient
C_{pre}	Pre-yield damping coefficient
D	Desired set-point gain of the linearised system
D	Feedthrough (or feedforward) matrix
D_{FS}	Desired set-point gain of fully active sky-hook system
D_{MR}	Desired set-point gain of the linearised sky-hook system
D_{SAS}	Desired set-point gain of the ideal semi-active sky-hook system
$\dot{e}(\cdot)$	State estimation error
F_d	Damping force
F_{ex}, and F_o	Structural Excitation force
F_{MR}	MR damping force
F_s	Spring force
F_y	Yield force
F_{fr}	Friction force
$\hat{F}_{MR}$	Estimated MR damping force
$\hat{F}_{desired}$	Estimated desired damping force
g	Ratio of natural frequencies
g_{opt}	Optimal frequency ratio
G	Feed-forward gain
I	Current
I_{max}	Switching current of the on/off controller
k	Linear stiffness represents the fluid compressibility
k_a	Absorber spring stiffness
$k_{a,opt}$	Optimal absorber spring stiffness
k_p	Spring stiffness
k_s	Structural spring stiffness
K	Optimal control gain
L	Observer gain matrix
m	Isolated mass
m_a	Mass of absorber
$m_{a,opt}$	Optimal mass of absorber
m_s	Mass of structure
$m_{s,opt}$	Optimal mass of structure

m_1	Mass representing fluid inertia
m_2	Mass of piston head
$\widetilde{m}_s$	Detuned structural mass
r	Forced frequency ratio
$u(\cdot)$	Input vector
V	Piston velocity
$x_b(\cdot)$, and $u_1(\cdot)$	Displacement of base
$x_m(\cdot)$, and $x_d(\cdot)$	Displacement of mass
x_r	Relative piston displacement
$\dot{x}_b(\cdot)$, and $u_2(\cdot)$	Velocity of base
$\dot{x}_m(\cdot)$, $\dot{x}_d(\cdot)$, and $x_v(\cdot)$	Absolute velocity of mass
$\dot{x}_r$	Relative velocity of piston
$\ddot{x}_b(\cdot)$	Acceleration of base
$\ddot{x}_m(\cdot)$, and $\dot{x}_v(\cdot)$	Acceleration of mass
$\underline{x}(\cdot)$	State vector
$\hat{\underline{x}}(\cdot)$	Estimated state vector
$\dot{x}_1$	Displacement of the mass representing fluid inertia
x_2	Displacement of piston head
X_a	Amplitude of absorber displacement
X_s	Amplitude of structural displacement
$y(\cdot)$	Output (or measurement) vector
$\hat{y}(\cdot)$	Estimated output (or measurement) vector
χ	Quasi-steady MR damping function
δ_{st}	Static deflection of the system
$\dot{\gamma}$	Shear rate
μ	Viscosity of MR fluid, and mass ratio in Chapter 7
$\mu_{optimal}$	Optimal mass ratio of tuned mass damper
$\mu_{retuned}$	Retuned mass ratio of tuned mass damper
η_a	Loss factor of absorber
$\eta_{a,opt}$	Optimal loss factor of absorber
η_s	Loss factor of main structure
τ	Shear stress
τ_y	MR fluid yield stress
ζ	Damping ratio
ζ_s	Damping ratio of main structure
ζ_a	Damping ratio of absorber
ω	Excitation frequency
ω_s	Natural frequency of the main structure
ω_a	Natural frequency of the absorber

1 Introduction

Vibration is usually undesirable and yet it occurs in most machines, vehicles, structures, buildings and dynamic systems. The resulting unpleasant motions and the dynamic stresses which may lead to fatigue and failure of the structure or machine [1]. A typical example of vibration could be swinging pendulum. The vibration theory deals with the oscillatory motion of bodies and the forces associated with them.

Scientists have been studying the theory of vibration since the first quarter of the twentieth century [2, 3]. Some of the earliest research was done by Timoshenko [2] and Den Hartog [3] who described the primary solutions to vibration problems of engineering structures. These solutions were achieved by applying passive devices to an engineering system such as a structure, turbine, vehicle, or bridge. However, the performance of passive devices suffers under wider ranges of excitation, due to passive systems being only optimal for specific conditions [4]. In order to overcome this limitation, scientists developed active and semi-active systems, which are able to change their absorbing behaviour according to measured data [3].

In the present day one of the most promising suspension systems is the semi-active system which deals with smart fluids. The flow resistance of these fluids changes very quickly and continuously by applying an electric or magnetic field [5].

This chapter is organised as follows. First relative merits of the passive, active and semi-active vibration control techniques are described which followed by the detailed explanation of the smart fluids. This chapter is concluded with the outline and objectives of present research.

1.1 The relative merits of passive, active, and semi-active suspensions

Passive suspensions devices are the most preferred solution to vibration control, due to their inherent simplicity, reliability and low cost. These passive devices are implemented in many engineering applications: automobiles, aircraft, locomotives, and buildings [6]. An example for the case of a passive suspension system is shown in Figure 1.1.

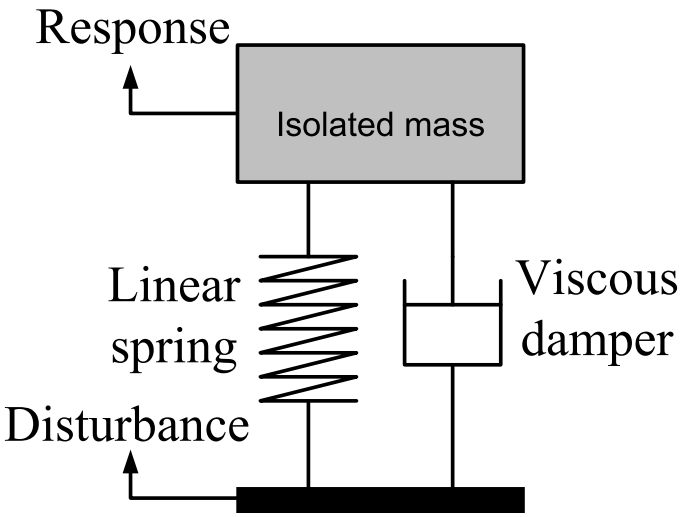

Figure 1.1: Passive suspension configuration (single degree of freedom mass isolator).

The passive suspension control involves modification of the stiffness, mass and damping of the vibrating system to make the system less responsive to its vibratory environment.

These three passive elements do not require any power sources [7]. Depending on the relative velocity of the damper, it dissipates energy [8, 9] which is not controllable as the suspension properties remain fixed. This makes the performance of the passive systems highly depended on the excitation bandwidth. For large excitation bandwidths the performance will decrease, due to passive systems only being optimal for specific conditions [4].

It is possible to classify the passive vibration control methods in four groups according to Mead [6].

- Vibration control by structural design
- Vibration control by localised addition
  - Passive, active, and semi-active vibration absorbers
- Vibration control by added damping
- Vibration control by resilient isolation

Even one of these solutions might be enough to deal with the vibration, but in some cases a combination of two or more of these could be implemented. Structural design is simply re-designing the structure according to the effect of the vibration so that the resonance frequency of a structure moves away from excitation frequency with great benefit. Localised addition is where the extra devices and materials are added and inserted to the main structure. This research will focus on this second stage where passive, active and semi-active vibration absorbers could be considered as an extra device locally added to the main structure. The commonly used method for vibration control by added damping is to include highly polymeric materials at strategic locations within the structure. The last method is

used to isolate the two interconnected structures from one another. An example of this is where engine mount devices are used to isolate the vibration created by the engines [10].

In the 1950's and 60's, active suspension systems started to get considerable attention in order to avoid limitations of the passive systems for vibration control [11]. The principle of a fully active suspension system is where a controllable actuator replaces the passive suspension device. Energy dissipation and storage from and to the vibrating system is achieved by a hydraulic actuator which supplies controlled forces to the structure. In this system, the flow rate of high-pressure fluid that is pumped into and out of the actuator is controlled by the electro-hydraulic servo-valves. The recorded measurements from the response and/or excitation are monitored by a controller (a computer) which, based on a pre-determined control algorithm, determines the appropriate control force signal for operation of the actuators [7]. As a result, better performance can be achieved over wide ranging excitation conditions by using appropriate sensors and control logic. For example, an active control system could increase the ride comfort of the passenger vehicle up to 35% [12]. However, the generation of control forces by electro-hydraulic actuators requires large power sources, which are on the order of tens of kilowatts for small structures and may reach several megawatts for large structures [13]. In addition to their high power consumption, the active system increases the cost, complexity and weight of the system. Due to these disadvantages active control system have not been introduced into the production of aircraft [14], and development of the active vehicle suspension has been dropped [12].

However, the performance of the semi-active systems are almost reaching that of active systems while keeping the weight, cost and complexity of the system similar to that of passive systems [15]. Based on feedback from the excitation and/or from the measured

response, the mechanical properties of these systems can be adjusted. As with an active control system, feedback measurements are monitored by the controller to generate a proper command signal for the semi-active device. The control forces are developed based on a pre-determined control algorithm to oppose the motion of the system. Semi-active systems provide a means to control energy storage and/or dissipation. But such systems cannot increase the energy of the system like active systems, so the power requirement of these systems are very low [4].

Researchers proposed different types of semi-active damper, where the semi-active control is achieved by altering the geometry of the oil flow passages or orifice. In 1974 Karnopp and his colleagues [16] introduced the electro-hydraulic semi-active device shown in Figure 1.2 where the fluid flow was controlled by the electro-hydraulic valves. In this work Karnopp et al. also described the most significant semi-active control, where the linear optimal control theory was used to derive the optimal control force for a single-degree-of-freedom (SDOF) system based on work by Bender *et. al.* [17]. This system is called the sky-hook system, as seen in Figure 1.3, the linear viscous damper is attached to the virtual ground to control the absolute velocity of the mass. The performance advantages of the sky-hook control is represented in Figure 1.4 in the sense of a transmissibility plot of a SDOF system. Comparing to the transmissibility of passive system (Figure 1.4-(a)) with the transmissibility of sky-hook control (Figure 1.4-(b)), a significant reduction of vibration amplitude at the resonance frequency is achieved without degrading the high frequency response by the sky-hook control. In reality, only the active system can emulate the sky-hook configuration, however, the clipped optimal approach was proposed to enable the semi-active devices to produce this sky-hook force when the energy dissipation are required by the Karnopp et. al. [16]. This passivity theory is displayed in Figure 1.5, where the semi-active force occurs when the sky-hook force has the same sign of the

relative velocity across the damper. On the other hand, the level of energy dissipation is minimised, or the no force at all is produced by the semi-active device when the energy input is required .

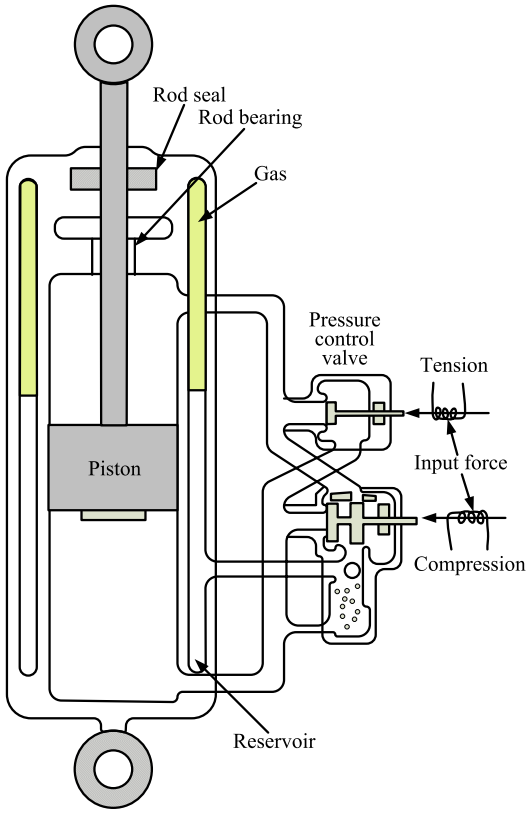

Figure 1.2: The electro-hydraulic semi-active damper proposed by Karnopp [16].

Hrovat et al. proposed the first application of semi-active control within the field of structural engineering for systems subjected to environmental loads [18]. Valve adjustable semi-active dampers for lorry suspensions were investigated by Cebon et al [19]. This work pioneered the hardware-in-the-loop-simulation (HILS) method, which enabled various controller designs to be investigated experimentally. HILS utilized a real-time computer simulation of a car model and the road excitation signal but not the semi-active suspension device. In this work by using the sky-hook based controller authors showed that car body acceleration could be reduced by 22% over optimally damped passive systems [19].

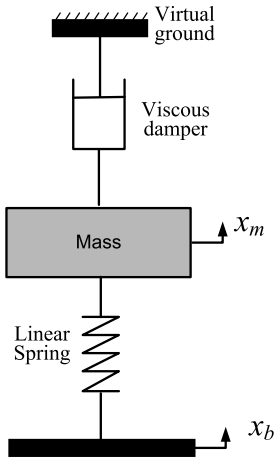

Figure 1.3: The sky-hook configuration.

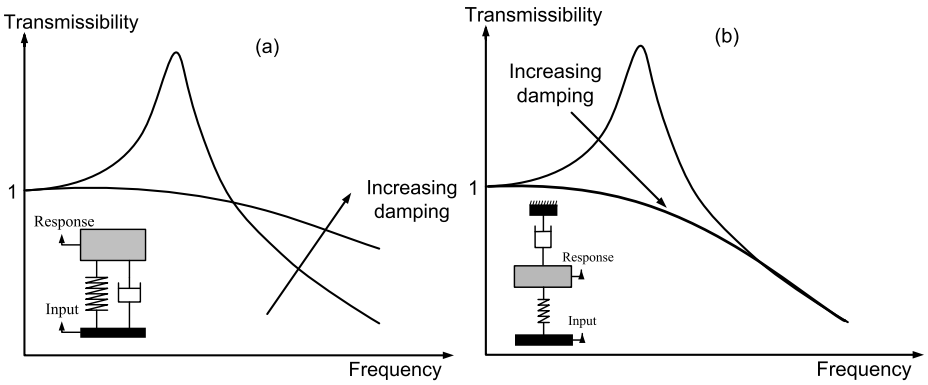

Figure 1.4: Transmissible plots (a) passive, (b) sky-hook SDOF system.

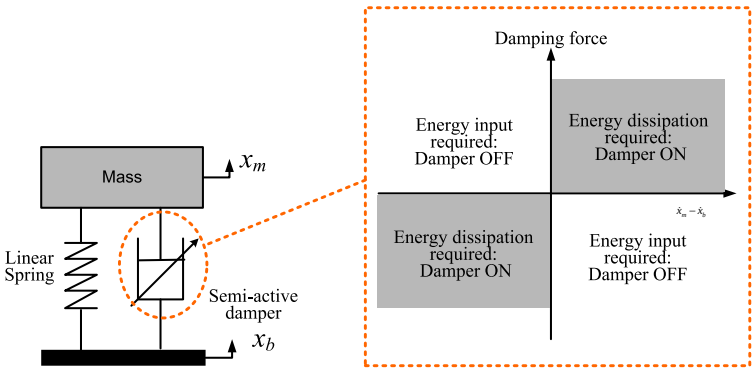

Figure 1.5: Semi-active clipped optimal approach.

Semi-active devices are able to reduce the power consumption of the active devices significantly, however, the method they use to control the semi-active force by utilising variable orifice methods are potentially infeasible. They can be as costly, complex, and bulky as active devices due to their similarity regarding the large number of moving parts, and components requirement that are often similar to those used on active systems (e.g. electro-hydraulic valves). However, smart fluids, provide an excellent, and arguably the most superior means to provide vibration control via alteration of the fluid properties rather than the flow geometry. Key advantages of smart fluids are summarised as:

- By using a low power electrical source the properties of smart fluid can be rapidly and reversibly changed. For example, the MagneRide ([20]) smart fluid damper has a peak power of 20W, and the root mean square (RMS) value is just a small fraction of this [21].
- The response times of smart fluids to the applied field are less than 10ms [21].
- Smart fluid devices have fairly easy and straightforward design stage within the constraints of existing passive designs.
- Carlson [21] noted that, the MagneRide shock absorber requires 60% fewer parts than their previous electro-mechanical semi-active damper system which implies that smart fluid devices do not require any small moving parts.

In conclusion, smart fluid devices combine the cost-effectiveness and simplicity of passive systems and performance of active systems, which makes them the best solution to vibration control [21]. Because of these advantages of the smart fluid devices, a semi-active magnetorheological (MR) damper which is made by smart fluid is used in this study. In the next section, more detailed description of smart fluids are given.

1.2 Smart fluids

In general, smart fluids are divided into two groups. The first group consists of micron-sized semi-conducting particles suspended in a dielectric oil and are called electrorheological fluid (ER), whereas the second group use micron-sized magnetisable particles suspended in a non-magnetisable liquid such as mineral oil, silicon oil or water and are called magnetorheological (MR) fluids. Under the appropriate electric or magnetic field, microscopically, polarisation causes the formation of the particles chain as seen in Figure 1.6-(a).

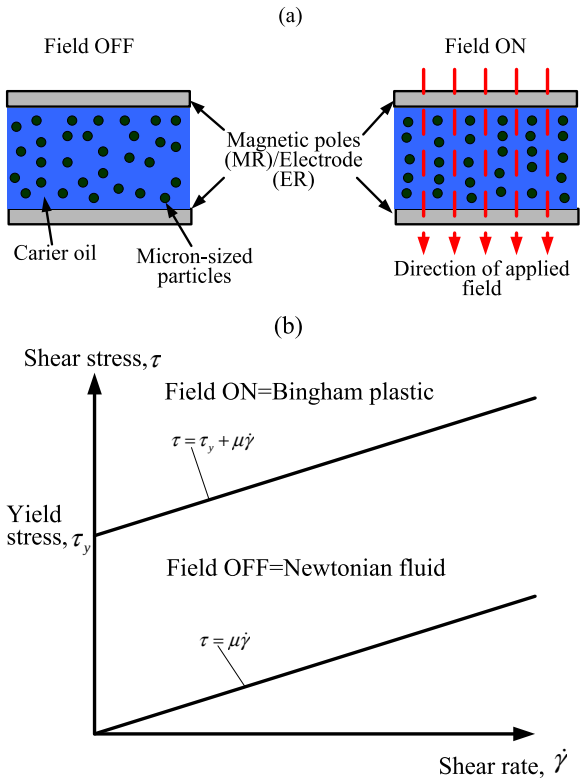

Figure 1.6: Smart fluids. (a) Formations of particle chains in smart fluids, (b) the resulting shear stress/shear rate response.

The intensity of the applied field determines the strength of these chains, hence change the viscosity of fluid and resist the fluid flow. This increased resistance behaves as a controllable yield stress in the form of a Bingham plastic as shown in Figure 1.6-(b). This

controllable yield stress approach led to the invention of highly controllable semi-active devices such as, dampers for vehicle vibration control, rotary brakes for aerobic exercise equipment, special purpose devices for medical rehabilitation, and erasable Braille displays for the blind, as well as for seismic damping and virtual surgery etc. [22]. If the applied field is set to zero volts or zero amperes, the smart devices behave as a Newtonian fluid as shown in Figure 1.6-(b) , where the shear stress is linearly proportional to the shear rate.

Production of practical ER fluids were started over thirty years ago [23, 24, 25], however practical production of ER devices have not got enough attention in the market yet. On the other hand, nearly a decade later, developments in MR fluid technology began and this was followed by significant commercial success, most notably in the automotive industry [21]. First MagneRide MR shock absorbers were introduced in the 2002 model year for General Motors' Cadillac and Corvette vehicles [26]. The system now appears on more than a dozen models from a wide variety of vehicles including: Audi TT, Audi R8, Buick Lucerne, Ferrari 599GTB, Holden HSV Commodore [27]. The reason for this present difference in commercial viability is largely associated with the fluid properties.

Controllable force levels of ER fluids are low, and in order to generate electric fields of up to 6kV/mm the requirement of voltages are very high [5]. Also, the working temperature range of ER fluids is narrow (typically between 15°C to 90°C [28]), which makes them unsuitable in hostile environments. This disadvantage has restricted commercialisation of ER fluids in the aerospace industry, owing to a reluctance to provide the necessary voltages [5]. However, MR fluids can operate in the wide range of temperature such between -40°C to 150°C and also can be powered by a low voltage source [21]. Consequently, MR fluids are are far better suited to aerospace applications, and interest in this

field has renewed due to the more recent developments in MR fluids.

However, the inherent non-linear behaviour of smart fluid devices, makes the target of tracking a prescribed force demand a challenging task. This problem has motivated researchers to propose a wide variety of relatively complex semi-active control strategies which are in use either experimentally or commercially. It is not clear how to perform the best automatic control yet. The inherent non-linearity of the MR fluids can be observed by considering the simplified behaviour shown in Figure 1.6-(b).

1.3 Aim, objectives and outline

The aim for the current research is to implement and experimentally validate a non-linear observer to simplify the sensing requirements for control of an MR damper. This can be completed with the following objectives

- Numerical modelling of:
  - MR damper
  - Linearised feedback control
  - Single-degree-of-freedom-system (SDOF)
  - Linear and non-linear observer.
- Development of MR linearised control methods based on sky-hook, on-off, and optimal control approaches.
- To build up an experimental SDOF mass isolation system incorporating a semi-active damping element (an MR damper).
- To test and verify the observer-based linearised control algorithms from the numerical and experimental study.

- Investigate the numerical and experimental (by using hardware-in-the-loop-simulations) performance of the proposed approach for a real engineering application.

The research in this thesis focuses on the observer based control of a smart fluid suspension damper (MR damper). The thesis starts with a review of the current literature concerning smart fluids and dampers. A brief history of the development of smart fluids is followed by a discussion of the properties and relative merits of modern ER and MR fluids. The various forms of smart fluids devices are then described, paying particular attention to the literature regarding the so-called flow damper which is used in this thesis. The literature review concludes by investigating the various modelling and control strategies that have been proposed to date.

The simple and economical way of converting highly non-linear smart devices (MR damper) into variable semi-active force generators are investigated in this thesis. In chapter 3, in order to achieve this target, observer based feedback linearisation of an MR damper is proposed. Aim of the proposed theory is discussed by giving brief historical developments and short descriptions of each parts (model of an MR damper, non-linear Luenberger observer, and linearised feedback control).

In chapter 4, the design and operation of the MR damper experimental test facility are described in detail, preliminary tests are described, to validate open loop and closed loop responses of the MR damper device. The experimental results show considerable agreement with the predicted model which makes the numerical model feasible.

Numerical analysis of the observer based linearised control of an MR damper are investigated in chapter 5 based on a single degree of freedom mass isolator system. Three different models of the MR damper device are proposed by modifying the Bingham plastic model,

with a proper controller and observer design. Later the performance of these models are presented by using a displacement transmissibility method under the harmonic excitation condition. Later on sky-hook based control algorithms are developed to overcome the non-linear behaviour of the smart fluid devices. The results are compared with basic on-off control scenarios under the broadband random excitation conditions by using the power spectral density (PSD) analysis.

The experimental investigation of semi-active SDOF mass isolation system are presented in chapter 6. An SDOF mass isolation system, consisting of an MR damper excited by a high response servo hydraulic actuator is described. The observer and controller were modelled in a real time digital simulation. The performance of the observer based feedback linearisation was investigated by implementing sky-hook controllers, where comparisons were made with more simplistic on/off controllers and the uncontrolled case.

In chapter 7, the focus is moved to the specific application of the proposed theory as a case study, where the tuned mass damper (TMD) problem is chosen. This is also relevant to smart fluid devices. Numerical and HILS experimental investigations of observer based adaptive semi-active tuned mass damper with a linearised MR damper that attempts to mitigate random vibrations of the main structure is described. Numerical models of the passive TMD with a linear viscous damper and adaptive TMD with an MR damper were evaluated. In order to estimate the necessary states and damping force a non-linear Luenberger observer was designed. Two control concepts for the MR damper have been presented in addition to force feedback linearisation. Damping performance of these control concepts has been tested by varying structural mass, over a wide range.

The frequency response results have been compared to the damping performances of the passive TMD and an ideal adaptive TMD where the ideal adaptive TMD has been determined as a benchmark for this study. Simulated and experimental results have demonstrated that the damping performance of the observer based adaptive TMD with a linearised MR damper exceeds that of a passive TMD significantly, depending on the change in the main structural mass.

Chapter 8 presents the key conclusion of this research and some recommendations for future work.

2 Literature review

2.1 A history of smart fluids

Smart fluid was first introduced by Willis Winslow, an American inventor in 1940's [29]. Winslow investigated the behaviour of different types of ER fluid by experimental testing. He used a variety of insulating oil (mineral oil, paraffin, and kerosene), with added solid particles such as starch, stone, carbon, and silicon to find out the how the viscosity of the fluid changes and the resistance to fluid flow varies under the applied field. At the beginning, smart fluids were used to implement the clutch and brake mechanism. Later damping devices and actuators were proposed based on smart fluid technology. The first ER device was also invented by Winslow, with a title of 'methods and means to translate electrical impulses to mechanical forces' [30].

However, the properties of Winslow's smart fluid were found to be abrasive, toxic, chemically unstable and they had a short life time [5]. Consequently, these drawback delayed the early commercial exploitation until the more stable and non-abrasive ER fluids were developed in the 1980's [23, 31]. The initial discovery and development of MR fluids and devices also goes back to the 1940's, an American inventor (Jacop Rabinow) developed MR fluid at the US National Bureau of Standards [32] and invented the first MR devices [33, 34, 35, 36]. Although, significant development of the MR devices took place in the

late 1980's and early 1990's [21, 37] most of these were presented by the Lord corporation [38]. This commercial exploitation of the MR fluid devices were also related to the improvement of other technologies such as microprocessors, sensor technologies, computer processing speeds and battery power [26].

In 1995 the commercialisation of MR fluid devices began with rotary brakes for sports equipment [39]. After two years, an MR damper was used for heavy-duty truck seat suspension. A few years later, MR fluid devices was introduced to primary vehicle suspension markets with mass production. The first MR shock absorber known as MagneRide [20] was manufactured for primary vehicle suspensions system by Delphi Corporation, and incorporated Lord Corporation's MR fluid [38]. This new suspension system was implemented on the Cadillac Seville STS by General Motors (GM), in 2002 [39]. Since 2002, GM have used MagneRide shock absorbers on the 2003 and 2005 Corvette, many of the Cadillacs models SRX and XLR (2004-09), STS sedan (2005-11), SRX roadster (2004-09), CTS-V (2009—), Escalade ESV (2009-), DTS (2006–11), XLR SUV (2005-09), and latest model of 2013 ATS [40]. In addition to GM vehicles, MagneRide suspension system have been replacing old suspension systems for many other worldwide companies on their primary vehicles, such as by Buick Lucerne CXS model [41], Ferrari 599 Fiorano (2006-) [42] and California (2008-) [43], Audi TT (2006-) [44], and R8 [45], and Range Rover Evoque [46]. Lord corporation have developed various other commercial MR fluid devices, which include MR rotary brakes for force-feedback elements in steer-by-wire systems, and large-scale MR dampers (up to 180kN) for civil engineering applications e.g. for earthquake protection. Lord's MR fluid production levels in 2004 were reached to the order of tens of thousands of litres to accommodate this wide range of commercial devices [39].

In 1995, the relative merits of ER and MR fluids are clearly identified by Carlson et al. [21], which explains the reason why MR fluids have had great commercial success, but the first mass-produced ER device is yet to be developed. The key point of this identification were described by Carlson as;

- Yield strengths displayed by ER fluids are in the range of 3-5kPa, whereas the capacity of delivering yield strengths of MR fluids reaches up to 100kPa.
- Operating temperature range of ER fluids (15 ^{o}C to 90 ^{o}C [28]) is narrower than MR fluids (-40^{o}C to 150 ^{o}C [21]).
- Voltage source requirement of the ER fluids (2-5kV [47]) to produce the necessary electric field strengths is higher than MR Fluids (12-24V [47]), which can be provided by more conventional power supplies. Due to the contrasting current requirements (1-10mA for ER, and 1-2A for MR), the power requirements of ER and MR devices are similar ($\approx$ 50W) [47].
- ER fluids are highly sensitive to the presence of contaminants [21].

It is clear that, MR fluids have a significant potential for commercial production.

2.2 Smart fluid devices

In order to classify the smart fluid devices the investigation about their working modes are suggested. Basically there are three modes of operation (1) flow mode, (2) direct shear mode, (3) squeeze-flow mode as illustrated in Figure 2.1.

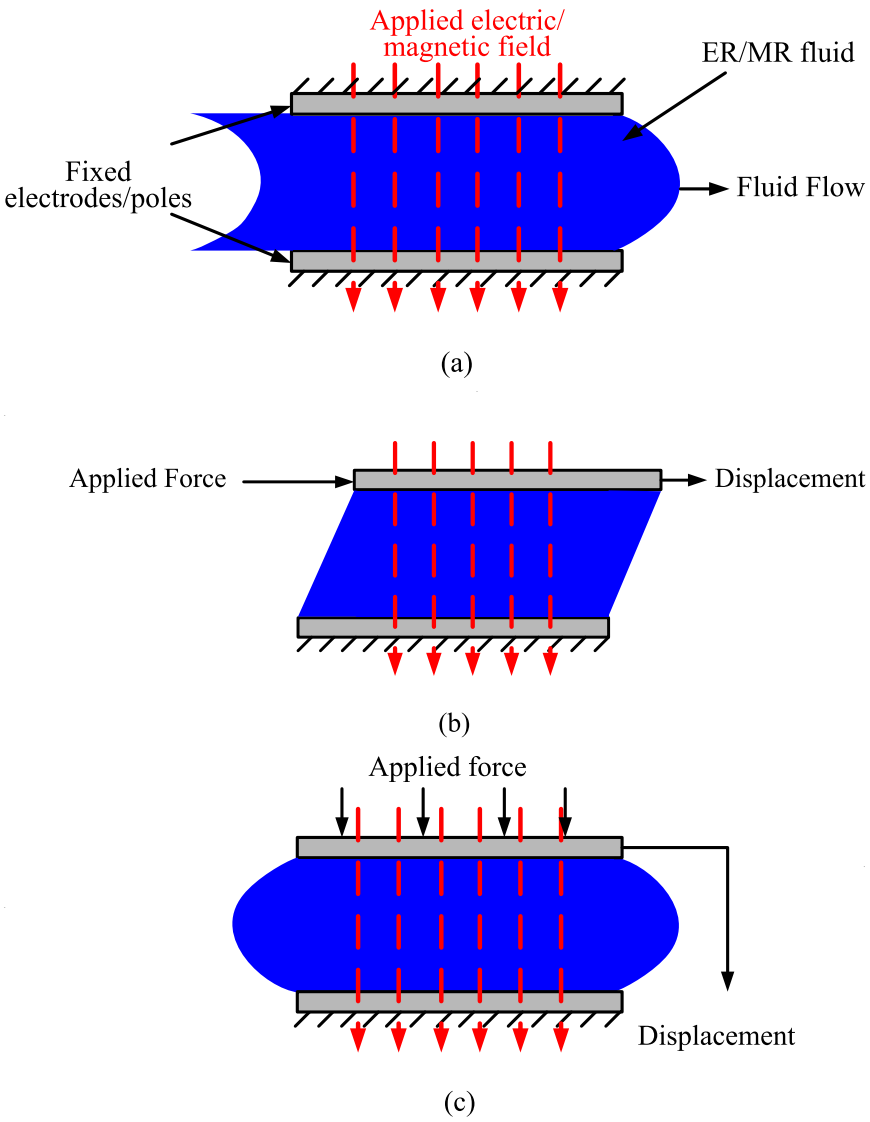

Figure 2.1: Smart fluid modes of operation. (a) Flow mode, (b) direct shear mode, and (c) squeeze mode.

• Flow Mode

The basic smart fluid devices are generally constructed with flow mode. Flow mode device first designed by Winslow [48]. This device mainly includes a pair of stationary electrodes (ER) or poles (MR) and controllable MR or ER fluid that is held between these electrodes or poles as shown in Figure 2.1-(a). Perhaps damping devices are the best ex-

ample of the flow mode devices as shown in Figure 2.2-(a). When the piston moves, smart fluids pass through the bypass circuit valve. Hence applied magnetic field increases the viscosity of the fluid therefore resistance to the piston increases as well [49]. Flow mode phenomenon could also be used to create actuator, servo valves and hydraulic control devices. A hydraulic actuator based on flow mode smart fluid devices was demonstrated by Kordonsky [50, 51], where the desired actuator motion were generated by controlling the flow rate through the two inlets (2 and 4) and the two outlets (1 and 3) as seen in Figure 2.2-(b).

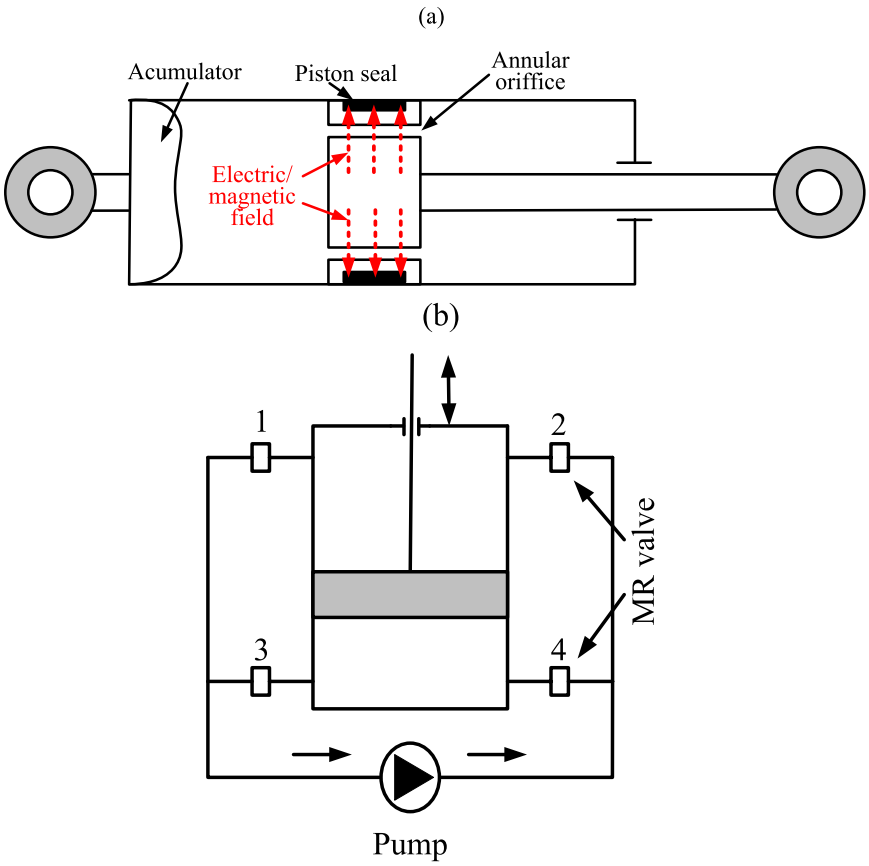

Figure 2.2: Flow mode devices (a) Smart fluid damper, and (b) smart fluid hydraulic control system.

• Direct Shear Mode

Here, smart fluid is shearing between two electrodes (ER) or poles (MR) where one or both of them are either rotating or sliding as shown in Figure 2.1-(b). As in flow mode, Winslow was the first inventor of the shear mode device, in 1947 [30]. If the electrodes (ER) or poles (MR) rotates then the device is a torsion damper, e.g. the Rheonetic MRB-2107 brakes that were developed by Lord Corporation in 1996 [21] in order to control aerobic exercise equipment by using the torsional direct shear mode. If the electrodes (ER) or poles (MR) translate then it is a linear damper. In addition direct shear mode is also used to build several types of ER/MR fluid devices such as, brakes [52, 53, 54], clutches [55, 56, 57], and structural dampers [58, 59]. Examples of rotary MR clutches are given in Figure 2.3. Such devices could replace torque converters in automatic drive line transmissions in order to provide better control during vehicle launch, and to improve high-speed efficiency (by reducing slip) [60].

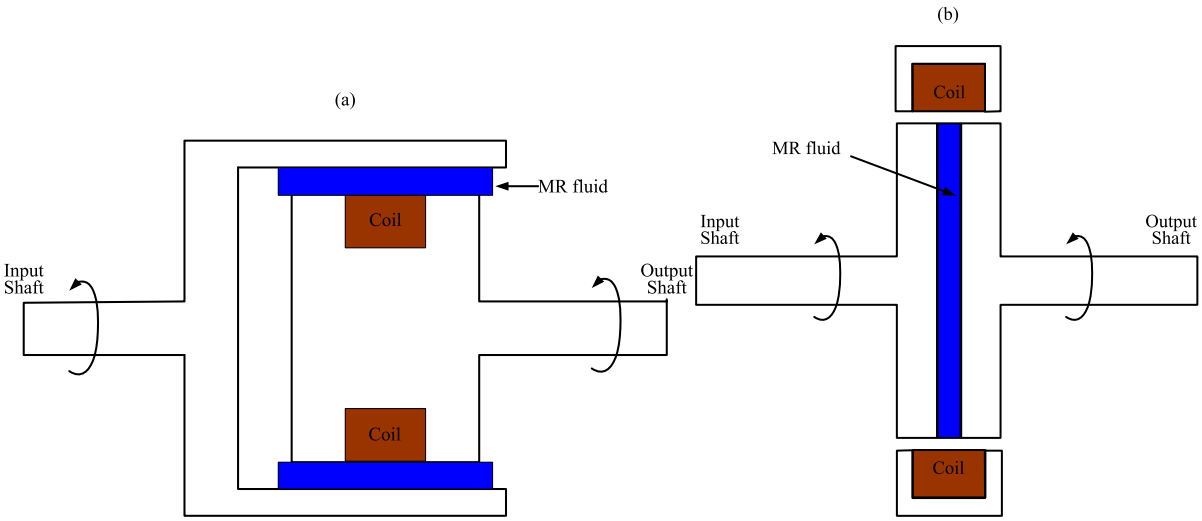

Figure 2.3: Shear mode rotary clutches [60]. (a) Cylindrical design, and (b) disk shaped design.

• Squeeze-flow Mode

In the squeeze-flow mode, the electrodes (ER) or the poles (MR) are free to translate in a direction parallel to the applied field as shown in Figure 2.1-(c). This movement depends on the fluid tension, compression, and shear forces [5]. When the system requires small displacement and large forces to control then this mode is perhaps the most suitable one [61], such as engine mounts [62]. In addition, squeeze flow mode devices have been used to control the vibration of flexible rotor systems [63, 64, 65, 66, 67].

For this research, the flow mode configuration of device is chosen, which is arguably the most suited to damper design.

2.3 Modelling of smart fluids

In reality, the highly non-linear characteristic of the smart fluids makes it quite difficult to design a proper model of the device. This non-linearity represents the relationship between the applied field and produced resistance force. In other words, the output (force) is the non-linear function of the inputs applied field. Increasing the accuracy of a smart fluid model will permit the effective design and sizing of devices, and will enable the development of high performance controllers.

Models of smart fluid devices are mainly divided in two groups. The first group estimates the behaviour of the smart fluid during the steady flow conditions i.e. where the fluid shear rate is constant. These are called Quasi-steady models. The second groups accounts for the transient flow behaviour, which can include effects such as fluid compressibility and fluid inertia. These dynamical models are better suited to precisely predicting device performance as part of a complete vibrating structure. As a result, dynamical model of smart fluids enable the more effective development of control strategies.

The most common way to represent the quasi-steady behaviours of the smart fluid is the Bingham plastic model (see Figure 1.6-(b)). According to this model, the onset of flow does not occur until the smart fluid is stressed beyond a critical yield stress, when it starts to flow like a Newtonian fluid with a constant viscosity. Experimental test results of the one-dimensional axisymmetric damper [68] have strongly supported Bingham plastic behaviour. However, the yield stress and viscosity predictions were not good enough, where fluid property values had to be updated before good correlation was achieved [68]. In addition, smart fluids may exhibit shear thickening or shear thinning behaviour. Figure 2.4 compares quasi-steady response for Bingham model with shear thickening or shear thinning behaviour where the apparent viscosity tends to increase or decrease with increasing shear rate [69]. Particularly the performance of smart fluids can vary from idealised Bingham plastic behaviour at high velocities.

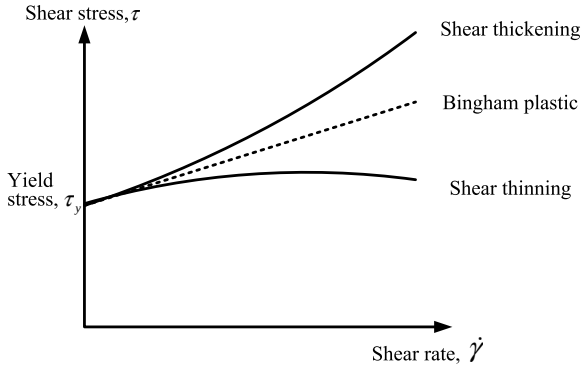

Figure 2.4: Shear thickening and shear thinning behaviour of smart fluids.

In order to illustrate this effect several solutions proposed such as, by using Herschel-Bulkley model with assumption of the shear stress is proportional to a power law of the shear rate [70, 71, 72, 73], by using simplified Herschel-Bulkley model where a region of high shear rate flow and a corresponding reduction (shear thinning) or increase (shear thickening) in the fluid viscosity were defined by using a bi-linear post-yield viscosity

function in the Bingham plastic equation [69], and empirical coefficients used to modify the equation for Bingham plastic flow between parallel flat plates as an alternative method [74].

The described models based on Bingham plastic theory were effective at predicting the post-yield quasi-steady response. They do not account for the significant dynamic behaviour that is observed in real devices. To give an example of this behaviour, Figure 2.5 compares force/velocity response of Lord Corporation's RD-8040-1 MR damper [75], and the quasi-steady response for Bingham plastic under the sinusoidal excitation. Figure 2.5 illustrates the shortage of the quasi-steady model under dynamic conditions. Also, the key dynamic effects has been attributed to fluid compressibility which appear in the form of a hysteresis loop with reference to the experimental response [76], and under-damped oscillations are associated with the fluid inertia [76]. Furthermore, viscoelastic behaviour appears in the pre-yield response, which assumes rigid pre-yield behaviour.

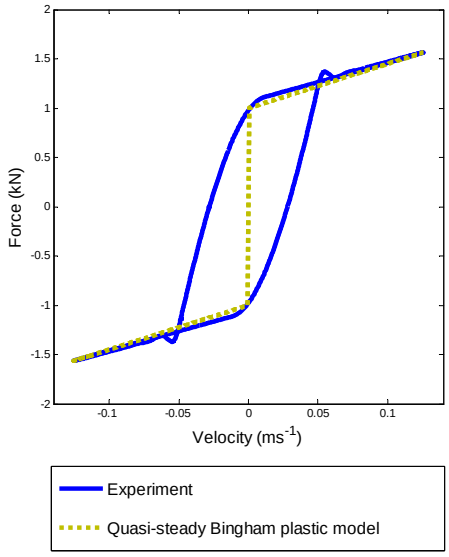

Figure 2.5: Experimental and numerical force/velocity response of Lord Corporation's RD-8040-1 MR damper [75] under 2 mm 10 Hz sinusoidal excitation.

In 1987, the first dynamical model of ER fluids was proposed by Stanway et. al. [77],

illustrated in Figure 2.6-(a). The model was designed for ER vibration damper and modelled as a parallel combination of a viscous damper (to model the post-yield response) and Coloumb friction element (to model the yield stress). Gamota and Filisko extended this model to three degree of freedom system by adding viscoelastic and plastic elements [78] as seen in Figure 2.6-(b). This later model was better able to predict the behaviour, but it also increased the complexity of the system, also the dynamic equations are stiff and so difficult to [59]. Later on, Spencer et. al. proposed the modified Bouc-Wen model [59]. This single degree of freedom Bouc-Wen model differs from the Bingham model with an additional parallel non-parametric element to account the hysteresis effects as shown in Figure 2.6-(c). The Bouc-Wen model was able to adequately predict the experimental response, but for significant accuracy of prediction an additional degree of freedom is required [59]. However, the Bouc-wen model requires the identification of large number of parameter and so the researchers have focused on the development of the effective system identification techniques [79, 80, 81, 82, 83, 84]. Also, it is claimed that "to account for the experimental force–velocity plots, an additional degree of freedom had to be introduced to the Bouc-wen model" by Sims [85].

Another dynamic modelling approach called the viscoelastic-plastic model, was proposed by Kamath and Wereley [86] where non-linear shape functions determine the weighting of two linear shear flow mechanisms – one that describes the pre-yield behaviour (parallel viscous damper and linear spring) and one that describes the post-yield behaviour (viscous damper), this is shown in Figure 2.6-(d). Researchers have been proposed many other non-parametric techniques for the dynamic modelling of smart fluid dampers. For example, Chebyshev polynomials were fitted to experimental data by Gavin, et al. [87], and 6th order polynomials were fitted by Choi, et al. [88]. A neural network of an MR damper were developed by Chang and Roschke [89]. In order to train the neural network

they used a Bouc-Wen model.

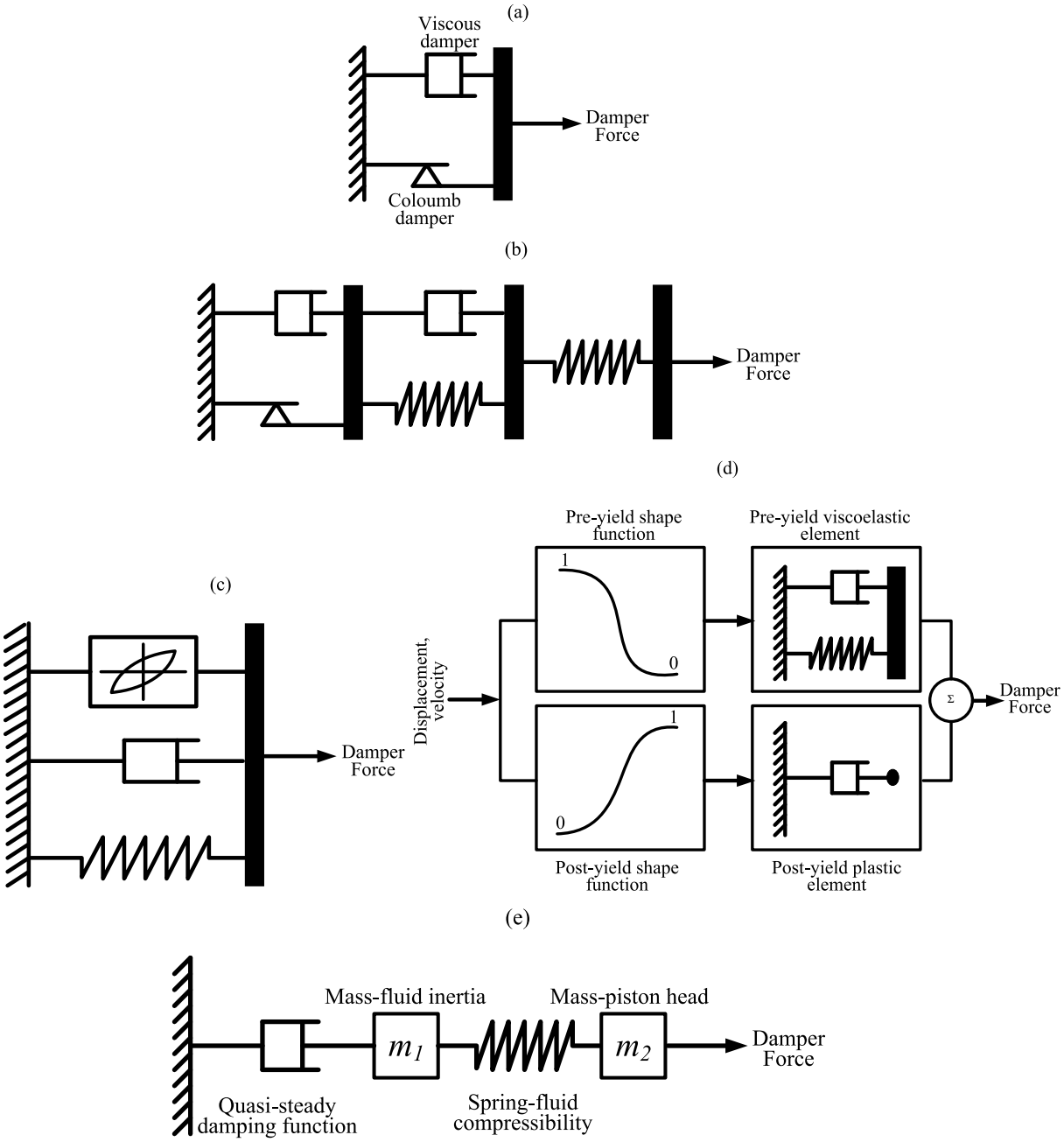

Figure 2.6: Lumped parameter model of some previous smart fluid dampers: (a) Bingham model [77], (b) extended Bingham model [78], (c) Bouc-Wen model [59], (d) viscoelatic-plastic model [86], and (e) unified MR model [85].

Many of the smart fluid device model formats discussed previously require the identification of many parameters and are highly complex. Besides, models are often developed in

parallel to existing laboratory devices and the parameters can often lack physical significance. So these models might be well suited to a particular device, and thus cannot be used for different designs. In order to overcome these potential drawbacks, Sims et. al. [85] have developed more a general modelling approach, which is shown in Figure 2.6-(e), and comprises a quasi-steady damping function in series with two masses and a linear spring. The mass m_1 represents the fluid inertia, whilst the mass m_2 represents the piston head mass, respectively the fluid compressibility k is represented by the linear spring. Analytical model of Bingham plastic equation for flow between parallel flat plates can be used to derive the quasi-steady damping function [76]. This indicates that, by using constitutive relationships between the fluid properties and the device geometry, the parameters of the model can be evaluated, rather than using observed experimental behaviour. This enables to design an accurate dynamical model before the device manufactured, which is vital for prototyping. In addition, this model also makes it possible to implement system identification method or the updating procedure. As a result, this model accurately represent many of real devices. An effective system identification method was explained by Sims, et al. [85]. Also, the authors showed that the resulting model is extremely efficient in reproducing an MR damper's behaviour with broadband mechanical and electrical excitation. This model is used in this thesis in order to develop effective control strategies for MR mass-isolators and vibration absorber problems.

2.4 Control of smart fluid devices

The significant non-linearity of the smart fluids damper complicates the proper control design, so as a result researchers have proposed wide range of control schemes. All of these control algorithms have aimed to find out;

1. The desired set-point damping force for optimal performance.

2. A method to determine the corresponding input current/voltage that achieves this desired force.

By combining these two targets, smart fluid devices were driven with an optimal calculated input current/voltage to track desired set-point damping force which is the biggest challenge in reality. To overcome this challenging task, relatively complex semi-active controllers were proposed by researchers, in an attempt to fully exploit their potential within automatic control systems. Several researchers implemented Lyapunov stability theory and clipped optimal control strategies with some success to structural control [90, 91, 92, 93, 94]. Yoshida and Dyke compared these methods with equivalent ideal semi-active and fully active systems [95]. Implementation of the neural networks for both structural [96, 97, 98] and automotive [99, 100, 101, 102] applications are investigated, as well as fuzzy control schemes [103, 104, 105, 106], quantitative feedback theory based controllers [107] and H_∞ controllers [108, 109]. Adaptive neural network techniques were proposed by Morishita and Ura [110] and implemented to the two-degree-of-freedom (2DOF) beam structure numerically and experimentally. Researchers have also proposed sliding mode control for aerospace [111], automotive [112, 113, 114, 115], and structural [116] applications. In addition Kim et al. designed a non-linear sliding mode control and experimentally investigated it a cantilever beam specimen [117]. Pole placement control method was used to reduce the tip deflection of a beam over frequencies of up to 100 Hz by S. H. Choi et al. [118]. Dyke et al. described the clipped optimal algorithm by using MR damper for structural application [90]. In a numerical study clipped optimal control implemented to the three-story building by using the measured acceleration signals. Also the experimental validation of optimal theory is done by Dyke et. al. [91].

Bang-bang or on/off methods are mostly preferred by researchers as algorithms to simply

achieve a proper force tracking of smart dampers. These methods simply switch the smart damper's current/voltage supply to a predetermined level when a dissipative force is required within the controllable range of the device, otherwise switch the smart damper's current/voltage supply to the zero or the minimum level [119, 120, 121]. It was shown by Sims et al. [15], that this simple on-off approach is very effective under the sinusoidal excitation but under more realistic random inputs the performance suffers.

Yoshida and Dyke investigated alternative force tracking methodologies include the development of approximate linear relationships between the control current and the desired damping force [95]. A polynomial model of an MR damper was used to analytically generate the inverse damper dynamics by Choi, et al. [88]. This methodology was used by Du, et al [108] to implement H_∞ control of an MR vehicle suspension where the authors concluded that due to the insufficiency of the polynomial model to describe the low velocity behaviour, the desired force could not be tracked accurately. By using the neural networks investigators have proposed more complex force tracking strategies, which are trained to predict the control current for a given force [122, 123, 124]. For example, it is shown that the force/velocity response could be linearised by using the experimental MR damper data to train neural networks [122]. A Bouc-Wen model is used for training by Chang and Zhou [123], and tracked force demands from optimal control laws for both single and multi-degree-of-freedom systems (MDOF).

So far, many of the control methodologies described above are derived using specific numerical or experimental behaviour which makes them sensitive to parameter uncertainty. In other words, if the behaviour changes due to differences in fluid properties or variations in viscosity of fluid, the force tracking accuracy will suffer. This problem motivated the researchers at the University of Sheffield, and they proposed an alternative approach to

controller design, where force feedback loop is used to linearise the force/velocity behaviour of a smart fluid damper [125, 49]. Accurate desired set-point force tracking is achieved by the feedback linearisation technique with in the control limits imposed by the fluid properties and device geometry. This control strategy enables effective implementation of the various control algorithms.

2.5 Observer base semi-active control

In a previous numerical study based upon an ER damper [126], feedback linearisation was shown to be effective for a single-degree-of-freedom (SDOF) mass-isolator with sinusoidal excitation. A later article [15] extended this work to investigate an ER vehicle suspension, where a 32% reduction in car body acceleration was demonstrated with the linearised controller. After that, Batterbee and Sims [127, 128] validated the force feedback linearisation algorithm under the actual roadway excitation conditions, by using the force transducer to measure the damping force, and an LVDT sensor to measure the piston displacement. Most of the proposed semi-active control algorithms implement the similar sensors techniques to measure these values, but implementation of these sensor in reality are difficult and increases the complexity of the system [129]. One target of this present thesis to overcome this complexity problem by estimating the force by using a non-linear observer.

Most of the control concepts proposed in the history of semi-active control also require the knowledge of the damping force and system states (velocity or displacement informations) [130] which were difficult to measure in practice [129]. The difficulty of measuring damping force and system states has motivated scientists to look for alternative ways to predict these values. Some of the proposed solutions use the measurement of semi-active relative displacement[131, 132], relative displacement and accelerations of the system

[133, 134], while some authors consider acceleration(s) alone [135, 136] to predict the required states of the system. Li et al [137] designed Luenberger [138] based non-linear dynamical neural network observers to isolate the vibration of the 20-story non-linear structure by using the relative displacement of first floor as the inputs of the observer. Giua et. al designed predictive observer by minimizing the H_2 norm of the transfer function matrix between the estimate error and the external disturbance [131]. Adaptive observers are developed for a class of non-linear systems by Rajamani et. al. [133] which use the measurement from two accelerations and an LVDT sensor. Yi et. al. present the observer uses easily accessible measurements such as accelerations and guarantees exponentially convergent state estimation for suspension deflections and velocities [136]. Dixit et. al. investigated sliding mode non-linear observers use the suspension deflection as a measured input [132]. H_∞/LPV linear parameter varying method was proposed by Aubouet et. al [139] to control the automotive suspension by using the relative displacement of the system.

Various methods have been proposed to estimate the velocities based on simple accelerometer implementation, such as simple bandpass filters, Kalman filtering, the decoupling technique, the sliding-mode technique, and gain scheduling among others [132, 131, 133, 135, 134, 136]. Acceleration based observers are designed especially for semi-active suspension system [140]. In this study, arguably the most applied simple Luenberger observer based on the measured accelerations are used. First observer designed according to linear model of the system and than updated to the non-linear observer form.

2.6 Summary of Chapters 1 and 2

The first two chapters in this thesis have described the limitations of traditional passive suspensions, whilst highlighting the advantages that can be gained using semi-active

devices. Moreover, magnetorheological fluid based devices were identified as a particularly superior means to provide semi-active vibration control.

Chapters 1 and 2 also drew attention to the non-linear behaviour of MR dampers. This makes the objective of achieving a desired force (and hence the application of classical control techniques) very difficult. Consequently, there is no general consensus on how to best perform automatic control. Previous research at the University of Sheffield has focused on a methodology known as feedback linearisation, which simplifies this force tracking issue. However, this research used the force transducer to measure the damping force same as the other controllers which in reality increases the complexity of the system. This motivates this thesis to implement a Luenberger observer by using the measured accelerations. The proposed observer, first is designed by using the linear model of the system and then by moving to a non-linear model.

The next Chapter aims to discuss the proposed observer based linearised control of an MR damper.

3 Theory

3.1 Introduction

Magneto-rheological, or MR, dampers are one of the most promising semi-active control devices for protecting civil engineering structures, vehicles, ships, or aircraft from the damaging effects of dynamic loading. They have many advantages over alternative technologies, such as low power requirement, reliability, and low cost. A wide range of control schemes have been considered for MR dampers, with no general consensus on the most appropriate approach. Research at the University of Sheffield has focused on feedback linearisation [125], but this requires measurement of the damping force which increases the complexity of the system.

The present research aims to overcome this problem by investigating the application of observer based control to the feedback linearisation of an MR damper. A single-degree-of freedom structure is chosen as the basis for this study, as shown schematically in Figure 3.1-(a). With reference to Figure 3.1-(b) and Figure 3.2, by replacing the passive damping element with a controllable MR damper the aim is to perform observer based force-feedback linearisation of the MR damper (so that it can perform as an arbitrary semi-active force generator) using an observation of the feedback force and states, rather than measured values. The proposed observer based linearised force feedback control of SDOF system consists of three basic components: the actual plant, non-linear observer

and the controller (combination of control concept and feedback linearisation) as seen in the Figure 3.2.

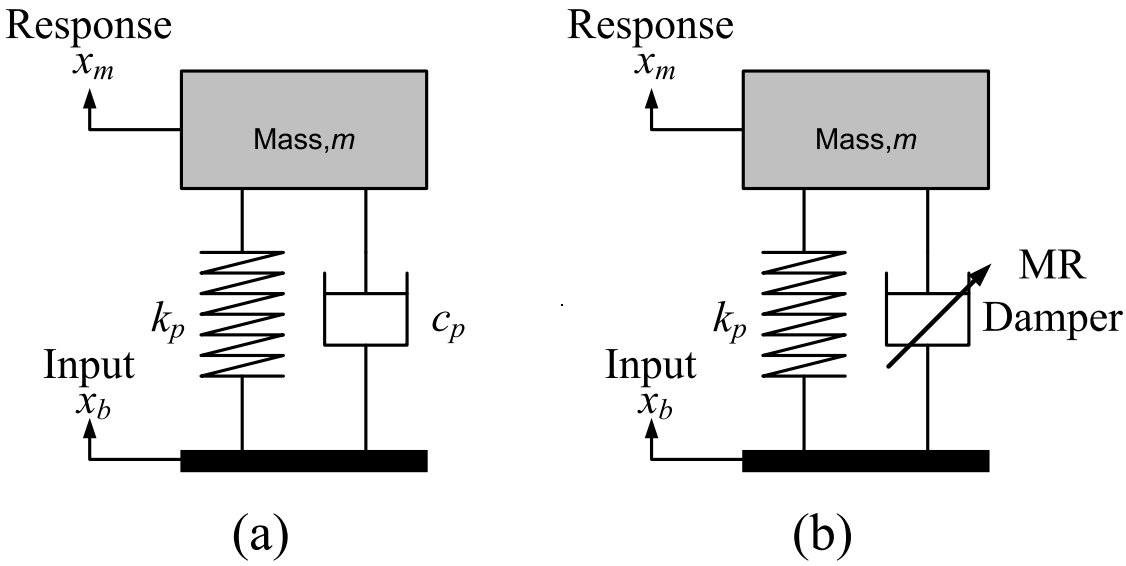

Figure 3.1: SDOF mass isolator configurations, (a) viscous damper model (b) MR damper model

The present chapter is organised as follows. First, there is a short discussion on the model of single degree of freedom system. After describing the model of the MR damper, an investigation of the observer design is then presented. Next, some attention is paid to the control algorithm. Lastly, it concluded with discussion and summary.

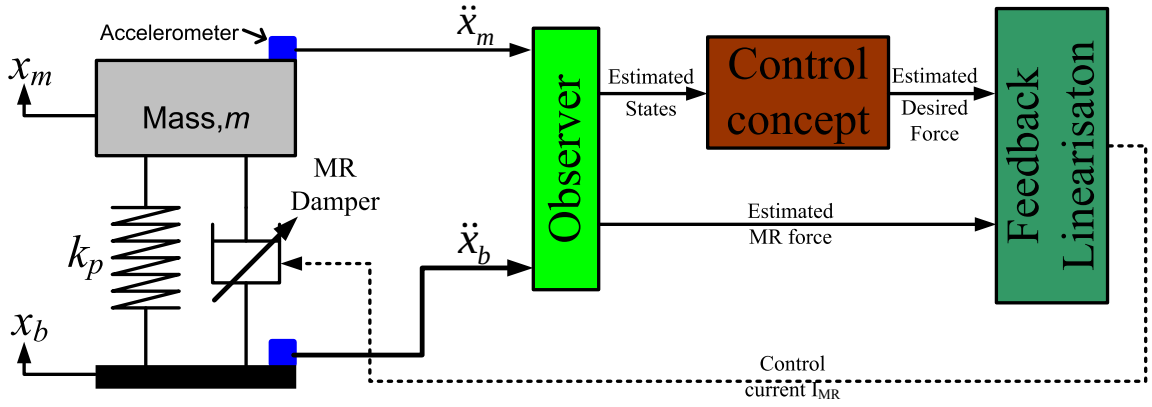

Figure 3.2: Observer based linearised control of the SDOF system.

3.2 Single degree of freedom system

A single degree of freedom system is created by an isolated mass (m), a linear spring (k_p) and a linear viscous damper (c_p) as shown in Figure 3.1-(a).

The equation of motion for the SDOF system is;

$$m\ddot{x}_m(t) = -k_p\left(x_m(t) - x_b(t)\right) - c_p\left(\dot{x}_m(t) - \dot{x}_b(t)\right) \tag{3.1}$$

where $x_m(\cdot)$, $\dot{x}_m(\cdot)$ and $\ddot{x}_m(\cdot)$ are the displacement, velocity and the acceleration of the mass. Also, $x_b(\cdot)$ and $\dot{x}_b(\cdot)$ are the displacement and the velocity excitation applied to the base.

For the case of harmonic excitation, the time domain solution is;

$$x_m(t) = X_m e^{i\omega t} \tag{3.2}$$

$$x_b(t) = X_b e^{i\omega t} \tag{3.3}$$

Substituting Equations 3.2 and 3.3 into Equation 3.1 yields

$$-m\omega^2 X_m = -k_p\left(X_m - X_b\right) - i\omega c_p\left(\dot{X}_m - \dot{X}_b\right) \tag{3.4}$$

and so the displacement transmissibility of the system becomes,

$$\frac{X_m}{X_b} = \frac{k_p + i\omega c_p}{-m\omega^2 + k_p + i\omega c_p} \tag{3.5}$$

Equation 3.5 illustrates the dynamics of the linear mass isolator problem. But, the performance of Lord Corporation's RD-8040-1 short stroke Magneto rheological (MR) [75] damper are investigated in this thesis. Because of this, the Equation 3.5 needs to be updated regarding MR damper rather than passive damper as seen in Figure 3.1-(b). The resulting equation of motion for MR damper mass isolation system becomes dependent on the MR damper force such as;

$$m\ddot{x}_m(t) = -k_p\left(x_m(t) - x_b(t)\right) - F_{MR}(t) \tag{3.6}$$

where $F_{MR}(\cdot)$ is the MR damper force. Because of the MR non-linearity, it is not possible to develop this equation further to evaluate the displacement transmissibility. However this non-linear model of SDOF system will be investigated numerically and experimentally in Chapter 5, and Chapter 6. At this point, a little attention is paid to the numerical model of an MR damper.

MR damper model

In reality the MR damper is a non-linear and hysteretic device due to highly non-linear characteristic of the magneto-rheological fluid. This non-linearity represents the relationship between the input and output. In other words the output (force) is the non-linear function of the electrical input (current applied) and the mechanical input (displacement of one end of the damper relative to the other end). Also the definition "hysteretic" is that

the output force is dependent not just on the instantaneous values of the inputs, but also on the history of the output [141] i.e. such a system has "memory". So a non-linear model of the MR damper is necessary.

Several types of numerical models have been designed to simulate the non-linear and hysteretic behaviour of the MR dampers. Shortly referring to the literature review, the most popular models of the smart fluid dampers were the model, proposed by Stanway [77] (Figure 2.6-(a)), Gamota and Filisko's model [78] (Figure 2.6-(b)), the modified Bouc-Wen model [59] (Figure 2.6-(c)), the viscoelatic-plastic model [86] (Figure 2.6-(d)), and the unified MR model (Figure 2.6-(e)) [85]. This was based on Lord Corporation's RD-1005-3 MR damper [142] and a schematic drawing and lumped parameter model of this device are shown in Figure 3.3. This is a flow mode device (Figure 2.1-(a)) where movement of the piston rod forces fluid through an annular orifice. An accumulator is also incorporated to accommodate for the change in the working volume caused by the presence of the piston rod. This introduces an element of stiffness to the damper response, however this was found to be insignificant when compared to the suspension stiffness terms in the SDOF models [127]. Consequently, the effect of the accumulator has been neglected in the development of the MR damper model (Figure 2.1-(b)). Here, the stiffness element represents the compressibility of the MR fluid, whilst the mass represents its inertia. The non-linear damper represents the Bingham plastic nature of the MR fluid flow. In earlier work the damping function was obtained by solving the Bingham plastic equations of flow.

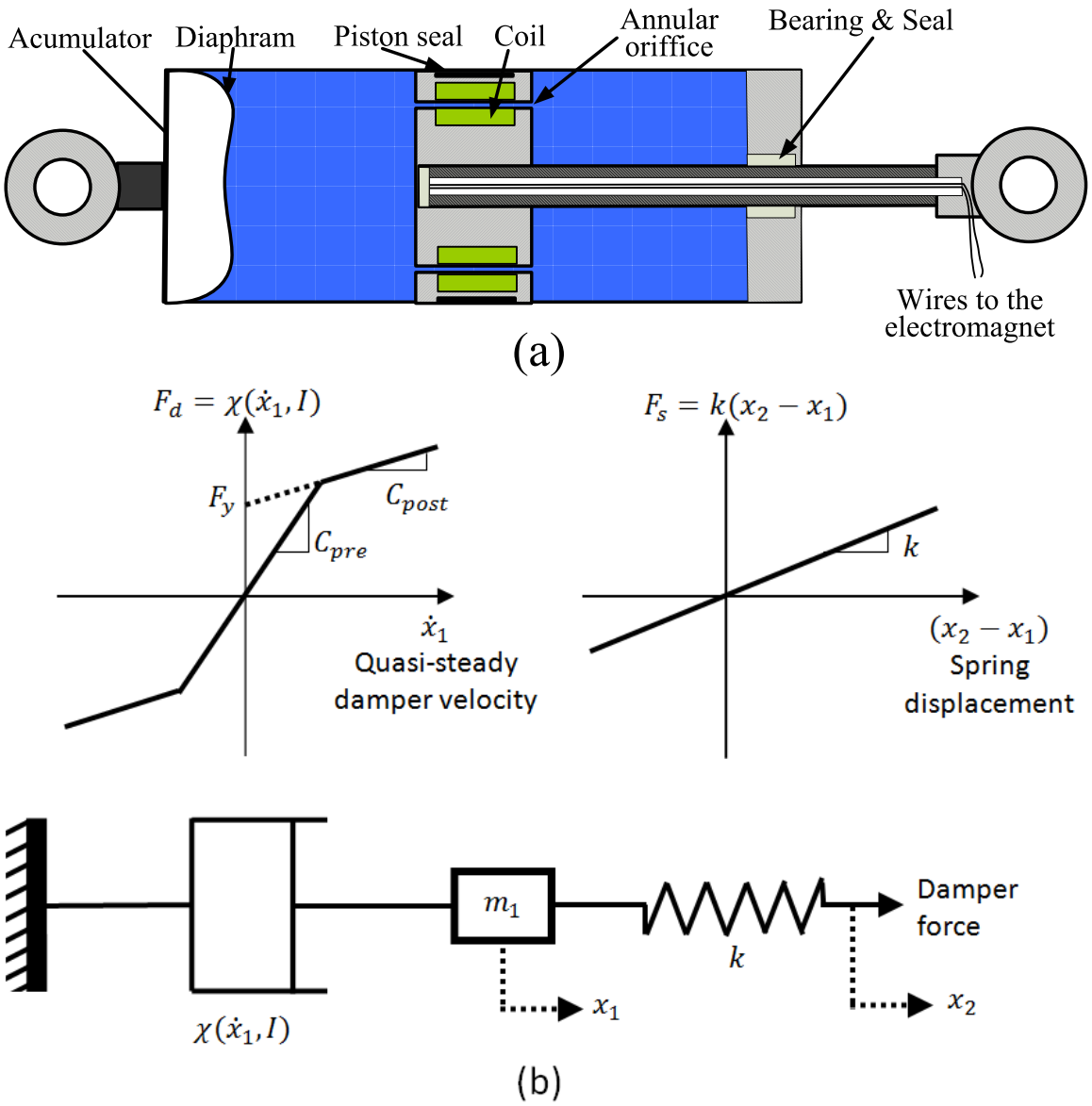

Figure 3.3: (a) Schematic diagram of the Lord Corporations RD-1005-3 MR damper [142] and (b) the lumped parameter model [85].

As it is been explained in the literature review that this unified model will be used in this thesis, due to not only it is flexibility in the choice of the model's damping function, but also the performance of the unified model has been proved by experimental testing of Lord Corporations RD-1005-3 short stroke MR damper by Batterbee and Sims [127] under the broadband mechanical excitation. This unified model is used in the present

study in order to develop effective control strategies for MR mass-isolators and vibration absorbers problems.

This unified model also will be summarised in Chapter 5 together with the other two types of non-linear models of MR damper.

3.3 Observer Design For SDOF System

All of the MR based semi-active control strategies require the system states (piston displacement and/or piston velocity) for control concepts, and the damper force (for feedback method), which are difficult to measure in practice. Direct measurements of these values are possible by the proper sensor applications (load cell, LVDT, and velocity transducers). However, the implementation of the load cell and LVDT sensors are difficult and expensive compared to accelerometers. This motivates proper observer design to predict states and the damper force from easily accessible measurements such as accelerations, for the implementation of the force feedback linearisation. There could be another way to measure this force such as using the acceleration signal directly, but it does drift when integrating the signal and also the observer concept could be extended for more complex systems to estimate the states. Implementing the observer reduce expense, reduce the working space of the system, and reduce the complexity.

Assume that there are two accelerometers, which are placed on the basement and mass to measure the accelerations of the basement and the mass. The question that arises here is whether an observer is able to estimate the velocity and displacement data of the base and the mass or not. In order to answer this question, firstly the state space representation of the SDOF system is derived. Then the observer gain is decided and implemented in Simulink.

If the estimated values of piston velocity and displacement are acceptable then the target is to estimate the force produced by the MR damper, which is installed between basement and mass to absorb the vibration by different values of applied current. If the force acting on the MR damper can be estimated, then the control algorithm could be developed to control the current applied to the MR damper according to force feedback linearisation.

State space model of the SDOF system

The equation of motion for SDOF system with linear viscous damper is already given in Equation 3.1.

$$m\ddot{x}_m(t) = -k_p\left(x_m(t) - x_b(t)\right) - c_p\left(\dot{x}_m(t) - \dot{x}_b(t)\right)$$

Where acceleration of mass is;

$$\ddot{x}_m(t) = -\frac{k_p}{m}\left(x_m(t) - x_b(t)\right) - \frac{c_p}{m}\left(\dot{x}_m(t) - \dot{x}_b(t)\right) \tag{3.7}$$

System inputs are $x_b(t) = u_1(t)$, $\dot{x}_b(t) = u_2(t)$, and the system output is the acceleration $\ddot{x}_m(\cdot)$ of the mass. The system states are designed to be displacement of mass $x_m(t) = x_d(t)$, and velocity of mass $\dot{x}_m(t) = x_v(t)$ so $\dot{x}_d(t) = x_v(t)$ and $\ddot{x}_m(t) = \dot{x}_v(t)$. Also

$$\dot{x}_v(t) = -\frac{k_p}{m}\left(x_d(t) - u_1(t)\right) - \frac{c_p}{m}\left(x_v(t) - u_2(t)\right)$$

The state space form for this SDOF system is ;

$$\begin{aligned} \dot{\underline{x}}(t) &= A\underline{x}(t) + Bu(t) \\ y(t) &= C\underline{x}(t) + Du(t) \end{aligned} \tag{3.8}$$

Which can be rewritten as:

$$\begin{bmatrix} \dot{x}_d(t) \\ \dot{x}_v(t) \end{bmatrix} = \begin{bmatrix} 0 & 1 \\ -\frac{k_p}{m} & -\frac{c_p}{m} \end{bmatrix} \begin{bmatrix} x_d(t) \\ x_v(t) \end{bmatrix} + \begin{bmatrix} 0 & 0 \\ \frac{k_p}{m} & \frac{c_p}{m} \end{bmatrix} \begin{bmatrix} u_1(t) \\ u_2(t) \end{bmatrix} \tag{3.9}$$

$$\dot{x}_v(t) = \begin{bmatrix} -\frac{k_p}{m} & -\frac{c_p}{m} \end{bmatrix} \begin{bmatrix} x_d(t) \\ x_v(t) \end{bmatrix} + \begin{bmatrix} \frac{k_p}{m} & \frac{c_p}{m} \end{bmatrix} \begin{bmatrix} u_1(t) \\ u_2(t) \end{bmatrix} \tag{3.10}$$

With reference to Figure 3.1-(b), the observed damper force was obtained using observations of the base and response motions, along with knowledge of the spring stiffness and payload mass:

$$F_{MR} = m\ddot{x}_m(t) - k_p\left(x_m(t) - x_b(t)\right) \tag{3.11}$$

This solution requires estimates of the payload mass acceleration and displacement, as well as the base motion. These can be obtained by designing a Luenberger observer [138], using as $x_b(t)$ system inputs, $\ddot{x}_m(t)$ as available output measurements, and $\hat{x}_m(t)$, and $\dot{\hat{x}}_m(t)$ as states to be identified. The frequency of the observer is chosen to make the observer dynamics considerably faster than the dynamics of the SDOF system. The mathematical model of the observer is defined as:

$$\begin{aligned} \dot{\underline{\hat{x}}}(t) &= A\underline{\hat{x}}(t) + Bu(t) + Lz(t) \\ \hat{y}(t) &= C\underline{\hat{x}}(t) + Du(t) \end{aligned} \tag{3.12}$$

where the difference between the measured outputs $y(t)$ and the estimated output $\hat{y}(t)$ is represented by:

$$z(t) = y(t) - \hat{y}(t) \tag{3.13}$$

The dynamics of the state estimation error is then given by

$$\dot{e}(t) = (A - LC)e(t) \tag{3.14}$$

where

$$e(t) = \underline{x}(t) - \underline{\hat{x}}(t) \tag{3.15}$$

where L is the observer gain matrix which is a 2x1 matrix for SDOF system. The pole placement method is used to find the observer gain matrix. Assuming the observer gain matrix is;

$$L = \begin{bmatrix} l_1 \\ l_2 \end{bmatrix}$$

Poles of the SDOF system are given by;

$$|sI - A| = 0$$

$$\left| \begin{bmatrix} s & 0 \\ 0 & s \end{bmatrix} - \begin{bmatrix} 0 & 1 \\ -\frac{k_p}{m} & -\frac{c_p}{m} \end{bmatrix} \right| = 0$$

Choosing the eigenvalues of the observer model at point a and b, implies that the desired characteristic polynomial of the observer is to be given by;

$$(s+\mathrm{a})(s+\mathrm{b})=0$$

$$s^2+(\mathrm{a}+\mathrm{b})s+\mathrm{ab}=0 \tag{3.16}$$

These chosen eigenvalues are the poles of the observer equation which is;

$$\dot{\underline{\hat{x}}}(t)=(A-LC)\underline{\hat{x}}(t)+Bu(t)+LCx(t)$$

where the eigenvalues are

$$|sI-(A-LC)|=0 \tag{3.17}$$

$$\left|\begin{bmatrix} s & 0 \\ 0 & s \end{bmatrix}-\left(\begin{bmatrix} 0 & 1 \\ -\frac{k_p}{m} & -\frac{c_p}{m} \end{bmatrix}-\begin{bmatrix} l_1 \\ l_2 \end{bmatrix}\begin{bmatrix} -\frac{k_p}{m} & -\frac{c_p}{m} \end{bmatrix}\right)\right|=0 \tag{3.18}$$

Comparing coefficients of Equation 3.18 with the desired characteristic polynomial Equation 3.16 the observer matrix could be evaluated.

Referring to Equation 3.12 the simulated model of the SDOF full state observer is shown in Figure 3.4 . The upper half of Figure 3.4 is the actual SDOF system and the lower half is the observer design for this system. This linear model could simply be converted to the non-linear observer model by replacing the linear damping element by the non-linear

model of the MR damper as seen in Figure 3.5. However, at this point it is worthy to ask whether the observer gain matrix (chosen based on the linear model), is able converge the system error dynamic (Equation 3.15) to zero in the presence of non-linearity? The answer to this question will be investigated numerically (in Chapter 5), and experimentally (in Chapter 6).

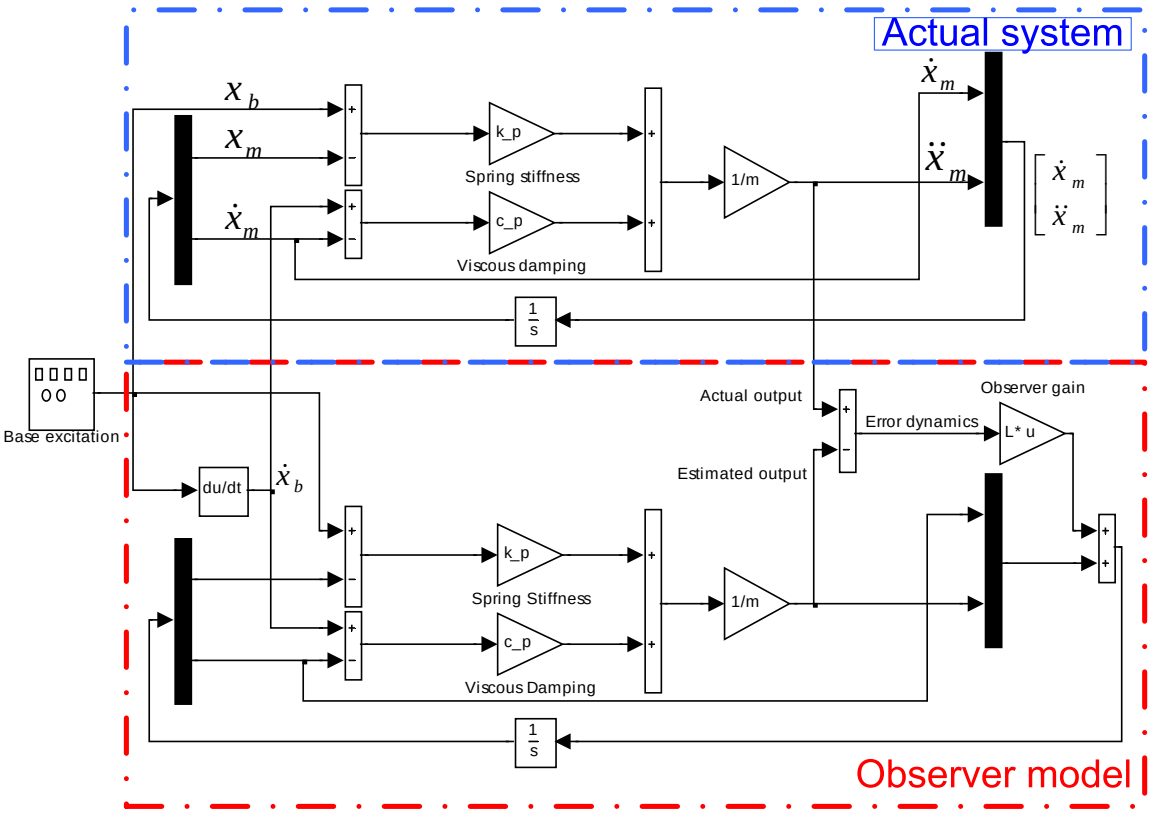

Figure 3.4: Linear Observer Design of SDOF system.

Next, a single degree of freedom linear observer system is designed based on the Luenberger [138] technique and a brief description of the non-linear observer design is given. Later, in Chapter 5, three types of non-linear SDOF observer models will be considered as well as the form of the non-linear MR model used to develop the SDOF observer system.

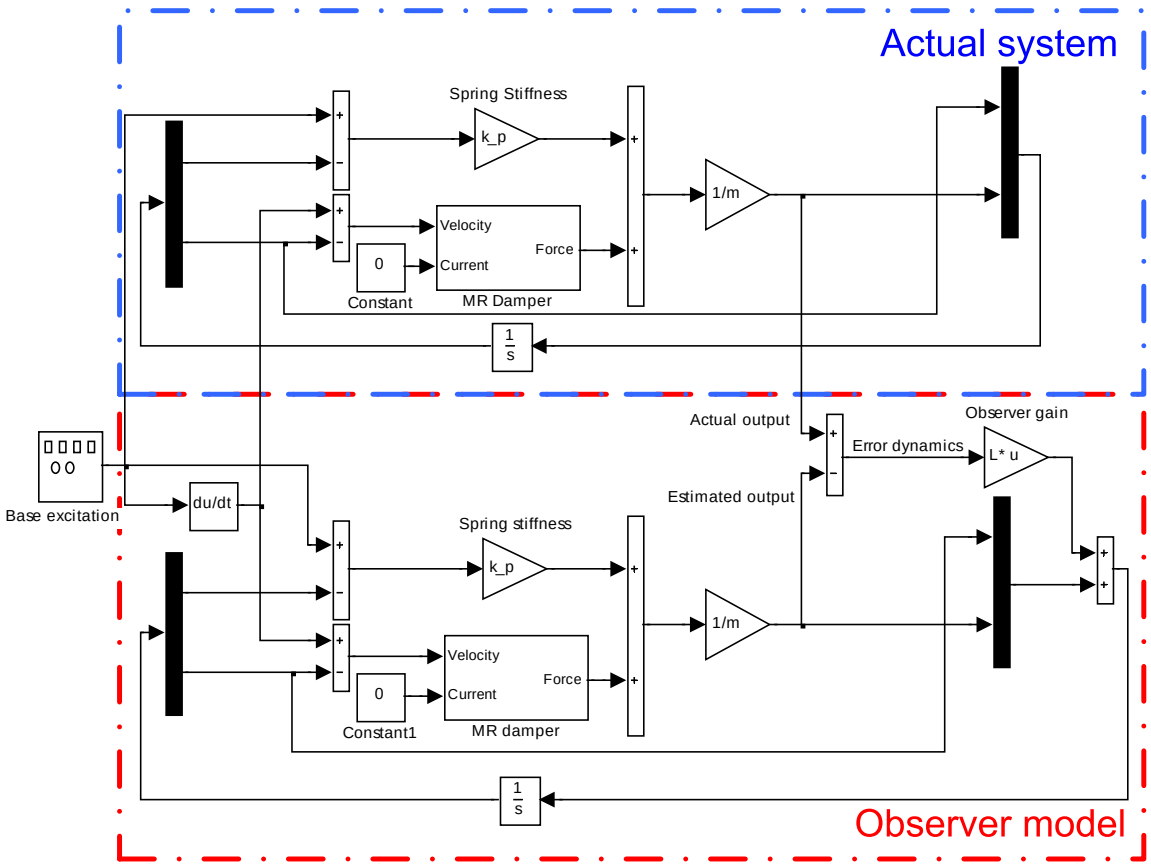

Figure 3.5: Non-linear Observer Design of SDOF system.

3.4 Feedback Linearised Control

Designing a proper control concept for smart fluid dampers is the key point to reach the maximum performance of the device due to their highly non-linear characteristic. Several types of control scheme have been proposed in the last two decades and these were summarised in the literature review. Kim et al. designed a non-linear sliding mode control and experimentally investigated on the cantilever beam specimen [117]. Adaptive neural network techniques was proposed by Morishita and Ura [110] and implemented to the 2DOF beam structure numerically and experimentally. Pole placement control method was used to reduce the tip deflection of the beam over frequencies of up to 100 Hz by S.

H. Choi et al. [118]. Dyke et al. described the clipped optimal algorithm by using MR damper for structural application [90]. In a numerical study clipped optimal control implemented to the three-story building by using the measured acceleration signals. Also the experimental validation of optimal theory is done by Dyke et. al. [91].

These non-linear controllers increased complexity of the system. It is been suggested by Sims et. al. [126] that using a linear control structure might be an alternative. Researchers at The University of Sheffield [125, 126] have developed simplistic feedback linearisation control method by using graphical techniques developed by West [143]. Using this model, a linear input/output characteristic can be obtained and also the slope of the line can be determined through the choice of a gain term in the controller, this linearised feedback control algorithm was chosen as the control strategy to be explored in this study.

The linearised feedback control strategy is shown in block diagram form in Figure 3.6. Here, feedback control is being used to implement a semi-active force generator. The proposed control system uses a measurement of the damper force to linearise the non-linear damping behaviour. Essentially, the controller gains B and G can be tuned so that the actual force closely matches the set point force. Here, the desired set point force is generated by the control law chosen separately by the users such as sky-hook, optimal, passive etc. However, the desired set point force could only be tracked by the MR damper if it lies within the control limits imposed by the device geometry and MR fluid properties. Figure 3.7 illustrates the control envelope of the MR damper. Feedback linearisation properly can track that force, if the desired set point force inclines within this envelope. On the other hand, the MR damper will remain in its 'off' state to minimise the energy dissipated if an energy input is required i.e. the desired force inclines within energy input quadrants, or if a dissipative force requirement is lower than that governed by the base

viscosity of the fluid (zero current), then this force cannot be achieved. On the other hand, if the desired force exceeds the upper boundary of the control envelope (maximum current), and is a dissipative one, then in order to maximise the energy dissipated, the damper current will saturate at its maximum level.

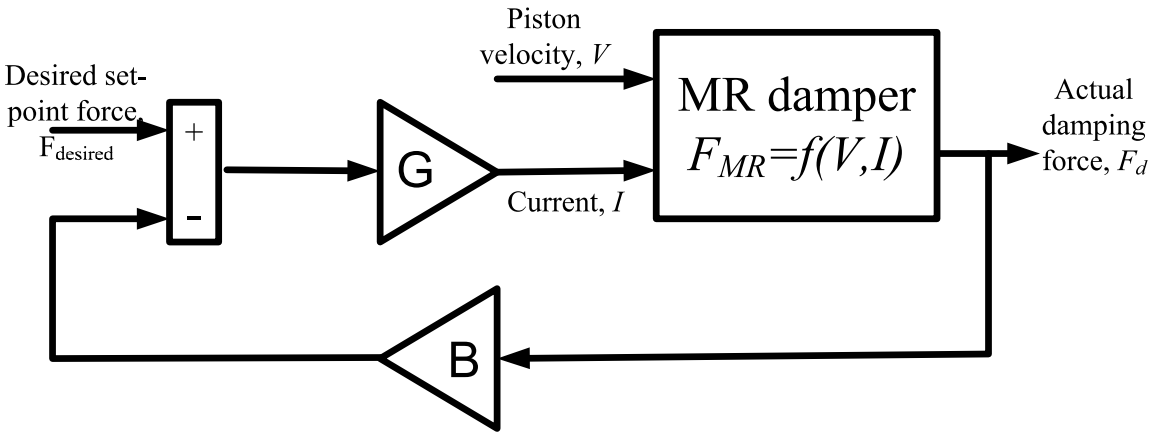

Figure 3.6: Semi-active force generator modified from [126].

Feedback linearisation control theory will be rediscover in Chapter 5.

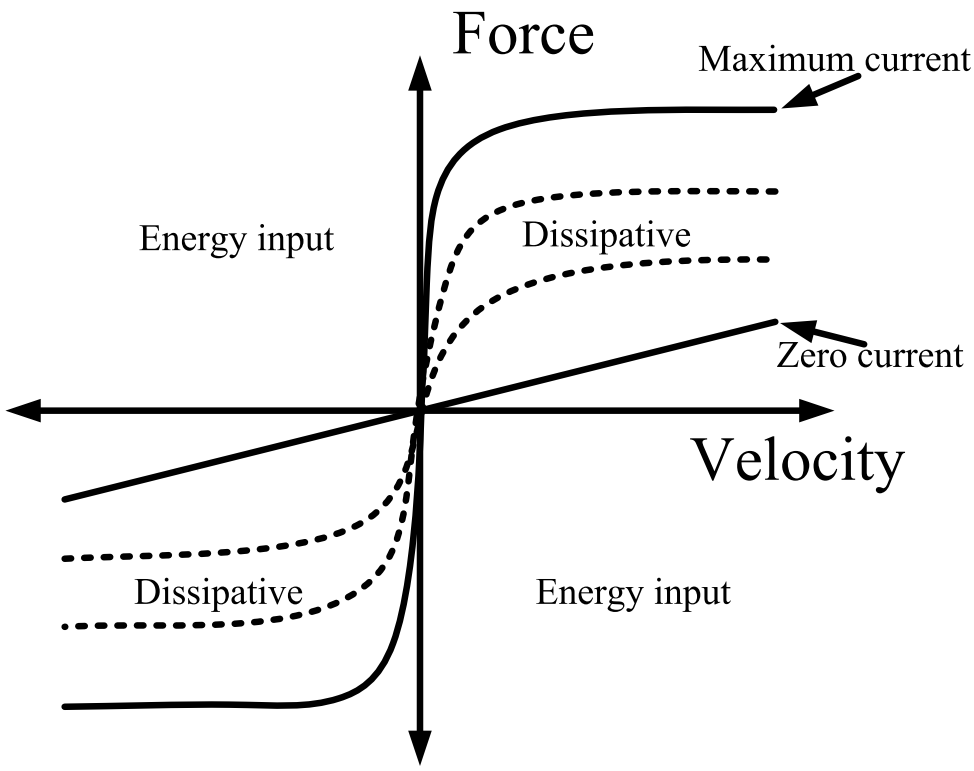

Figure 3.7: Control envelope of MR damper.

3.5 Summary of chapter 3

The proposed observer based feedback linearisation theory aims to convert a highly non-linear smart device (MR damper) into a variable semi-active force generator. This chapter has demonstrated the basics of the proposed theory by giving a brief theoretical descriptions of each aspects, a unified model of an MR damper; non-linear Luenberger observer; and linearised feedback control. Detailed designs for each part will be developed in Chapter 5.

First, however, it is useful to describe the comprehensive experimental test facility that will be used as a basis for designing, testing, and validating the proposed control system. This will be the focus of Chapter 4.

4 Experimental test Facility

4.1 Introduction

The present chapter is organised as follows. First, a description of the experimental test facility is illustrated, and this is followed by the set-up of the real model for the proposed single-degree-of-freedom system. Some experimental test results will be used to validate the numerical model of the MR damper and the proposed linearised control method under the broadband random excitation. Preliminary test results are used to compare the open loop responses of the numerical and experimental SDOF model under sinusoidal base excitation. The chapter is concluded with a discussion of the results.

4.2 Test facility

The experimental damper test facility is shown in Figure 4.1, and a corresponding schematic diagram is also illustrated in Figure 4.2 and Figure 4.3. Figure 4.2 illustrates experimental testing of an MR damper alone whilst Figure 4.3 illustrates experimental testing of a complete SDOF system. These two Figures 4.2-4.3 explain the interaction between the various hardware and software components.

Figure 4.1: A photograph of the experimental facility .

An Instron PLL25K servo-hydraulic actuator [144] was used to excite the system, which is able to deliver $\pm$25 kN force, $\pm$50 mm displacement and velocities of up to $\pm$1 ms^{-1}. This was controlled by two high response Moog servo-valves [145] and an Instron 8400 digital controller [144]. The desired control current and displacement to the MR damper can be controlled externally using real-time control software. Where a Kepco BOP amplifier [146] is used to provide this high-bandwidth dynamic desired control current for the MR damper. The excitation signals and test scripts are produced by a host PC running xPC target [147]. Simulink software was used to code the excitation signals and test scripts. These were then compiled as a C-programme, and afterwards downloaded onto a target PC. The real time control of the actuator was performed by the target PC, which comprised a 1.3GHz AMD Athlon processor with 128Mb of RAM. This was booted from a floppy disk containing the xPC operating kernel.

National Instruments PCI-MIO-16XE-10 data acquisition card [148] was used to achieve data logging, with sample rates up to 100kHz and supported an interface board with eight 16-bit analogue differential input channels (A/D conversion) and two 16-bit analogue output channels (D/A conversion). Data stored on the target PC's RAM was uploaded to the host PC after a test had completed, the measurement ready for post-processing.

In order to achieve accurate actuator position (sinusoidal excitation or random excitation), the measured data from inductive displacement transducer (LVDT) was compared with the desired actuator positions. The error between these two signals are minimised by the Instron 8400 digital controller which uses the PID feedback control algorithm.

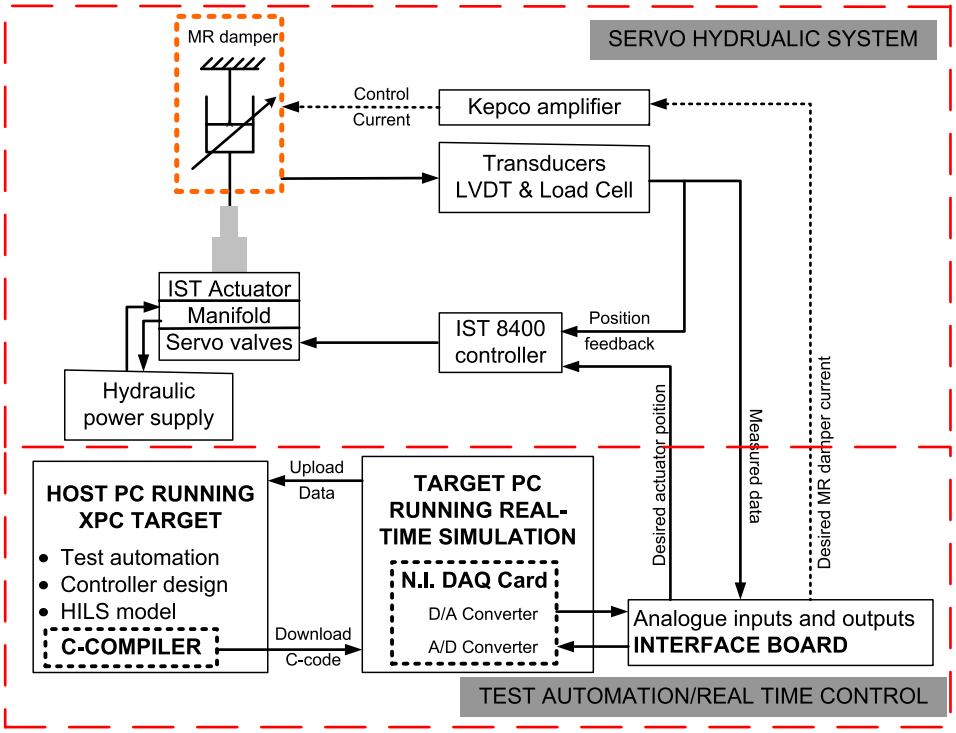

Figure 4.2: Schematic diagram of the experiment facility for MR damper testing.

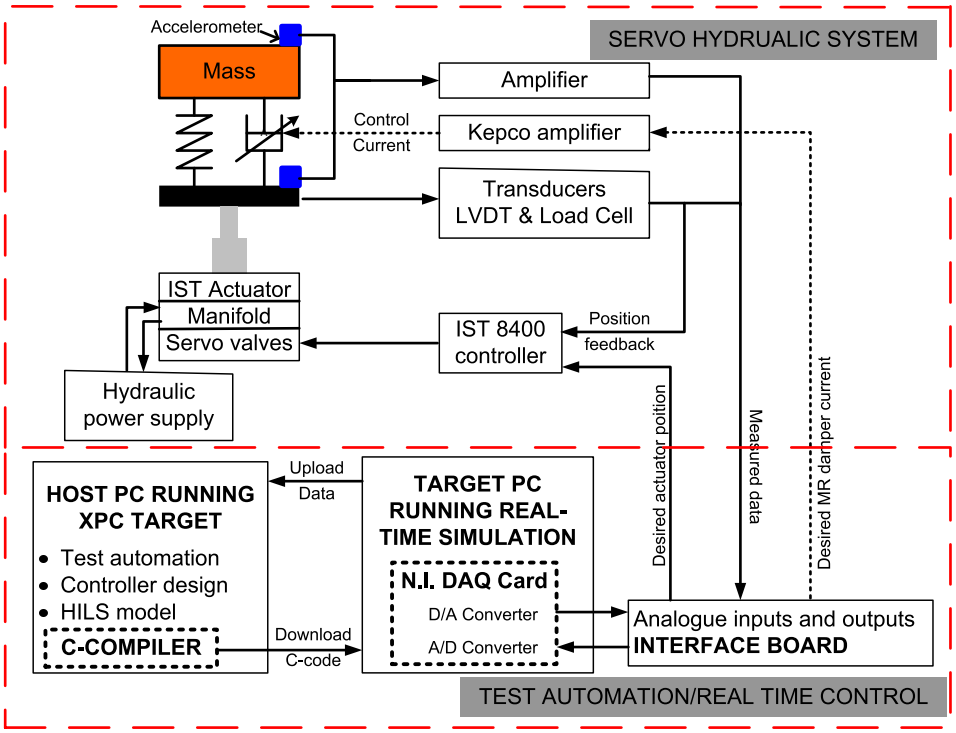

Figure 4.3: Schematic diagram of the experiment facility for SDOF testing.

Referring to Figure 4.2 the measurement data from an inductive displacement transducer (LVDT) also was used to investigate the dynamics of the MR damper with measured data from an Instron ±25kN load cell (IST Dynacell [144]). However, for SDOF experimental testing, the measurement data were acquired from two PCB piezotronics 3741 accelerometers [149] which were used to measure the base excitation and mass response with sensitivity 200 mv/g as seen in Figure 4.3.

Finally, to permit continuous testing without overheating of the MR damper, approximately 10 minutes breaks are given between each test and simultaneously the temperature of the damper is measured by the commercially available K type RS thermocouples [150].

4.3 SDOF study

A single degree of freedom system is created by an isolated mass (m=112 kg), a linear spring (k=63 kN/m), and a MR damper as shown in Figure 3.1-(b). The natural frequency of the system is equal to 3.75 Hz. The desired spring was manufactured and tested by Valley Spring Co Ltd [151]. The MR damper is a type of seat suspension damper (RD-8040-1), which is produced by Lord Corporation [75]. Damping ratio of the MR damper ($\zeta = 0.2$) is evaluated by testing the MR damper in an "off" state to characterize the linear behaviour of the damper. The linear spring and damper are shown in Figure 4.4.

Figure 4.4: Photo of linear spring and MR damper.

The design of the experimental SDOF test rig is shown in Figure 4.5 which enables the damper's nominal compression to be set separately from the spring compression where the damper has the full stroke of 55 mm. The assembly drawing of the designed system is in Figure 4.5-(a), where the damper is connected to a screw thread to be able to move the damper down separately by winding. 112 kg mass will compress the the spring about 15 mm and the maximum nominal stroke of the damper is set to 27.5 mm. The actual system build is shown in Figure 4.5-(b), and excited with different types of base excitation input which are initially, sine waves (to first confirm the system frequency response function (FRF) by comparison) and random broadband displacement excitation.

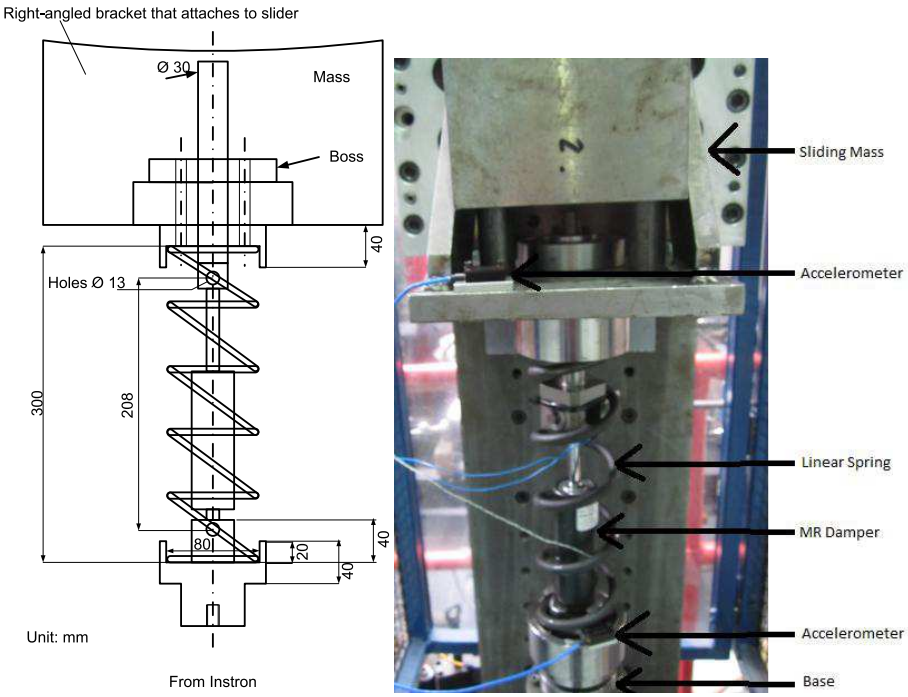

(a) (b)

Figure 4.5: (a) The rig assembly drawing. (b) Real model of the proposed SDOF system.

4.4 Model validations

The proposed linearisation technique was shown to be effective for an ER damper under sinusoidal mechanical excitation [125] and for a commercially available MR damper (RD-1005-3) under non-sinusoidal mechanical excitation [127]. However, the present study was based upon a model of a commercially available brand new MR damper (RD-8040-1). Consequently it was necessary to validate this model under closed-loop conditions with a broadband mechanical excitation and in addition, before this, it is necessary to validate the predicted open loop response of an MR damper with experimental open loop response of this brand new device under sinusoidal excitation.

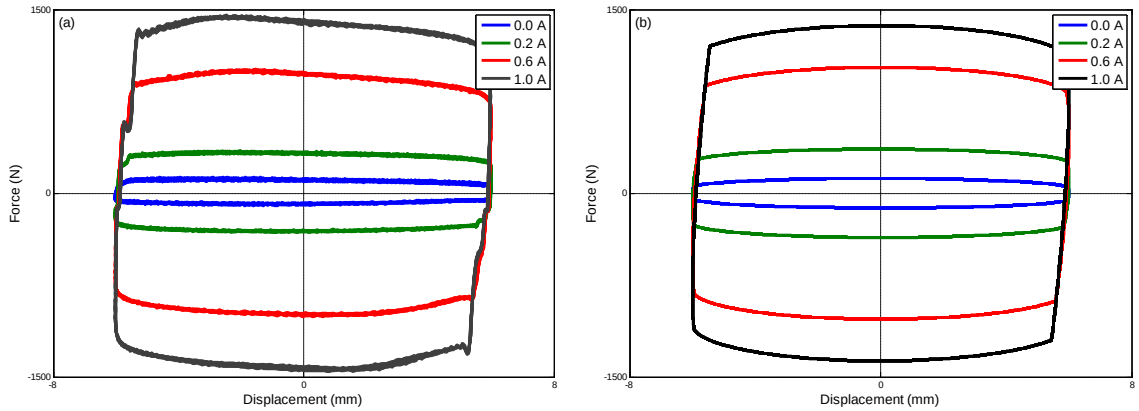

Figure 4.6: Force/displacement characteristic of MR damper. (a) Experimental test, (b) numerical test. 6mm, 2Hz sinusoidal excitation.

To validate the numerical model, the MR damper was mounted in the servo-hydraulic test machine as shown in Figure 4.2. A sinusoidal signal is used to excite MR damper with a chosen constant current to validate the model. For this study, the actual data from test rig has been used, such as actual MR damper force (Instron Load Cell) and actual piston displacement (LVDT sensor). Energy dissipation of the MR damper under constant current are displayed in Figure 4.6 for 6mm 2Hz sinusoidal excitation. Figure 4.6-(a) illustrates experimental data whilst Figure 4.6-(b) shows numerical results under identical conditions. This clearly identifies the increase in energy dissipation with increased current. In order to get a better understanding of the dynamics of the MR damper, the force/velocity characteristic of the MR damper was investigated at constant velocity amplitude, where the frequency and amplitude combination of the sinusoidal signal were chosen to be 2 Hz, 6 mm, 3 Hz, 4 mm, 6 Hz, 2 mm, and 12 Hz, 1 mm. These excitations conditions give a velocity amplitude of approximately 0.08 ms^{-1} which is measured by evaluating by the differential of the displacement signal (LVDT). In addition, the MR damper has driven with varying constant current: 0, 0.2, 0.4, 0.6, 0.8, 1.0 A. Experimental force/velocity characteristics of MR damper have compared with the typical model prediction in Figure 4.7, over a range of excitation conditions. First of all the results displayed in here,

illustrate extremely good agreement between the identified model predictions and the experimental data. However, at lower excitation frequencies the model's pre-yield damping is slightly lower than that observed experimentally. The second observation from these results is the relationship between the piston excitation frequency and the size of the hysteresis loop.

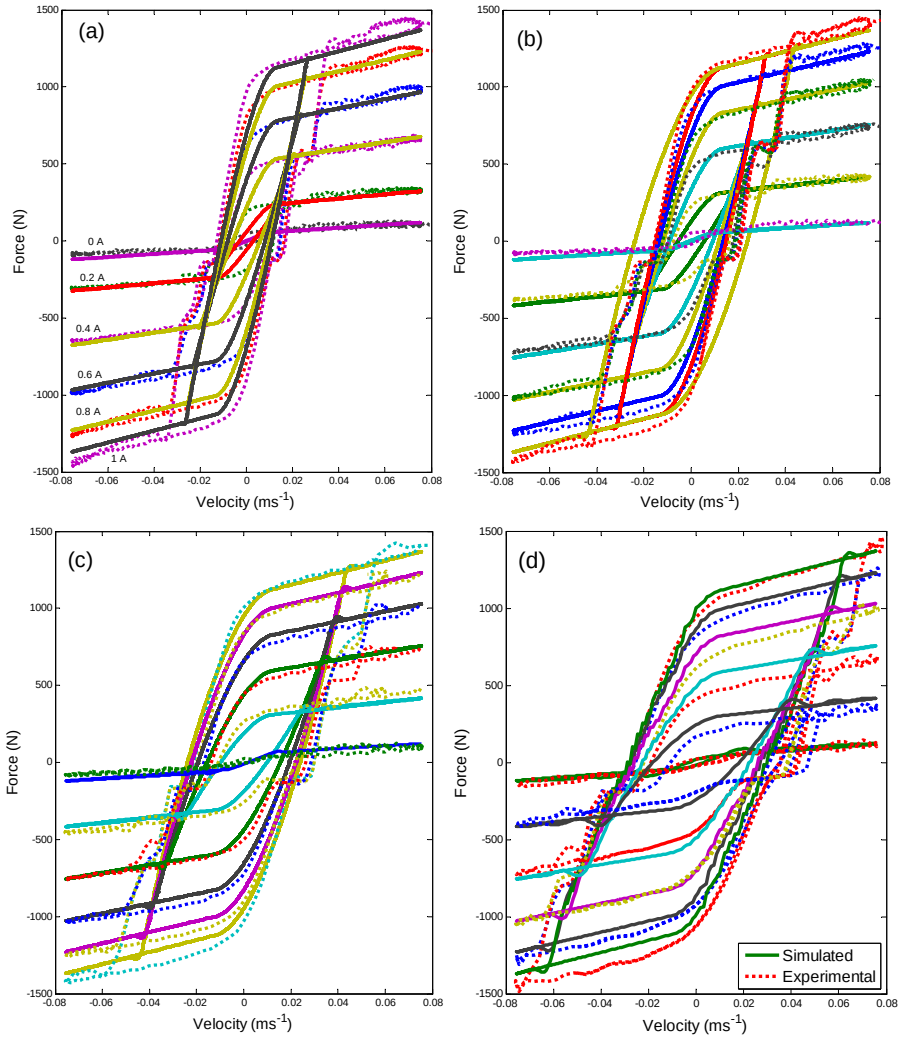

Figure 4.7: Simulated and experimental force/velocity plots of an MR damper; 0,0.2,...1.0A; (a) 2 Hz, 6 mm; (b) 3 Hz, 4 mm; (c) 6 Hz, 2 mm; (d) 12 Hz, 1 mm.

Proposed open loop model validation of MR damper is followed by exciting the MR

damper with a broadband command signal to validate the linearised feedback control of an MR damper. This command signal was generated by filtering a white noise signal to reduce its high frequency content (i.e. above 15Hz) to within the duty of the MR damper as shown in Figure 4.8. At the same time, the feedback linearisation strategy was implemented by using the xPC real-time digital signal processing system (see Figures 4.2). With reference to Figure 3.6, the desired set-point force $F_{desired}$ was chosen to be proportional to the piston velocity such as:

$$F_{desired} = \mathrm{D}V \tag{4.1}$$

Here, V represents the relative velocity of damper and D represents a controller set-point gain. The feedback strategy should result MR damper to emulate the viscous damping behaviour with an effective damping rate equal in value to the controller gain D. Choosing a larger control gain D will cause saturation to the damper force in order to catch the desired set-point force. The values of B and G were previously determined through extensive simulation testing on the MR damper (RD-1005-3), which led to the feedback controller gain B=0.6 N/N, and feedforward controller gain G=0.0015 A/N for the MR damper model [127]. Due to the perfect matching between the numerical (RD-1005-3) and experimental (RD-8040-1) results (see Figures 4.6, and 4.7), these gains are used for the testing of RD-8040-1 MR damper as well.

Figure 4.8 shows a sample of the input displacement signal and Figure 4.9-(a) shows the resulting experimental force/velocity responses for a range of set-point gains, D=1kNs/m, 3kNs/m, and 6 kNs/m. Shown superimposed are straight lines of slope D, which represent the idealised responses. Very good linearisation is demonstrated for values of D between 1kNs/m and 3kNs/m thus validating the controller's behaviour under broadband excita-

tion. For the set-point controller gain D=6kNs/m, the control limits of the MR damper can be observed. For example, the force beyond ± 0.3m/s is less than the ideal viscous force, resulting in a non-linear response (owing to saturation). To validate the model under closed-loop conditions, Figure 4.9-(b) shows the simulated linearised responses under identical excitation and controller conditions as for the experiment. Again, highly linear characteristics can be observed with the actual responses closely matching the ideal responses. In addition, the simulated results match very well with the experiment and the saturation in the response (D=6kNs/m) is predicted accurately.

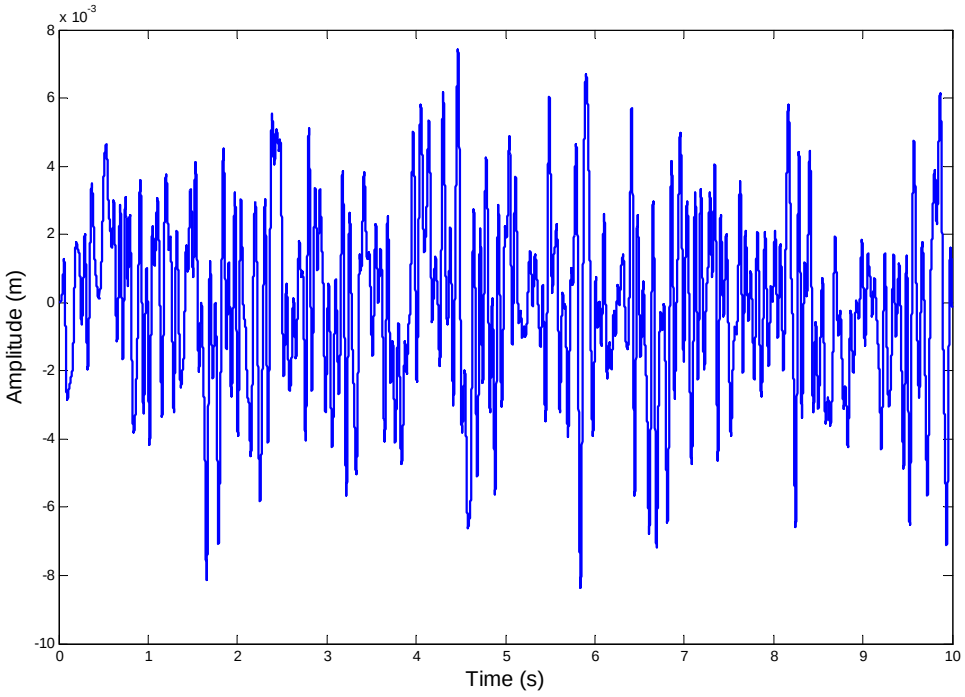

Figure 4.8: Broadband excitation used for experimental validation of feedback linearisation.

This has demonstrated the validation of the predicted model of the brand new MR damper and the proposed linearisation theory, however, still the whole model of the proposed mass isolator system was not validated yet. In order to do so, referring to Figure 4.3 the real

model of the SDOF mass isolator system (see Figure 4.5-(b)) was mounted in the servo-hydraulic, and some preliminarily test were carried out under broadband excitation (Figure 4.8) without any control, ie the MR damper driven with 0A current. The 'Tfestimate' method of the Matlab software was used to evaluate the open loop frequency response of the experimental and the numerical models. These frequency responses were compared in Figure 4.10 with perfect matching. However, at the resonance frequency the experimental system showed slightly higher damping level, which might be due to accumulator stiffness of MR damper is neglected in the numerical model.

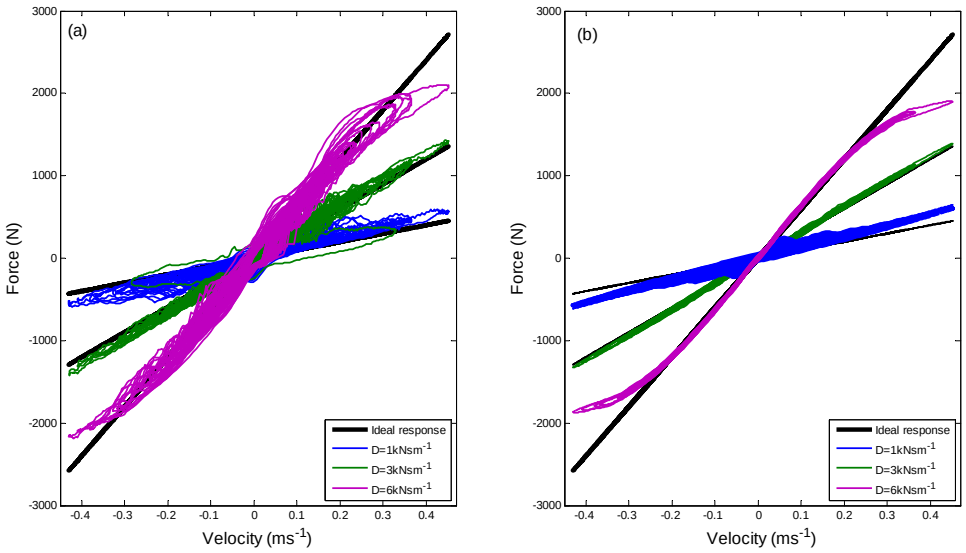

Figure 4.9: Linearised force/velocity responses. (a) experimental and (b) simulated. G=0.0015 and B=0.6.

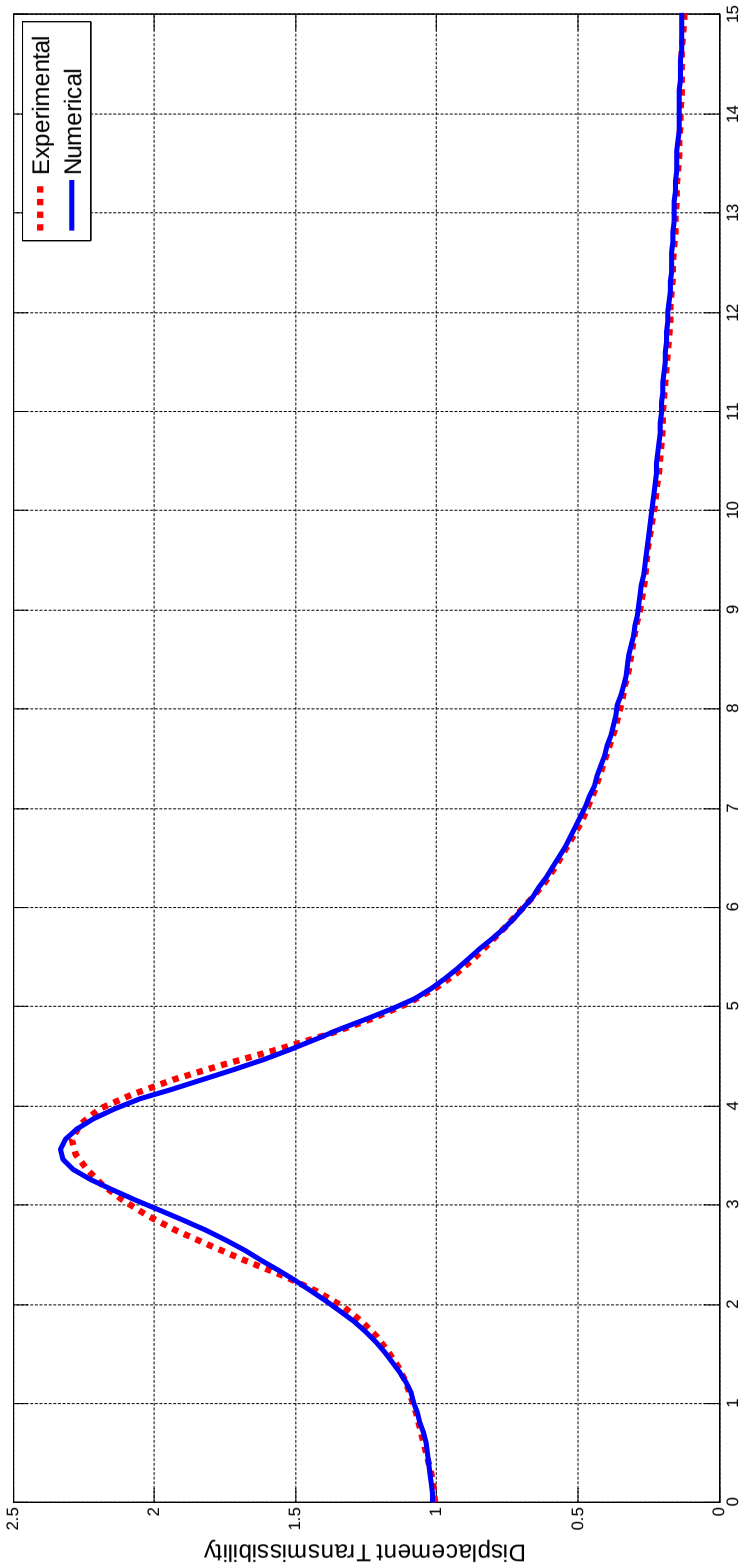

Figure 4.10: Open loop frequency response comparison of SDOF system (m=112 kg, k=63 kN/m, and $\zeta = 0.2$).

4.5 Summary of chapter 4

This chapter has described the design and operation of the MR damper experimental test facility in detail. Preliminary tests were used to validate open loop and closed loop responses of the MR damper device under sinusoidal and broadband random excitations with both constant and linearised control currents. The experimental results show considerable agreement with the predicted model which indicates that the numerical model is feasible. In the next chapter, the proposed observer based linearised control of an MR damper study will be considered by numerical investigation.

5 Numerical investigation

5.1 Introduction

In Chapter 3, the basics of the observer-based control of an MR damper theory (Figure 3.2) was explained by giving a brief theoretical descriptions of each aspects: a unified model of an MR damper; non-linear Luenberger observer; and linearised feedback control. This was followed by the description of the comprehensive experimental test facility and validation of the proposed numerical model in Chapter 4.

Referring to Figure 3.2, the lumped parameter model of the proposed system is illustrated. A schematic block diagram is shown in Figure 5.1. Here, the observer is designed to estimate the system states and damping force (MR damper) by using as base displacement (x_b) and the desired control current (I) system inputs, and mass acceleration ($\ddot{x}_m(t)$) as available output measurements. In practice the base displacement is provided by the measurement of base acceleration (Chapter 6), but it is assumed that for the numerical testing the required base displacement is available as measured data (Figure 5.1). For the experimental testing in the Chapter 6, it will be discussed how to evaluate this base displacement from the measured acceleration. In addition, linearised feedback control of SDOF system is designed as seen in Figure 5.2, which was used to validate the results of the observer based linearised force feedback control of the SDOF system. Here, perfect

knowledge of the damper force and states are assumed.

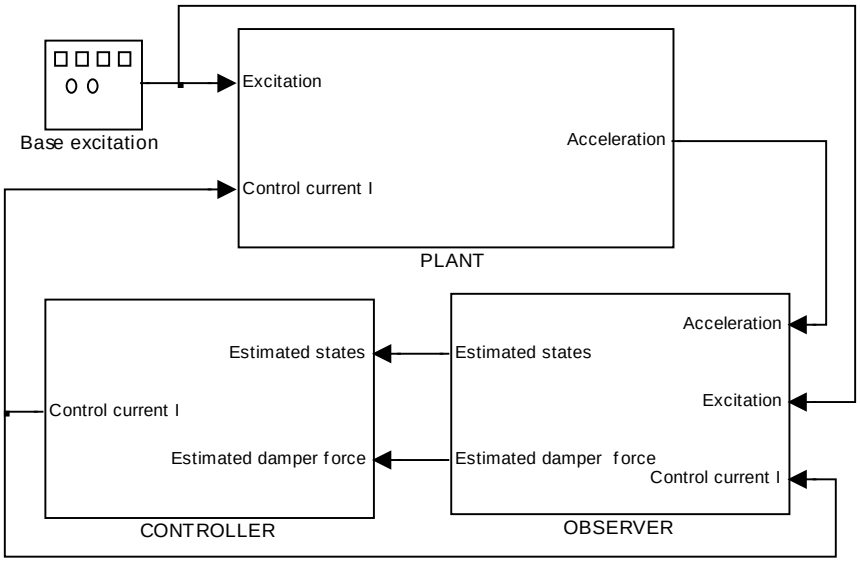

Figure 5.1: Observer-based linearised control of the SDOF system.

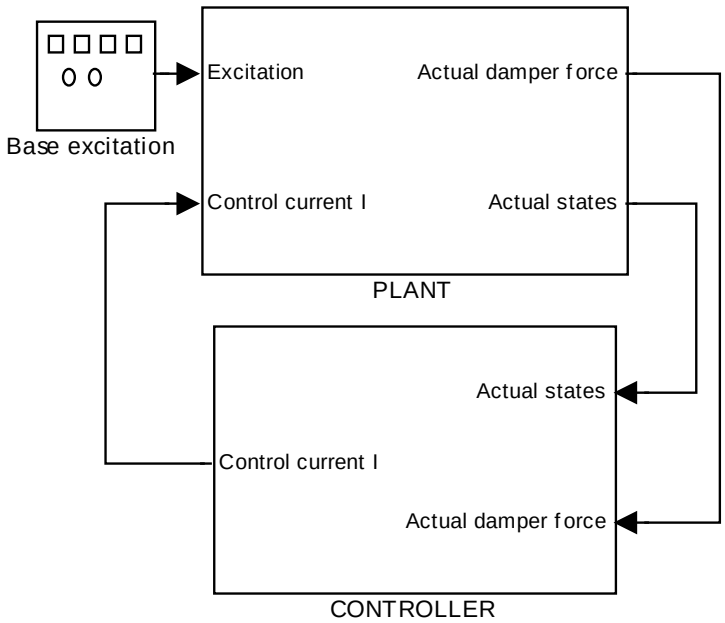

Figure 5.2: Linearised control of the SDOF system.

During the development stage of this research, nine different types of model were pro-

posed to investigate the performance of the observer-based control of SDOF system, which are summarized in Table 5.1. These different types of the SDOF system basically depend on the models of the MR damper used in plant and the observer which will be discussed in detail in the next section. All the models use the same linearised force feedback controller, but the last three models of these were using the actual values (no observer).

However, for conciseness, four of these system (last column of Table 5.1) are presented in this thesis. For these scenarios, the unified model of the MR damper is used to design the plant due to the excellent validation of the numerical unified model with the experimental model (Chapter 4).

The present chapter begins by performing numerical investigation of the observer-based control of SDOF system subject to sinusoidal and broadband random excitation. The same system parameters are used for this study as in section 4.3. Sky-hook based controllers will be used to illustrate the effectiveness of observer based feedback linearisation. These are compared against observer based on-off and linearised optimal control schemes as well idealised passive, semi-active and fully active dampers.

The present chapter is organised as follows. First the basics of observer based SDOF system are discussed by describing three possible models of an MR damper. Regarding these MR damper models, proper linearised control schemes and observers models are designed. Next, passive control, observer-based semi-active sky-hook, observer-based on/off, observer-based optimal control, and observer-based fully active control are explained before presenting the corresponding results. Finally, discussion and conclusion are drawn. Some parts of the research described in this chapter were presented at the Eur-

oMech Colloquium 530: Structural Control and Energy Harvesting conference in Bristol, United Kingdom [152], and at the 10th World Congress On Computational Mechanics (WCCM 2012) conference in São Paulo, Brazil [153].

		MR MODELS IN PLANT			
		BASIC	COMPLEX	UNIFIED	
MR MODELS IN OBSERVER	BASIC	X	X	X	LINEARISED FORCE FEEDBACK CONTROLLER
	COMPLEX		X	X	
	UNIFIED			X	
NO OBSERVER		X	X	X	

Table 5.1: Observer base linearised force feedback control of SDOF system models.

5.2 Numerical modelling

In this numerical modelling section, to get a better understanding of proposed system the detailed description of each parts (MR damper, non-linear observer, controller) will be given which were briefly discussed in the theory chapter.

5.2.1 MR damper Modelling

In reality the MR damper has highly non linear characteristics, and so a non-linear model of the MR damper is necessary. In this section three different non-linear models of the MR damper will be investigated. These will be referred to as the 'basic', 'complex', and

'unified' MR damper models.

Referring to Figure 2.6-(a), the simplest model of a smart damper is a parallel summation of viscous and the Coulomb friction elements. This is known as the Bingham plastic model [77]. The resulting equation of motion is

$$F_d = F_{fr} sgn(V) + c_p V \tag{5.1}$$

where F_{fr} is friction force, c_p is the viscous coefficient and V is the piston velocity.

The simulated model designed according to Equation 5.1 is displayed in Figure 5.3 below.

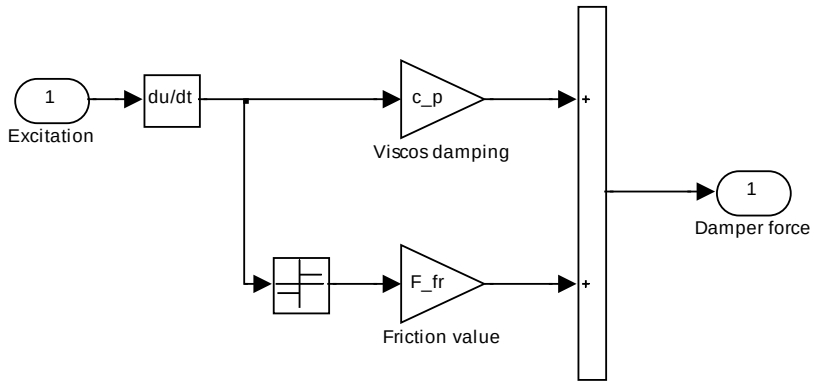

Figure 5.3: Non-linear basic MR damper model (coulomb and viscous element).

The basic model of an MR damper enables good progress for developing the observer while simplifying the parameters. But as discussed by Gamota and Filisko [78], this basic two-parameter model is not able to observe the viscoelastic response which is clearly observed in the pre-yield region without an elastic element. In order to model this non-linear behaviour of the MR damper, a complex model of MR damper is developed based

partly on the unified model [85] (Figure 3.3). However, the damping function (quasi-steady valve flow) for the complex MR model was obtained by solving equation 5.2:

$$\chi(\dot{x}_1, F_{fr}) = F_{fr} sgn(\dot{x}_1) + c\dot{x}_1 \tag{5.2}$$

where the equation of motion becomes

$$k(x_2 - x_1) - \chi(\dot{x}_1, F_{fr}) = m_1 \ddot{x}_1 \tag{5.3}$$

The force produced by the damper F_d is;

$$F_d = k(x_2 - x_1) \tag{5.4}$$

Where k represents the fluid compressibility, m_1 is fluid inertia, $\dot{x}_1$ is the quasi-steady velocity, x_2 is displacement motion of the piston, and χ is the quasi-steady valve flow (non-linear equation).

The complex MR damper model becomes;

$$k(x_2 - x_1) - F_{fr} sgn(\dot{x}_1) - c\dot{x}_1 = m_1 \ddot{x}_1 \tag{5.5}$$

where the acceleration is:

$$\ddot{x}_1 = \frac{k}{m_1}(x_2 - x_1) - \frac{F_{fr}}{m_1} sgn(\dot{x}_1) - \frac{c}{m_1}\dot{x}_1 \tag{5.6}$$

The simulated model of Equation 5.6 is shown in Figure 5.4.

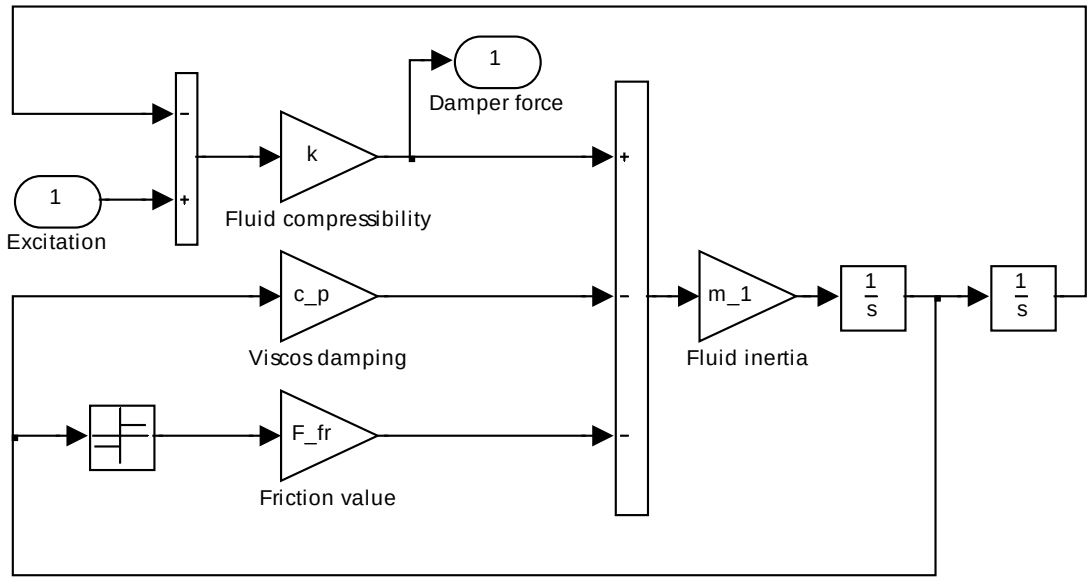

Figure 5.4: Non-linear complex MR damper model (coulomb friction, viscous, fluid inertia and fluid compressibility).

This complex model has got a little difference from the unified model, where the quasi-steady valve flow is formulated. The complex model defines it as a function of quasi-steady velocity ($\dot{x}_1$) and the control friction force (F_{fr}), (Equation 5.2) while the unified model defines its as a function of quasi-steady velocity ($\dot{x}$) and control current (I) applied to the damper as seen in Equation 5.7. It is worthwhile to investigate the dynamic performance comparison of these two approaches. The unified model uses a bi-viscous model to define the quasi steady valve flow.

$$\chi(\dot{x}_1, I) = \begin{cases} C_{pre}\dot{x}_1 & |\dot{x}_1| \leq F_y/C_{pre} \\ C_{post}\dot{x}_1 + F_y sgn(\dot{x}_1) & |\dot{x}_1| > F_y/C_{pre}. \end{cases} \tag{5.7}$$

Where,

$$\begin{aligned} F_y &= -0.0115 + 1.3063 tanh(1.1946I) \\ C_{post} &= 0.6167 + 3.7383 tanh(1.3629I) \\ C_{pre} &= 4.1357 + 99.4736 tanh(1.0697I) \end{aligned} \tag{5.8}$$

These values are separately calculated by curve fitting techniques [85]. The simulation of the unified model is displayed in Figure 5.5 which is designed based on Equation 5.9.

$$k(x_2 - x_1) - \chi(\dot{x}_1, I) = m_1\ddot{x}_1 \tag{5.9}$$

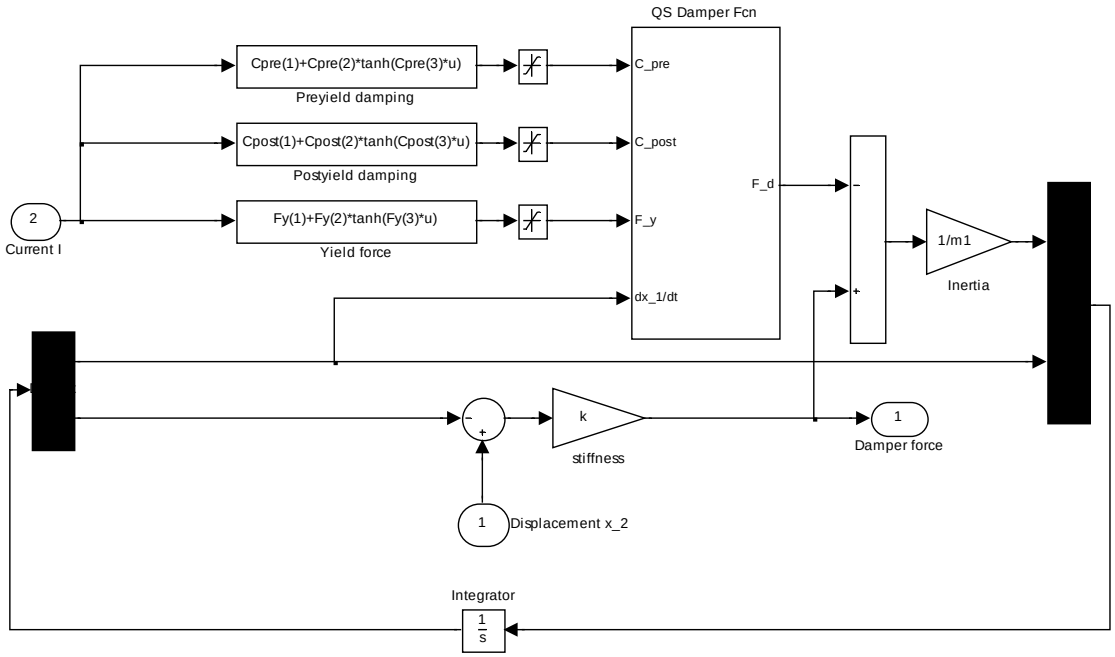

Figure 5.5: Non-linear unified MR damper model [85].

Until now the non-linear modelling of the MR damper is discussed. Although, in this section numerical models of basic, complex, and unified models are evaluated, as indicated before the unified model will be used for analytical and experimental investigation of the proposed theory. The next section will model non-linear observers considering these three MR damper models. Proper design of the linearised force feedback control strategies will also be developed to make MR the damper, behave as a semi-active force generator.

5.2.2 Modelling of Force Feedback Linearisation

In Chapter 3 the proposed feedback linearisation control was explained (see Figure 3.6), which was developed for the unified model of an MR damper. However, replacing the unified MR damper with basic or complex MR damper, the control algorithm has to be modified. Referring to Figure 5.6-(b), the input of MR damper is the control current (I), but for the basic and complex MR model the input is the friction force (F_{fr}). This new

modified linearised control scheme is illustrated in Figure 5.6-(a).

Here, feedback control is being used to implement a semi-active force generator. The proposed control system uses measurement of the damper force to linearise the non-linear damping behaviour. Essentially, the controller gains B and G can be tuned so that the actual force closely matches the set point force. In Figure 5.6, this desired set-point force is chosen to be proportional to piston velocity, so that the MR damper behaves as a linear viscous device.

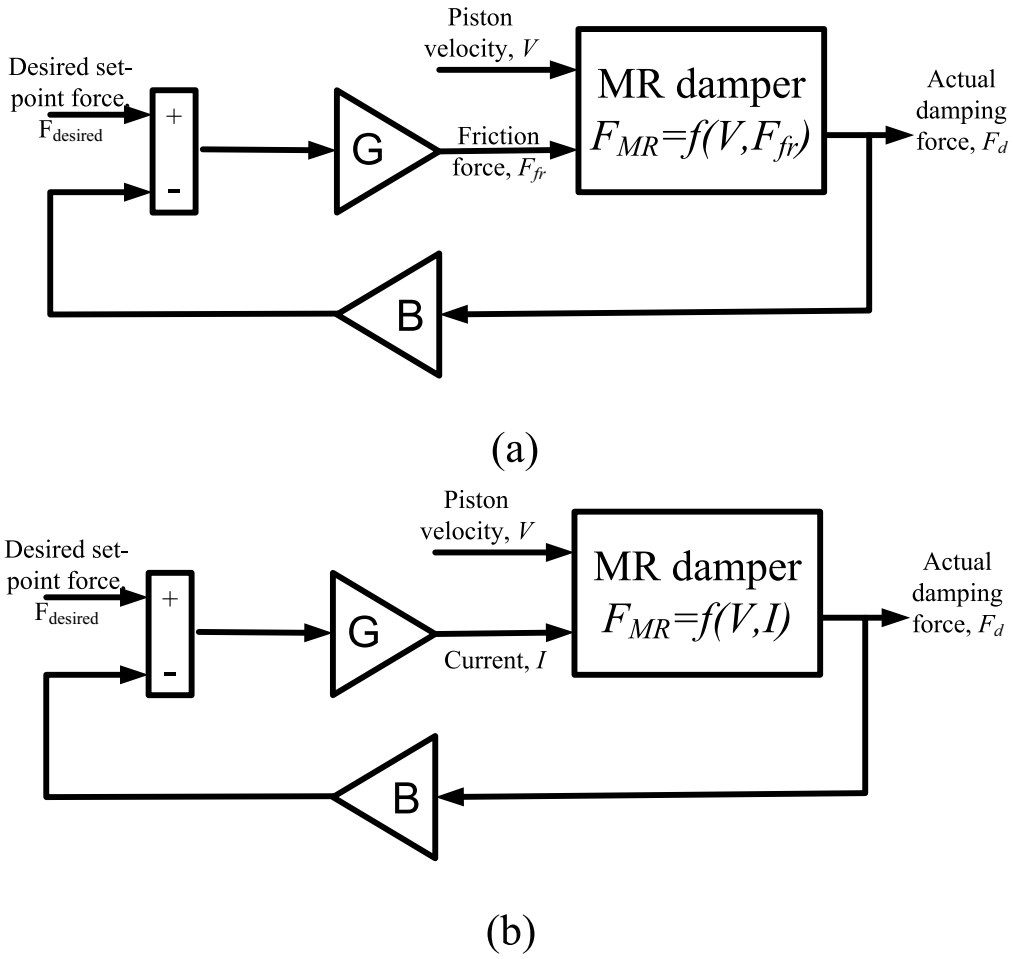

Figure 5.6: Models of force-feedback linearisation control; (a) Friction control model; (b) Current control model.

The values of B and G (B=0.6 N/N and G=0.0015 A/N) for the current control model

were presented in Chapter 4. These values are required to be modified for the friction control model, These are determined through extensive simulation testing on the MR damper, which led to the feedback controller gain B=0.6 N/N and the feedforward gain G=0.925 N/N. It is clear that, the both of the control model linearise the non-linearity of the damper with same feedback gain while the feedforward gain alters. This alteration implies the direct relationship between the desired control current and the desired friction force. This identity will be used to create the observer-based control model where the plant and observer uses the different MR damper model in the next section.

5.2.3 Observer Design For SDOF System

Referring to Equation 3.12, a linear observer model was designed (Figure 3.4) and this was extended to the non-linear observer model (Figure 3.5). By substituting the non-linear MR damper with the 'basic', 'complex' and 'unified' models of MR damper in Figure 3.4, three types of non-linear observer is created. Having validated the unified model as a true representation of the system's response (Chapter 4), afterwards this model will be used to design the plant of the system. The proposed three observer are shown in Figure 5.7 (basic MR model for observer), Figure 5.8 (complex MR model for observer), and Figure 5.9 (unified MR model for observer). The linearised feedback controller (current control model) is used to generate the desired control current (see 5.6-(b)), but which is converted to the friction force by the Current-Friction gain (I_FR) in case of basic observer or complex observer (Figures 5.7, and 5.8) is used. This gain is evaluated by using the direct relationship between the desired control current and the desired friction force as described previously. The I_FR gain is determined through extensive simulation testing of observer-based control system, which led to the Current-Friction, I_FR=1200 N/A.

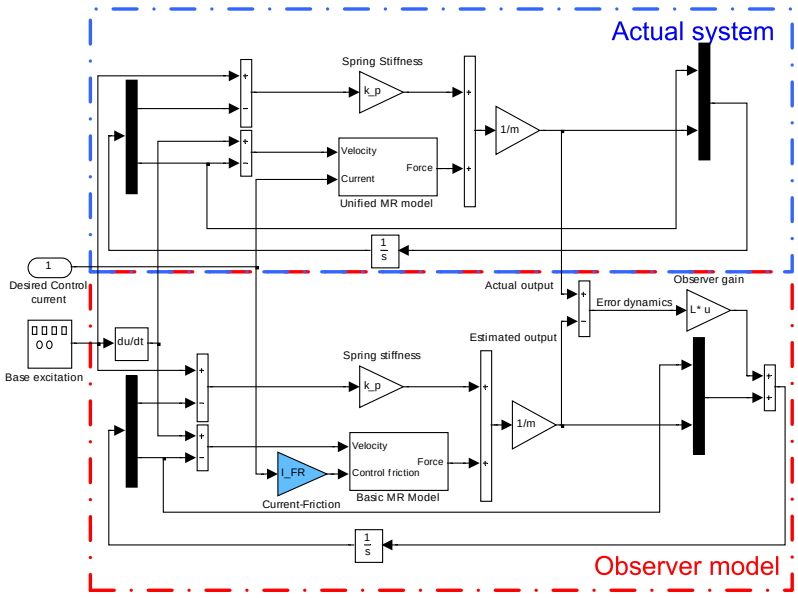

Figure 5.7: Simulated model of observer for SDOF mass isolation system (plant is designed with unified model of the MR damper while the observer is designed with the basic model of the MR damper).

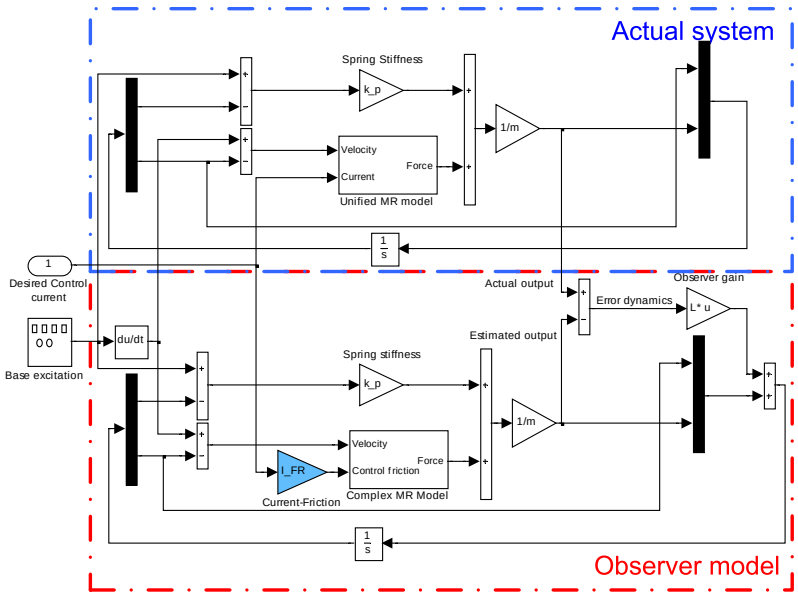

Figure 5.8: Simulated model of observer for SDOF mass isolation system (plant is designed with unified model of the MR damper while the observer is designed with the complex model of the MR damper).

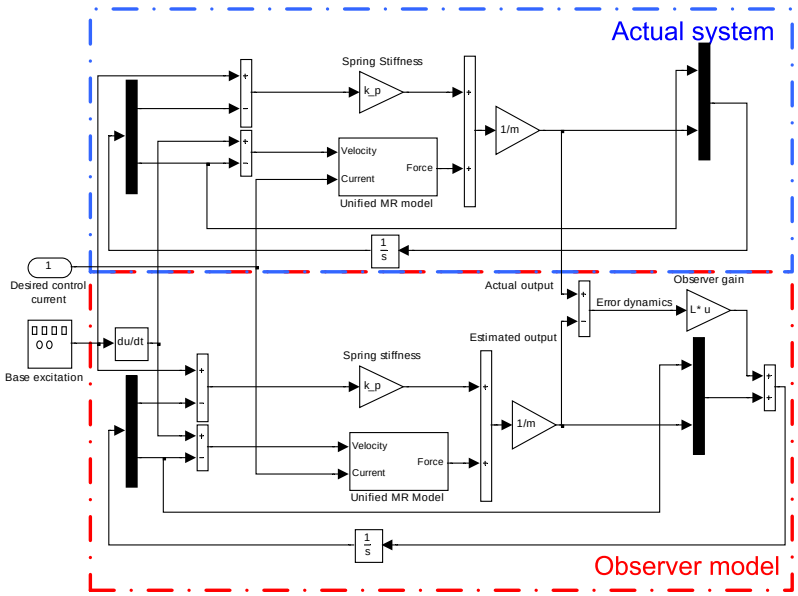

Figure 5.9: Simulated model of observer for SDOF mass isolation system (plant and observer are designed with unified model of the MR damper).

The key point of the observer design step is the decision of the observer gain matrix. In Chapter 3 it has been discussed that regarding to [154], for acceptable estimation of the states, the dynamic of the observer model has to be faster than the dynamics of the controller. The control force is generated by the MR damper, and because of the unmodelled friction inside the MR damper, the dynamics of the MR controller is already slower than the dynamics of a linear system. In other words, choosing the dynamics of the observer faster than the linear model will forward the poles of the observer far away from the poles of the controller (on the left side of the imaginary axis), which will cause an unwanted saturation of the estimated values [154]. In order to avoid this problem (referring to text book [154]), the observer gain matrix is chosen to be a little bit slower than the dynamics of the linear system so, it is going to be enough faster than the dynamics of the controller. By using the pole placement method the dynamics of the observer was chosen to be 25 percent slower than the actual passive system. In addition, different gains could be chosen based on system requirements, so this is not the best one.

$$L = \begin{bmatrix} -0.0060 \\ 0.4375 \end{bmatrix}$$

5.2.4 Numerical modelling results

The performance analysis of the proposed non-linear observer system is started by comparing the estimated states of the non-linear observer ($\dot{\hat{x}}_m$, $\hat{x}_m$) with the actual system states ($\dot{x}_m$, x_m). Linear observer models for the SDOF system have excellent performance for estimating the unmeasured states of the system. However, for the non-linear observer, when the friction value inside the damper is unknown or unmeasurable, the estimated values for the velocity and displacement seem to have small errors.

To get a better understanding of the non-linear performance of the observer the test system was designed such that the actual system (unified MR model) and observer (complex MR model) were modelled with a different model to allow investigation of model mismatching between the actual and observer system. Sinusoidal displacement excitation was used to excite the system. The unified model was driven with constant current levels of 0A, 0.4A and 1A, referring to paper [85] these reflect the coulomb friction levels of 65N, 500N, and 1000N which were used to drive the complex model as well. The results are displayed in Figure 5.10 and 5.11, where the excitation frequencies were chosen around the system natural frequency.

Comparison of the estimated and actual displacement of the mass (x_m, and $\hat{x}_m$) are displayed in Figure 5.10, while the estimated and actual velocities ($\dot{x}_m$, and $\dot{\hat{x}}_m$) are shown in Figure 5.11. These two figures clearly illustrates that if the friction value inside the MR damper is known and applied to the observer model as well then the estimated values are

matching almost perfectly to the actual values.

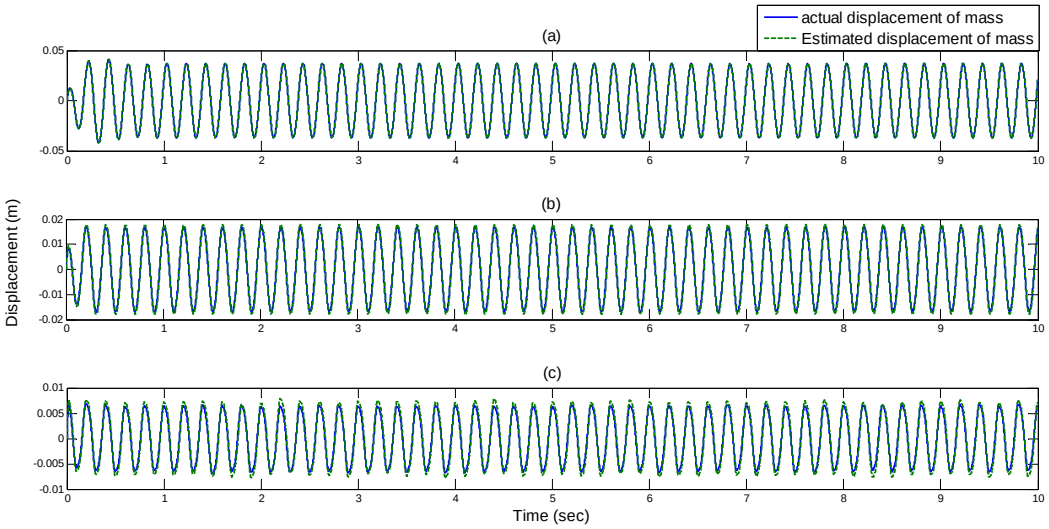

Figure 5.10: Comparison of estimated and actual mass displacement for 5 Hz, 20 mm sinusoidal base displacement. (a) 0A current, and 65N coulomb friction, (b) 0.4A current, and 500N coulomb friction, and (c) 1A current, and 1000N coulomb friction.

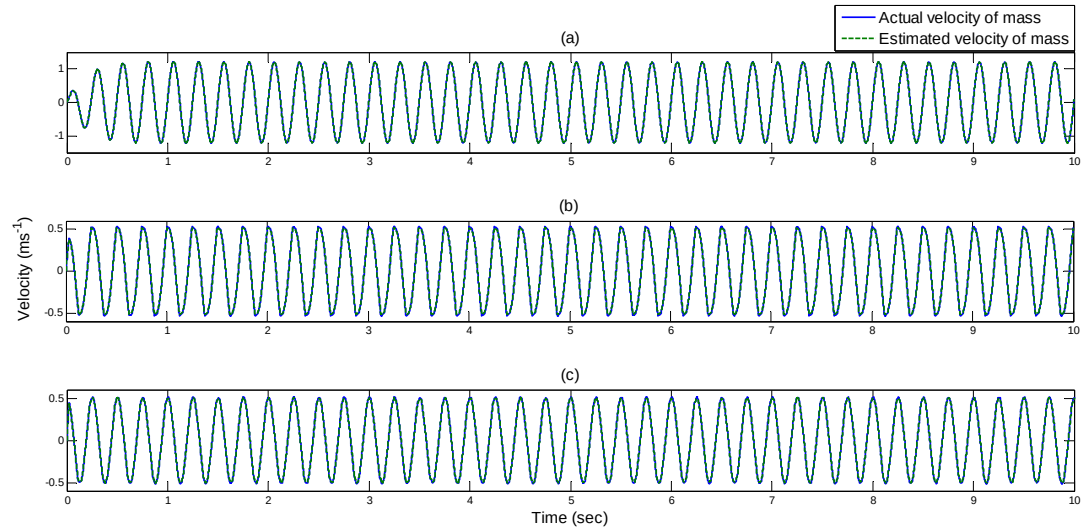

Figure 5.11: Comparison of estimated and actual velocity of mass for 4 Hz, 20 mm sinusoidal base displacement. (a) 0A current, and 65N coulomb friction, (b) 0.4A current, and 500N coulomb friction, and (c) 1A current, and 1000N coulomb friction.

Having made sure that the non-linear observer is able to estimate the velocity and displacement of the actual system as expected, the closed loop dynamical response of the three MR damper models (basic, complex, and unified) is now investigated under sinusoidal excitation. This step was carried out by applying the linearised force feedback algorithm to the each of the MR damper models so that the force produced by the MR dampers will be linearised.

Figure 5.12 illustrates simulated performance of the SDOF system with feedback linearisation based upon the actual damping force[1]. As expected, the damper's force-velocity behaviour emulates that of a linear viscous device with tunable damping rate (D).

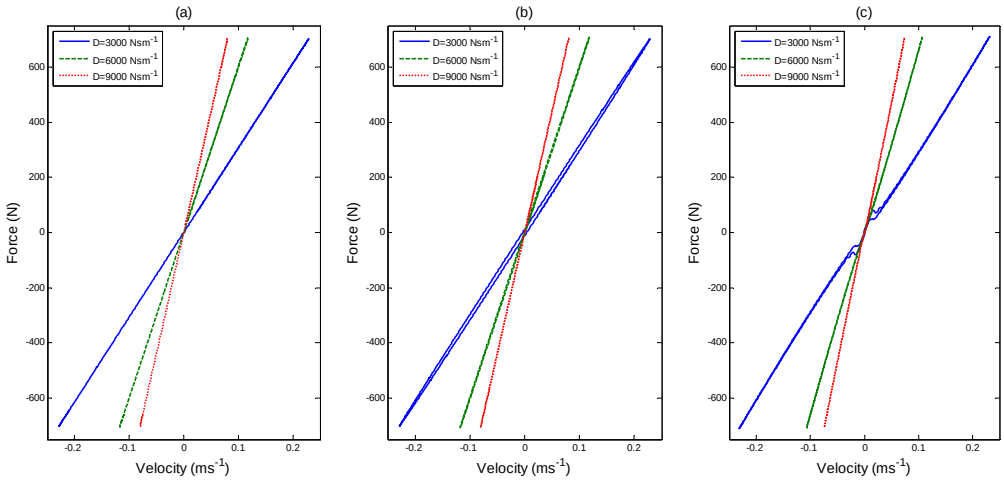

Figure 5.12: Force-velocity graphs of the different MR damper models for force feedback linearised control of SDOF system; (a) basic MR model; (b) complex MR model; (c) unified MR model. System was excited with 10 mm, 4 Hz sinusoidal.

These results are repeated in Figure 5.13, where the feedback force signal is obtained using the observer based control approach. Here, the linearised force feedback control (current control mode) is implemented for each test to generate the desired control current.

[1]Systems have no observer, i.e. perfect knowledge of the damper force is assumed.

The desired control current is converted to the desired friction force for basic and complex model as explained previously in subsection 5.2.3. As seen from Figure 5.13 around the origin the linearisation of the force velocity plots seems to have slightly unexpected behaviour, except 5.13-(c). This happens at the pre-yield region where the velocity of the piston due to change from positive to negative. After several investigation it is found that this problem is related to the fluid inertia. When the sign of the piston velocity changes from positive to negative the velocity of the fluid inertia causes oscillation. One of the solutions to this problem could be the decreasing the fluid inertia to lower the effective mass. Also it is seen from Figure 5.13-(c) this unexpected behaviour seems to have disappeared. This is because the MR models are the same for the observer and actual system.

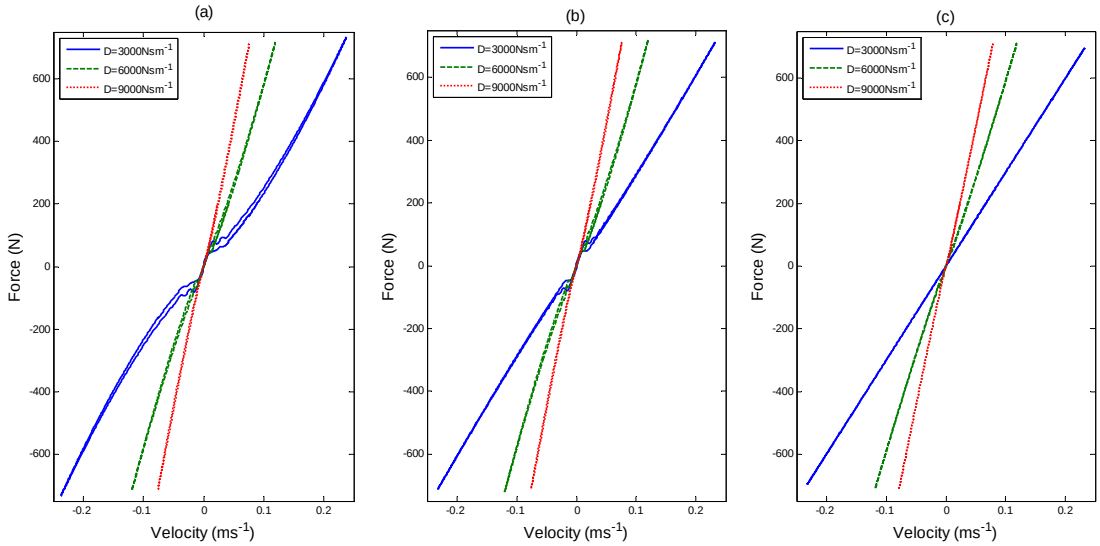

Figure 5.13: Force-velocity graphs of the different MR damper models for observer base linearised control of SDOF system; (a) basic MR observer; (b) complex MR observer; (c) Unified MR observer. System was excited with 10 mm, 4 Hz sinusoidal.

In Figure 5.14, the observed frequency responses of the three different observer-based control system are compared with the frequency response of the actual system (unified

MR model) under the sinusoidal base excitation with frequency range of 0 Hz to 15 Hz. The Figure 5.14-(a) and Figure 5.14-(b) illustrate slightly higher response around the resonance and slightly lower response at the high frequency level. This is due to mismatch between the models of the plant and observer, which cause the observer to underestimate or overestimate the damping level. It is clear that, this problem disappeared in Figure 5.14-(c). This result explains that, if there are discrepancies in system matrices (A, B, and C) in the observer and actual system, the observer is no longer able to estimate the states properly [154].

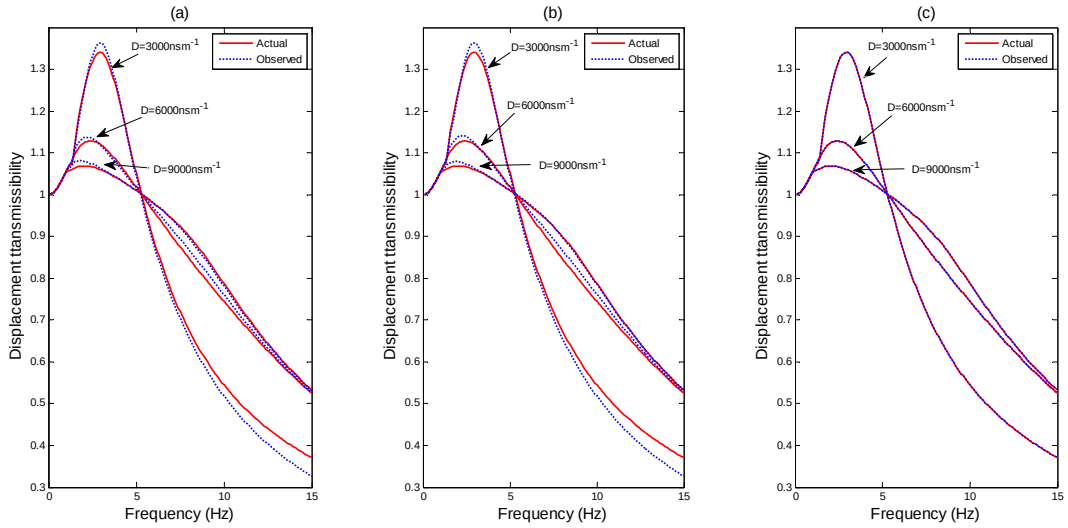

Figure 5.14: Comparison of the displacement transmissibilities of actual system (Figure 5.1) and observer-based systems (Figure 5.2); (a) unified MR model for actual and basic MR model for observer; (b) unified MR model for actual and complex MR model for observer; (c) unified MR model for actual and unified MR model for observer.

5.3 Control Theories

In this section, referring to Figure 3.2, control concepts for proposed observer based control of an MR damper are discussed. Mainly, seven different damper configurations were investigated and these are summarised in Table 5.2. This will now be explained in detail.

Control law	Control strategy	Actual Model
Passive	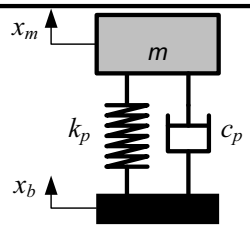	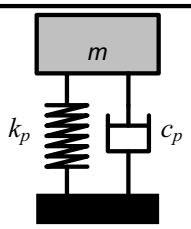
MR linearised feedback	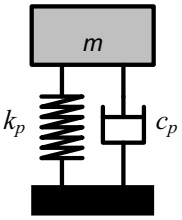	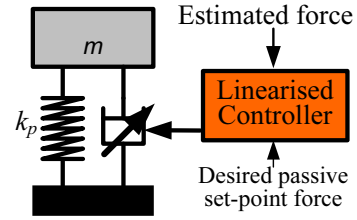
MR linearised sky-hook	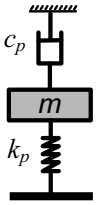	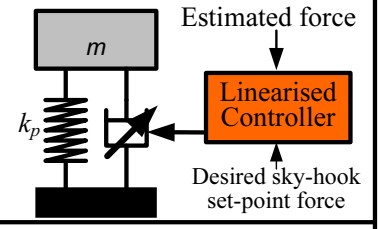
MR linearised optimal	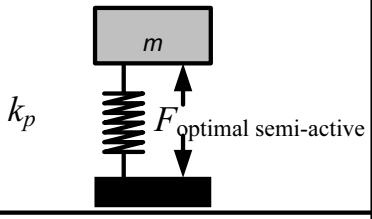	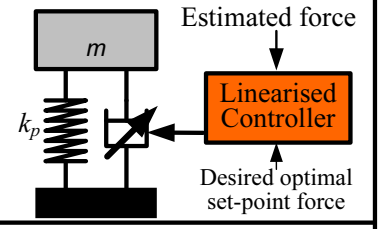
On-Off sky-hook	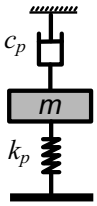	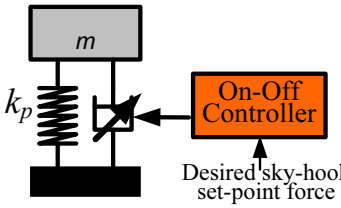
Fully active sky-hook	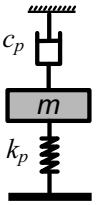	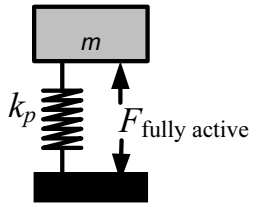
Ideal semi-active sky-hook	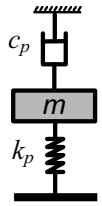	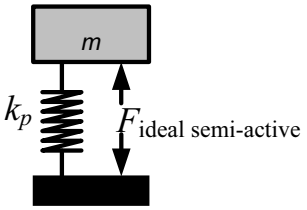

Table 5.2: Implementation of control theories for SDOF system.

5.3.1 Passive system

As shown in Table 5.2-(second row), instead of using the MR damper in its "on" or "off" state to create a passive system, a more realistic viscous damper is used to generate damping force in the present study;

$$F_d = c_p \dot{x}_r \tag{5.10}$$

where the relative velocity is $\dot{x}_r = (\dot{x}_m - \dot{x}_b)$, and c_p is viscous damping coefficient. The simulated model of passive system is shown in Figure 5.15.

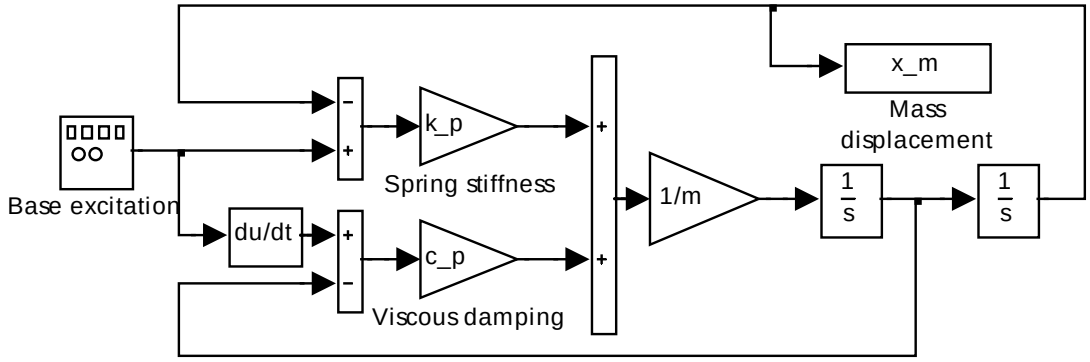

Figure 5.15: Simulated model of single degree of freedom system (viscous damping).

5.3.2 Observer based MR linearised feedback control

This technique linearises the non-linear dynamics of the MR damper and makes it to behave as a linear viscous damper with a linear damping rates. To achieve this, feedback linearisation uses the desired set point force to the semi active force generator that is proportional to the relative velocity between mass and base of the SDOF system. Implementation of MR linearised control algorithm requires the relative velocity of the SDOF system and MR damper force which were estimated by the observer. With reference to Table 5.2-(third row); estimated desired set-point force is given by;

$$F_{desired} = \mathrm{D}\dot{\hat{x}}_r \tag{5.11}$$

where the estimated relative velocity is $\dot{\hat{x}}_r = (\dot{\hat{x}}_m - \dot{x}_b)$.

The simulated model of the observer based linearised MR control is shown in Figure 5.16.

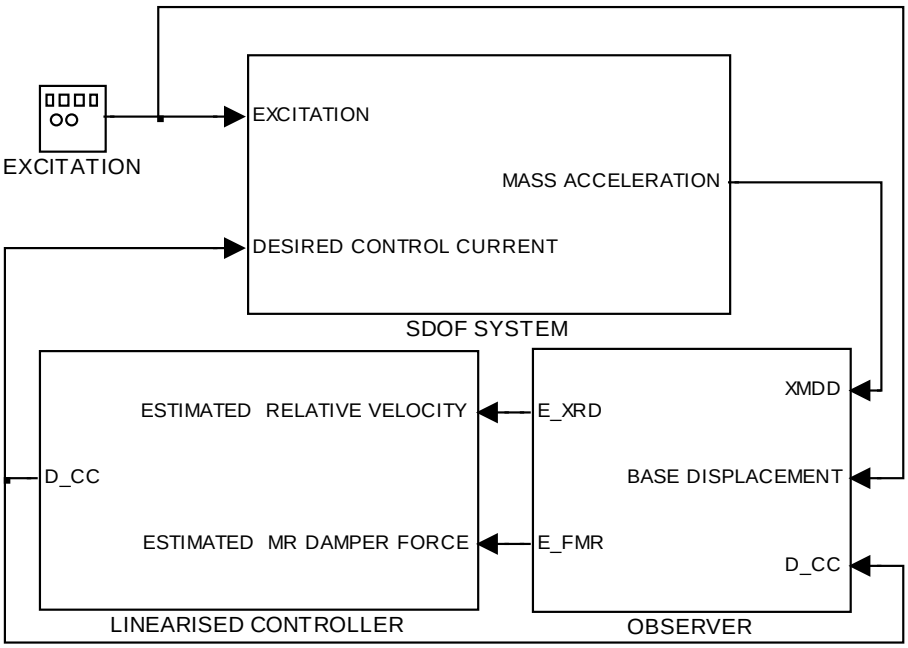

Figure 5.16: Simulation of observer based linearised MR damper control model.

5.3.3 Observer based MR linearised sky-hook control

Sky-hook control is the optimal for an SDOF isolation system and enables resonant vibrations to be suppressed without any performance reduction of the higher frequency response. The sky-hook control concepts are where the damping force is proportional to the absolute velocity of the isolated mass. This absolute velocity of the isolated mass

will be estimated by the observer while also estimating the damper force for feedback linearisation. Although sky-hook control requires an energy input under certain conditions, feedback linearisation can be utilised to accurately achieve the sky-hook force within the semi-active limits of the MR damper as seen in Figure 3.7. Referring to Table 5.2-(fourth row), the desired set-point force is given by;

$$F_{desired} = \mathrm{D_{MR}}\dot{\hat{x}}_m \tag{5.12}$$

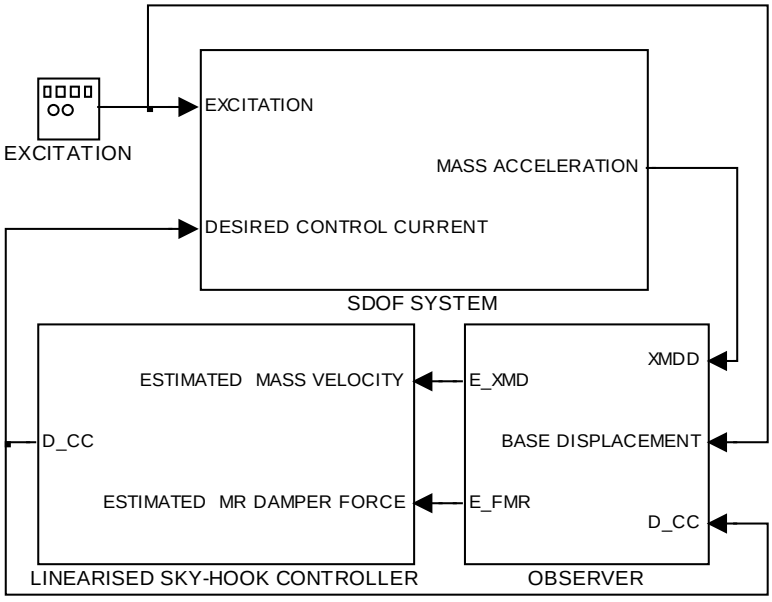

Figure 5.17: Simulated model of observer based MR linearised sky-hook control of SDOF system.

Implementation of the MR linearised sky-hook needs the absolute velocity of mass and MR damper force which were estimated by the observer as seen in Figure 5.17.

5.3.4 Observer based MR linearised optimal control

In this study, to improve the performance of the system, the desired set point force is chosen to be the optimal control force. The implementation of the optimal control theory requires the measurement of the system states which are the absolute displacement and velocity of the mass as shown in Figure 5.18. These states are provided by the observer as well.

Observer based MR linearised optimal control approach uses a force-feedback loop to induce the MR damper to produce approximately a desired control force $F_{desired}$. In order to achieve $F_{desired}$, a linear optimal control gain K is then designed based on the measured states. This optimal control force is not possible to be achieved by the MR damper in active region where the energy is injected to the system by the force generator. Due to this passivity limitation of the MR damper, the set point force is set to zero at the active region, by checking the product of the estimated damper force and the estimated piston velocity. This has to be positive to satisfy the passivity theory of Karnopp [16]. The desired optimal control force is designed referring to Table 5.2-(fifth row);

$$F_{desired} = \left\{ \begin{array}{cc} \mathrm{K} \begin{bmatrix} \hat{x}_m \\ \dot{\hat{x}}_m \end{bmatrix} & \dot{\hat{x}}_m(\dot{\hat{x}}_m - \dot{x}_b) > 0 \\ 0 & \dot{\hat{x}}_m(\dot{\hat{x}}_m - \dot{x}_b) \leq 0 \end{array} \right\} \tag{5.13}$$

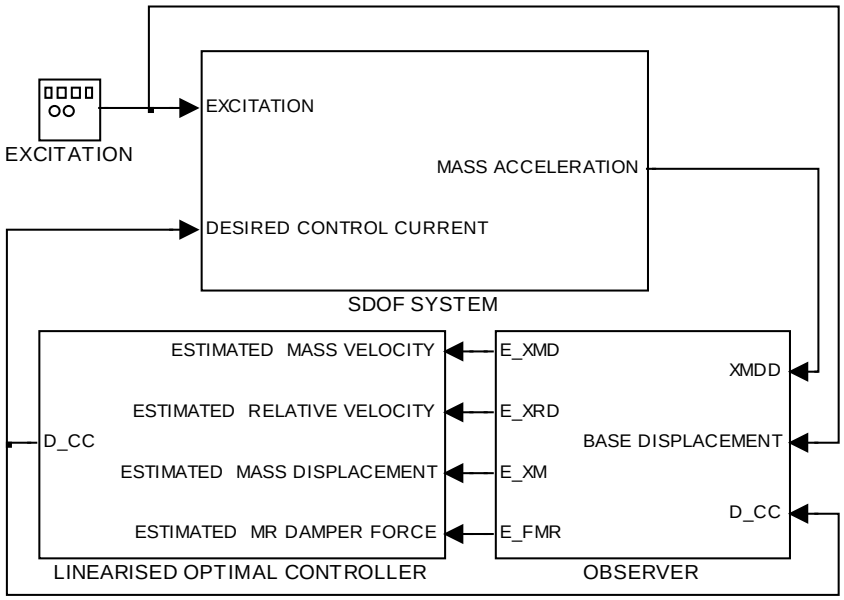

Figure 5.18: Simulated model of observer based linearised optimal control of SDOF system.

The optimal gain K is obtained by the LQR strategies because of their successful application in other engineering structural control applications [155, 90, 156]. The matrix K is the full state feedback gain for deterministic regulator problem given by [157];

$$K = B^{'}P/R \tag{5.14}$$

Here P is the solution of the algebraic Ricatti equation given by

$$0 = PA + A^{'}P - PB^{'}BP/R + C^{'}QC \tag{5.15}$$

Here Q and R weighting matrices minimize the performance index;

$$J = \int_0^\infty (\underline{x} Q \underline{x}' + F_d' R F_d) dt \tag{5.16}$$

After several numerical investigations the best values of the weighting matrices are found as, $Q = \begin{bmatrix} 1 & 0 \\ 0 & 1 \end{bmatrix}$, and $R = 10^{-7.5}$. A block diagram of this semi-active control system is shown in Figure 5.18.

- Results of passive and MR linearised control theories

The performance of the passive control and MR linearised control theories (MR linearised feedback, MR linearised sky-hook, and MR linearised optimal) was investigated under the broadband random base excitation. The random displacement signal was produced by passing the white noise signal to the low pass butter-worth filter with 15 Hz cut off frequency. In the case of MR linearised control scenarios, the actual and the observer systems were designed with the unified MR damper model, and the linearised feedback controller (current control mode, see Figure 5.6-(b)) was used to generate the desired control force. The frequency responses of the system for different controller gains are compared. In order to obtain the frequency response the tfestimate method is used.

First, the passive control system is compared with the observer-based MR linearised control where the MR damper replaces the linear viscous damper, which is shown in Figure 5.19. Both of the system is able to reduce the resonance frequency response with a little degradation in the high frequency response with increased control gain. Also, observer-based MR linearised system exhibits quite good matching with the passive system, which indicates that the proposed observer is able to estimate the state properly, and that by im-

plementing linearised feedback control the MR damper can emulate the passive damper.

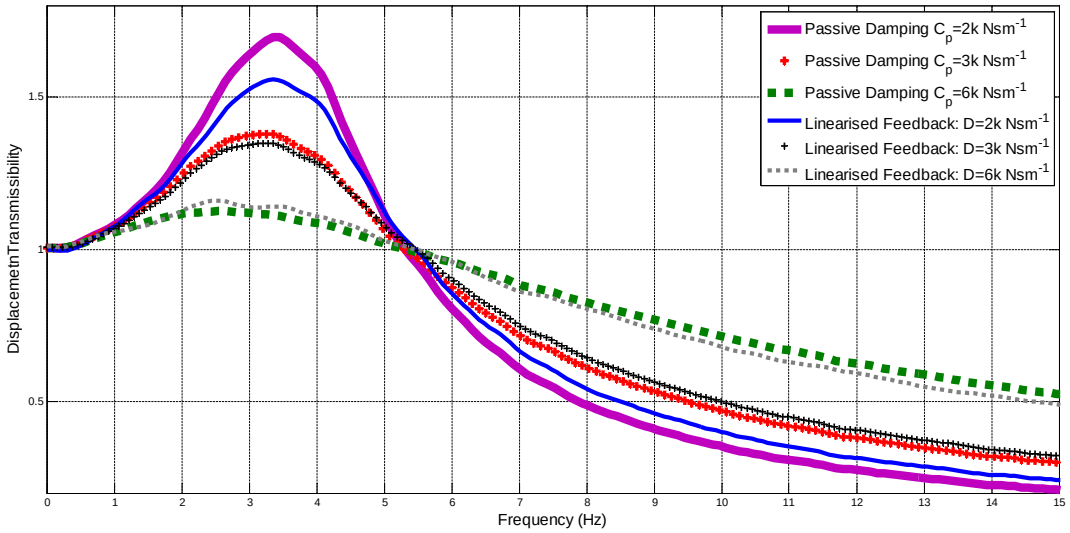

Figure 5.19: Transmissibility comparison between passive and MR linearised feedback systems.

In Figure 5.20, the response of the MR linearised sky-hook system is compared with the response of the MR linearised optimal control. No control response is also shown, where the MR damper is driven at OFF position. Since no current was applied to damper, this represents the passive response equivalent to a damping ratio of 0.2. Control gains for optimal system are identical to the linearised MR sky-hook gains so the performances of both systems are quite similar to each other. Both of the control theories show significant improvement over the passive system.

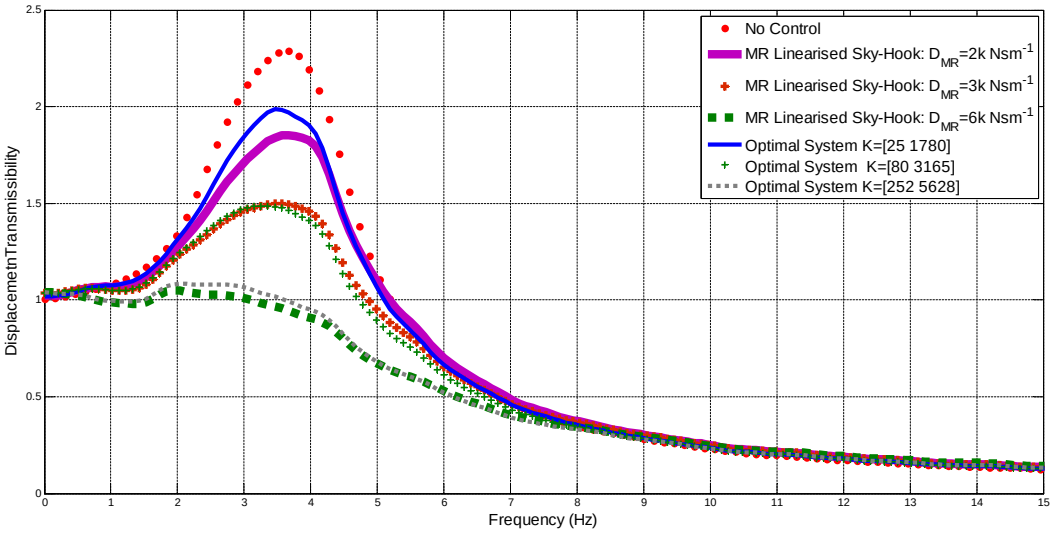

Figure 5.20: Transmissibility comparison between linearised MR sky-hook and optimal systems.

5.3.5 Observer based On-Off sky-hook control

On-off sky-hook control algorithms are mostly investigated in semi-active vibration control [19, 158]. In this control theory, the input current is switched to a predetermined and constant level if the force required by the sky-hook control law is dissipative one, otherwise it is switched to the zero. The representation of this system is shown in Table 5.2-(sixth row). In the content of the unified MR damper model, the control law:

$$\left\{ \begin{array}{ll} I = I_{max} & \dot{\hat{x}}_m(\dot{\hat{x}}_m - \dot{x}_b) > 0 \\ I = 0 & \dot{\hat{x}}_m(\dot{\hat{x}}_m - \dot{x}_b) \leq 0 \end{array} \right\} \tag{5.17}$$

If the current driven to the MR damper is I_{max}, then energy dissipation is required and the damper is in the on condition, otherwise $I = 0$ for the energy input requirement and the

damper is in the off condition. It is obvious that there is no need for a force feedback loop, which simplifies the implementation of on-off control. The controller only requires the absolute velocity of the isolated mass and the velocity of the base, which are estimated by the observer as seen in Figure 5.21.

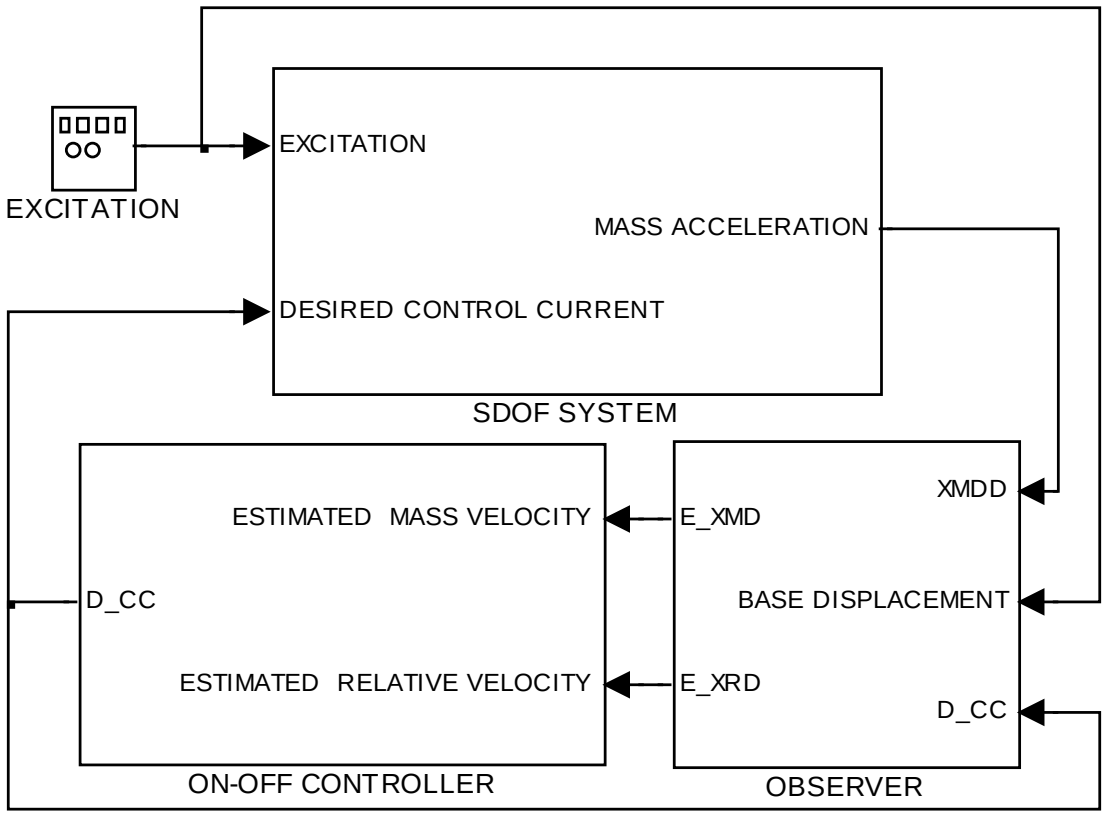

Figure 5.21: Simulated model of observer based on-off sky-hook control of SDOF system.

5.3.6 Observer based fully active sky-hook control

Referring to Table 5.2-(seventh row), the desired damping force is chosen to be the fully active sky-hook force. It is assumed that, this force could be generated by the ideal actuator, which is capable of dissipating and supplying energy in to system. Simulated model of the observer based fully active system is shown in Figure 5.22, where the fully active

force is chosen by,

$$F_{full} = \mathrm{D_{FS}}\dot{\hat{x}}_m \tag{5.18}$$

As seen in equation 5.18 , fully active sky-hook system requires only the absolute velocity of isolated mass which will provided by the observer. The fully active sky-hook control is the benchmark performance for the MR damper system.

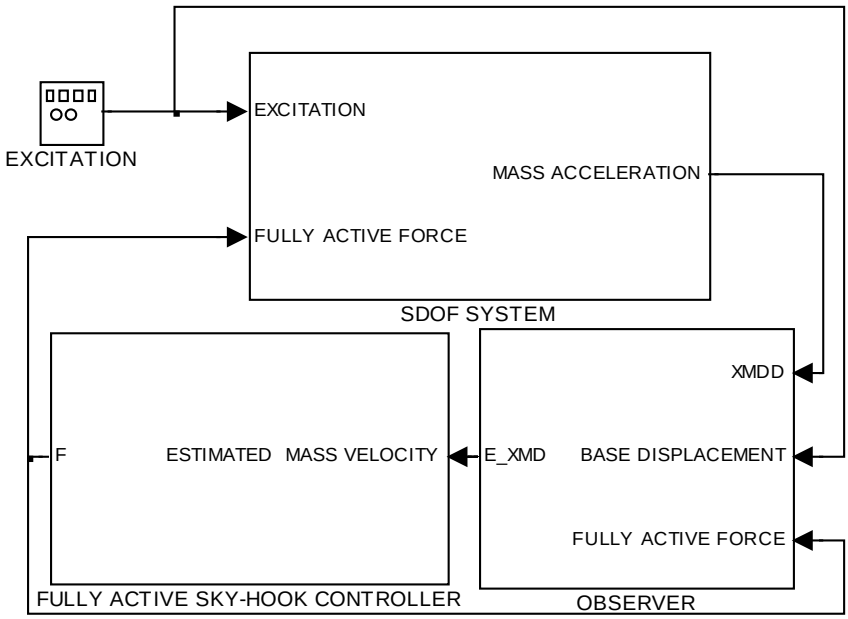

Figure 5.22: Simulated model of fully active sky-hook control of SDOF system.

5.3.7 Observer based ideal semi-active sky-hook control

This system is a modified version of the observer-based fully active sky-hook control. The desired sky-hook force is generated when the damping force is dissipative. Otherwise zero desired damping force is applied to the system;

$$F_{desired} = \left\{ \begin{array}{ll} D_{SAS}\dot{\hat{x}}_m & \dot{\hat{x}}_m(\dot{\hat{x}}_m - \dot{x}_b) > 0 \\ 0 & \dot{\hat{x}}_m(\dot{\hat{x}}_m - \dot{x}_b) \leq 0 \end{array} \right\} \tag{5.19}$$

The ideal semi-active control system requires the knowledge of the damper force, absolute velocity of isolated mass, and the relative velocity of the damper. All of these required states and MR force are estimated by the observer as seen in Figure 5.23.

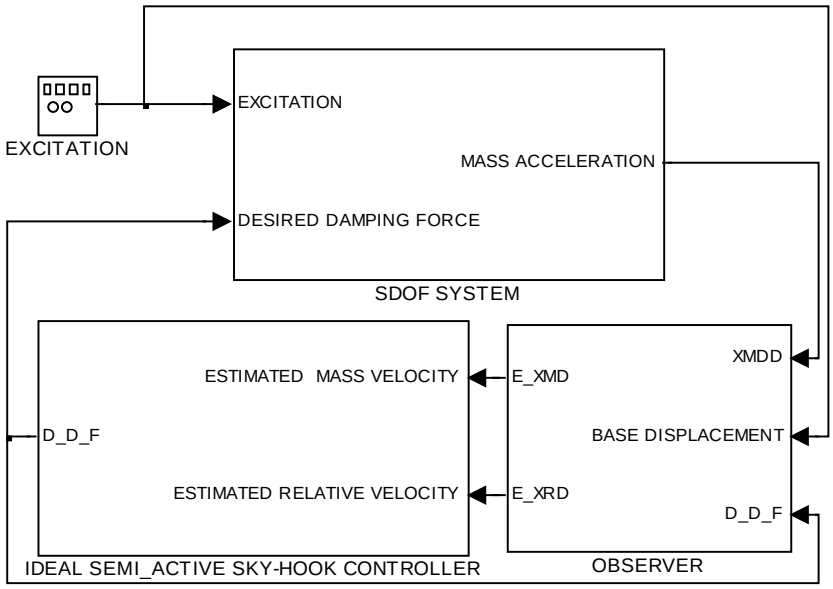

Figure 5.23: Simulated model of observer based ideal semi-active sky-hook control of SDOF system.

- Results of on-off, fully active, and ideal semi-active sky-hook theories

In order to analyse the performance of the observer-based linearised feedback control, the response of the observer-based MR linearised sky-hook system is compared with responses of observer-based on-off sky-hook, observer-based fully active sky-hook, and ideal semi-active sky-hook, under the same random displacement input. Again, the observer is designed with unified MR damper model.

Figure 5.24 compares the transmissibility curves between the linearised MR sky-hook and the on/off MR sky-hook systems. The performance of observer-based on-off sky-hook control slightly reduces with increased control gain I at the high frequency level like a passive system. For example, for large gains the low frequency response of observer-based on-off is superior to the observer-based MR linearised system, but at the same time, at high frequency response the performance of on-off reduces compared to both MR and passive systems.

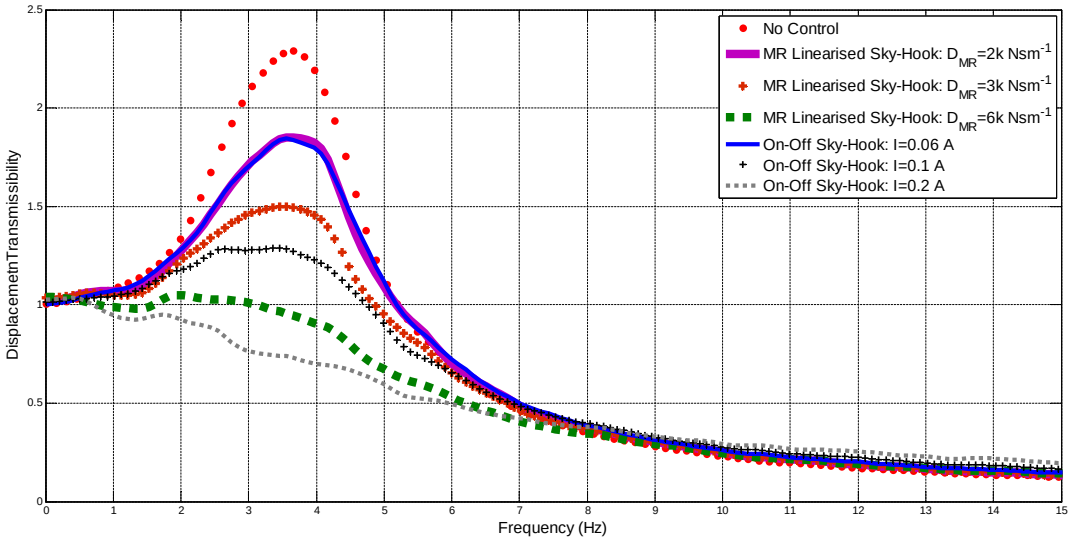

Figure 5.24: Transmissibility comparison between linearised MR sky-hook and on-off sky-hook systems.

The next transmissibility curves comparison is made between the observer-based linearised MR sky-hook system and observer-based fully active sky-hook system, which is shown in Figure 5.25. As expected, the observer-based fully active system improves both the low and high frequency response with increasing controller gain D_{FS}. This is superior to the observer-based MR system where the linearised MR sky-hook achieve a good performance.

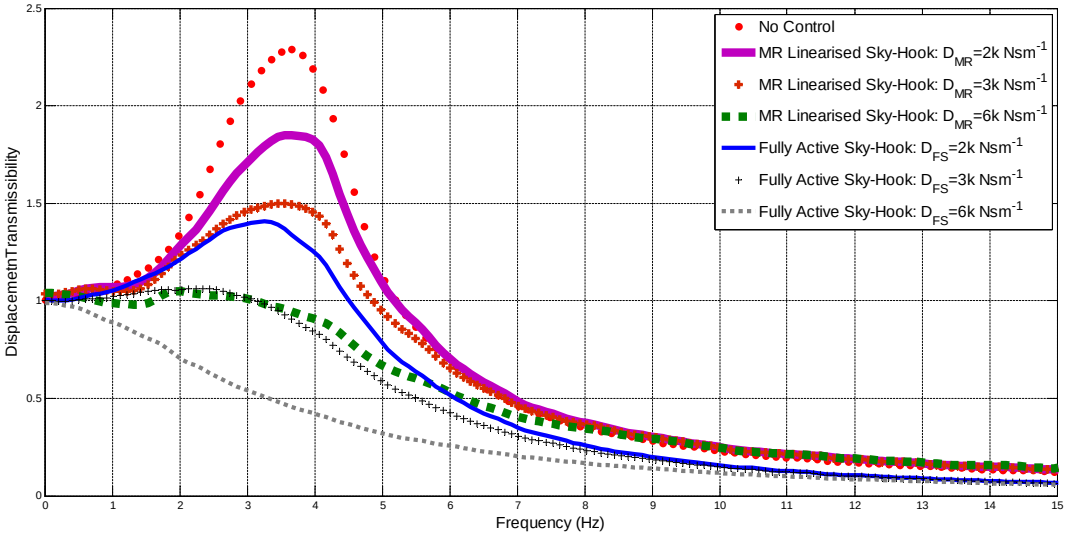

Figure 5.25: Transmissibility comparison between linearised MR sky-hook and fully active sky-hook systems.

Lastly, Figure 5.26 illustrates the comparison of the transmissibility curves between the observer-based linearised MR sky-hook system and the observer-based idealised semi-active sky-hook system, which represents a more realistic performance benchmark. It is clear that, the observer-based ideal sky-hook system improves the both low and high frequency response same as observer-based fully active sky-hook control. In addition, at high frequency performance of observer-based MR linearised sky-hook is close to the ideal case.

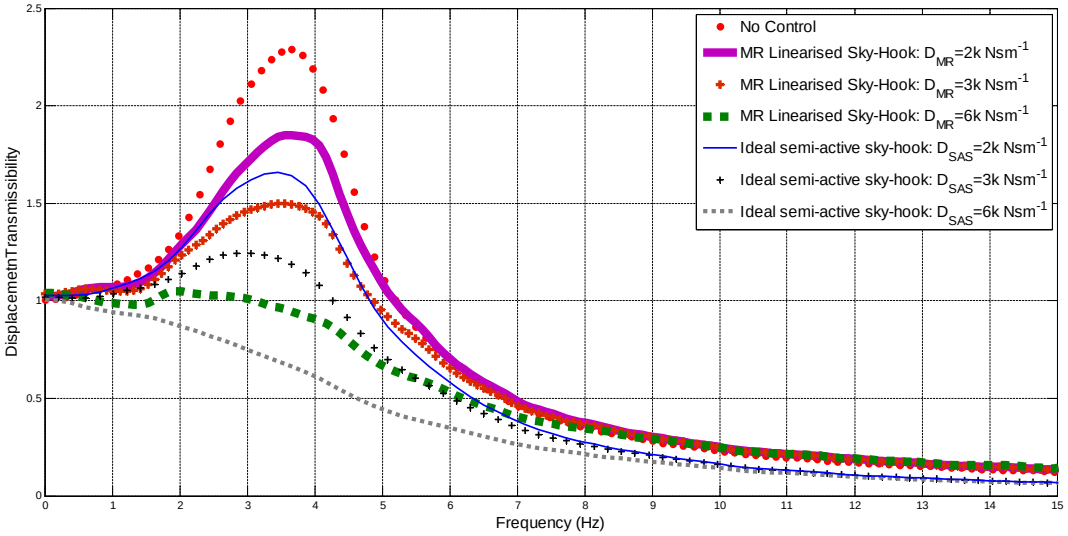

Figure 5.26: Transmissibility comparison between linearised MR sky-hook and ideal semi-active sky-hook systems.

5.4 Summary of Chapter 5

In this chapter, the author numerically investigated the observer-based feedback control of vibration isolation systems using MR dampers. The SDOF mass isolator system were investigated using broadband random excitations, and the results have been benchmarked against ideal passive, observer-based semi-active, and observer-based fully active systems.

Three types of MR damper model are investigated, basic, complex and unified model. In order to validate the performance of the proposed non-linear observer, each of these MR models are used to implement the SDOF system with a proper feedback linearised controller. The numerical results have showed that the non-linear observer is able to estimate states with small error even when the modelling of friction inside damper has been mismatched with real value. Also, using sky-hook based control laws, observer

based feedback linearisation was shown to outperform the equivalent passive systems, whilst approaching that of more simplistic observer-based on/off, observer-based ideal semi-active, and observer-based fully active schemes.

It can be concluded that the proposed numerical observer consisting of a unified MR damper model, is a valid design to estimate the system states and the damping force wide variety of controllers (sky-hook, optimal, and fully active).

In the next chapter of this thesis the performance of the observer based feedback linearisation of MR damper based on SDOF study will be investigated experimentally.

6 Experimental investigation

6.1 Introduction

The performance of the observer-based feedback linearisation theory has been investigated by numerical simulations and proposed observer appears to be effective.

The present section aims to build upon this work by performing experiments of the observer-based single-degree-of-freedom (SDOF) structure subject to broadband excitations. In this study, sky-hook, optimal and on-off based controllers will be used to illustrate the performance of the observer based feedback linearisation. The experiments are performed by using a real SDOF system (see Figure 4.5-(b)) on the test rig (see Figure 4.3). Using D/A conversion, the desired digital control current from observer-based feedback linearisation simulation is then used to modify the damping level of the MR damper by the current amplifier. Simultaneously, an A/D converter provides the simulation with base and mass accelerations data. Although they are not needed in this study, the force transmitted to the basement and the base displacement were measured by an Instron $\pm$25kN dynamic load cell (IST Dynacell [144]) and linear variable differential transformer (LVDT) for verification purposes. The continuous testing of the experiment without overheating of the MR damper is achieved by giving approximately 10 minutes breaks between each test.

This chapter is organised by explanation of the experimental configuration, followed by the associated control theories and concluded with the general discussion of the results.

6.2 Experimental configurations

The real time testing appraoch is shown in Figure 6.1, where the PCI-6030E National Instron Analog Output and Input blocks are used to convert analogue data (base and mass accelerations) to digital data for real time control and digital data (base excitation and desired control current) to analogue data to run the test rig. The real time observer, and the control systems are solved in MATLAB/Simulink using the ode4 (Runge Kutta) solver with the sampling rate of 5k Hz. The observer is designed by using the numerical unified model of MR damper (Chapter 5.2.1), where the inputs of the observer were base displacement (x_b), the mass acceleration ($\ddot{x}_m$), and desired control current (I).

Referring to Figure 6.1, the base excitation signal is scaled from $\pm$50mm (maximum range of the test rig) to $\pm$10V, respectively the measured displacement (LVDT) signal is calibrated from $\pm$10V to $\pm$50mm for data processing. The desired control current generated by the controller is scaled according to output/input relationship of the current amplifier [146], which is 1A/2V. At the same time, the measured signal from the force transducer is converted from Volts to Newtons according to set-up of the Instron [144] controller which is specified to be 1V/800N by the user. Lastly, the measurement of acceleration signals (analogue voltage) are first amplified, and then are converted to the acceleration ($1\text{V}/0.251 * 9.81\text{ms}^{-2}$). Also these signals receive an offset problem which is solved by added constant acceleration (-9.83ms^{-2}).

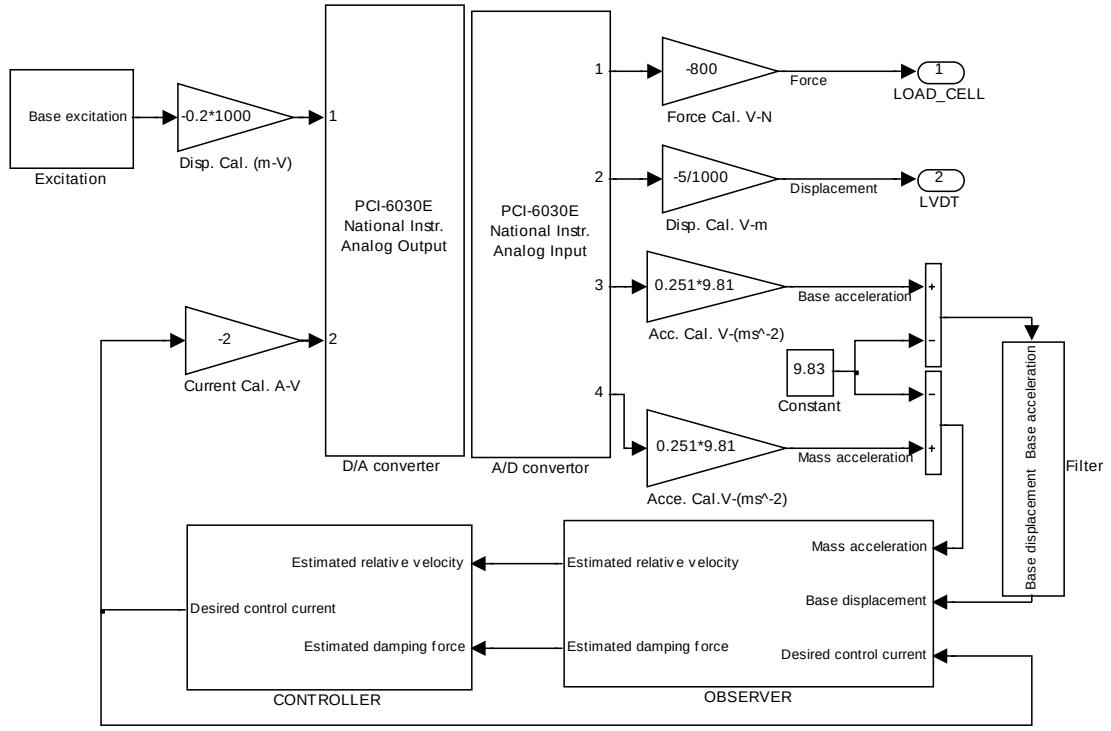

Figure 6.1: Experimental system for observer-based SDOF control testing.

As explained previously, implementation of the proposed theory requires the base displacement (x_b) for the proposed observer model which was provided by double integration of the measured base acceleration. This acceleration signal was integrated two times to produce the base displacement. However, this displacement signal drifts due to integration process. One of the possible solution to this drifting problem proposed was to employ high-pass filtering of drifted base displacement by properly choosing a cut-off frequency [159]. So, the drifting problem of the displacement signal was overcome by passing displacement signal through the high pass Butterworth filter. All of these integrations and filtering process were represented by the Filter block in Figure 6.1.

The accuracy of this filtered base displacement signal depended on the passband edge frequency of the filter. In order to optimise the pass band edge frequency several exper-

imental tests of observer-based control were carried out with different frequency of the filter (0.5 Hz to 7 Hz). For these tests, the desired set-point force was chosen to be proportional to the relative velocity of the piston, and the system was excited with the random broad band excitation which was used in Chapter 5. The frequency response function was used to compare the performance of each filter frequency by comparison to the frequency response of the system where the actual base displacement is used by the observer instead of the integrated acceleration as seen in Figure 6.2.

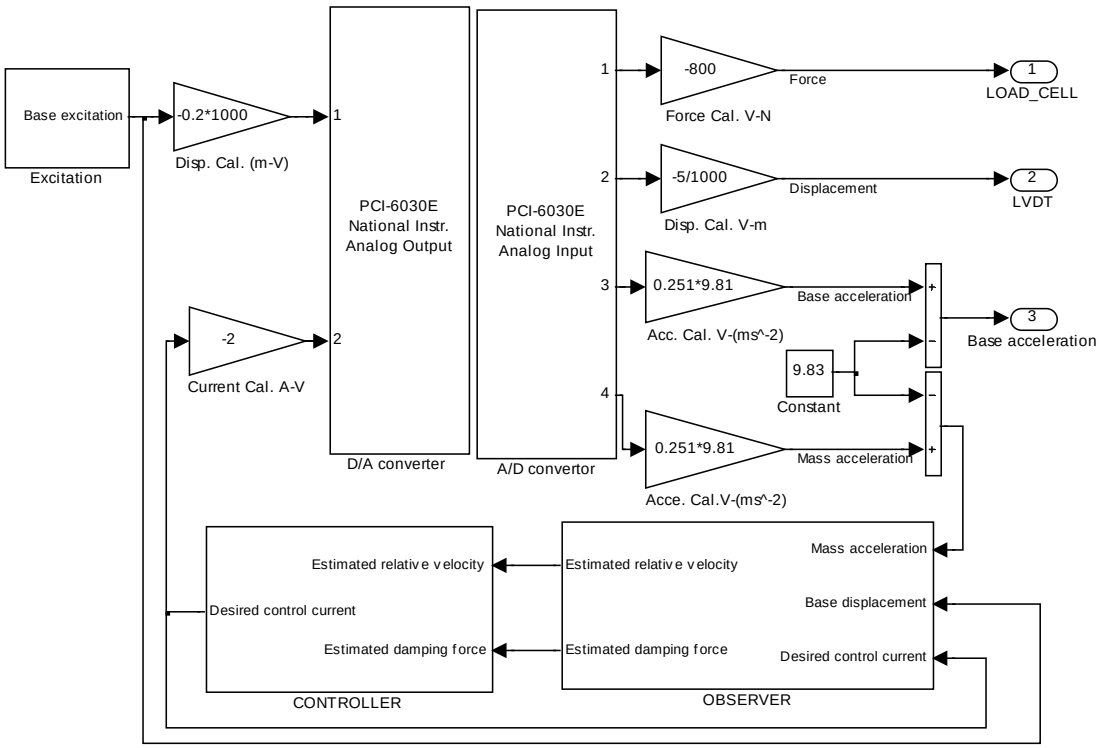

Figure 6.2: Experimental system for observer-based SDOF control testing where the actual base displacement signal is used.

The frequency response comparisons are shown in Figure 6.3. This figure indicates that, perfect matching appears between two systems when the frequency of high pass filter is chosen 1 Hz. Also, it shows that, when the passband edge frequency chosen is closer to the natural frequency of the system (3.75 Hz) or even higher than that, it is possible

to avoid the drifting problem but, in this case the filtered displacement signal receives phase/shifting and attenuation [159], which results in inaccurate estimation of the base displacement. In a similar manner, if the cut-off frequency was chosen lower than 1 Hz, the filtered displacement signal still drifts and so the observer could not estimate the state properly.

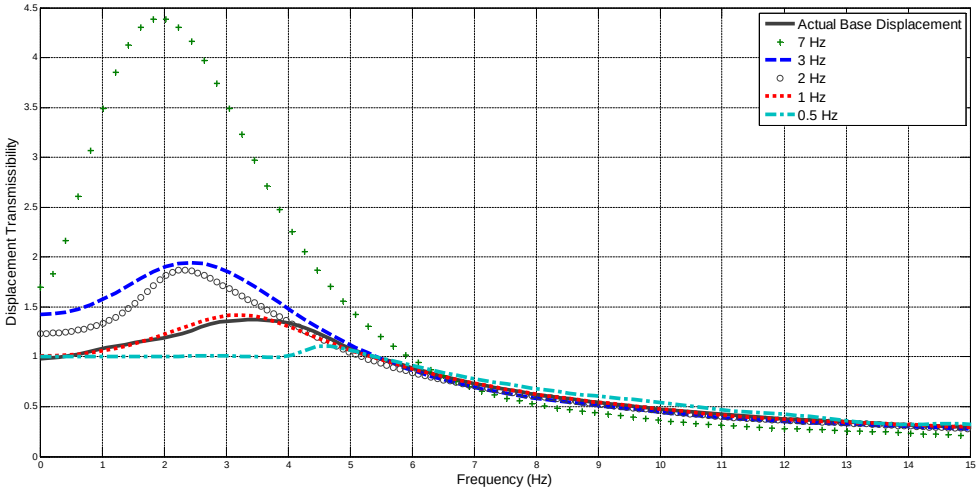

Figure 6.3: Comparison of the displacement transmissibility plots observer based feedback linearisation of SDOF system (D=3000 Ns/m).

In conclusion, 1 Hz passband edge frequency is chosen for the high pass Butterworth filter in this study.

6.3 Control Theories

Four different types of SDOF control strategies were performed for experimental investigation;

1. Observer-based MR linearised feedback control

2. Observer-based MR linearised sky-hook control

3. Observer-based MR linearised optimal control

4. Observer-based MR linearised on-off control

These control theories were already described in the Section 5.3.

6.4 Results and Discussion

The four observer-based control systems were all tested under broad band conditions. The base displacement excitation signal is produced by passing the white noise signal through a low pass Butterworth filter with 15 Hz cut off frequency, in the Simulink environment. The frequency response of the system for different controller gains are compared. In order to obtain the frequency response the Tfestimate method of the Matlab program is used. This frequency response method is useful for the input/output relationships of the linear system. However, the semi-active theory involves highly non-linear characteristics. Due to this, it is more proper to compare the power spectral density (PSD) of the mass acceleration for each control theory.

The first two results, compare the performance of the observer-based MR linearised feedback control with the observer-based MR linearised sky-hook control as seen in Figures 6.4-6.5. Figure 6.4 shows the comparison of the transmissibility curves and Figure 6.5-(a) illustrates spectral density of base displacement, whilst the Figure 6.5-(b) compares the PSD of the mass acceleration for the uncontrolled case and controlled case with chosen control gains $D = D_{MR} = 2,3,6 \text{kNs/m}^{-1}$. The uncontrolled case is where no current is applied to the MR damper, to illustrate the passive characteristic of the system.

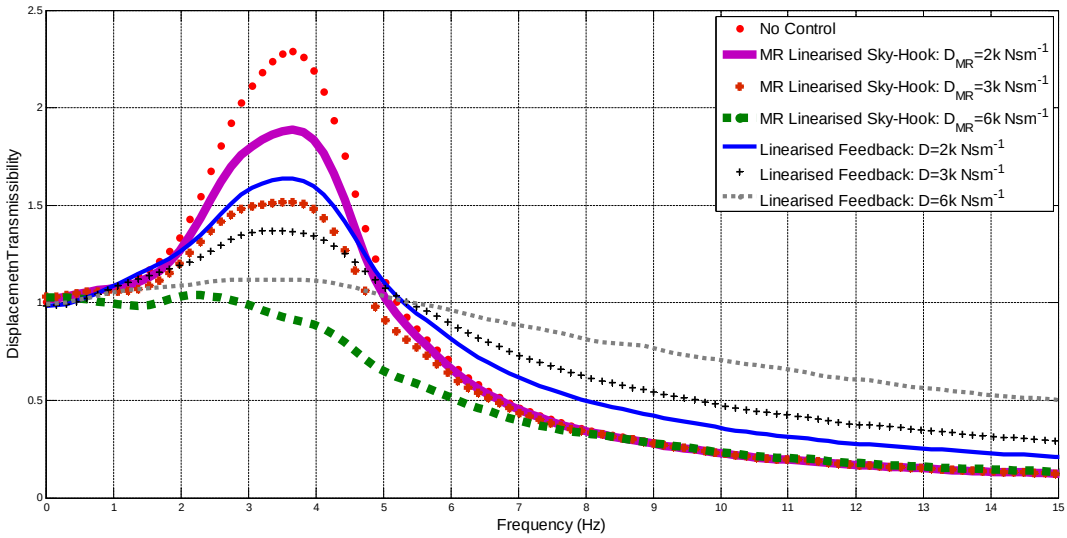

Figure 6.4: Transmissible comparison between linearised and MR linearised sky-hook system for different control gains.

Figure 6.4 indicates that observer-based MR linearised feedback control of an MR damper achieved a significant improvement over the uncontrolled case, where some degradation in the higher frequency response is observed with increased control gain D. Also, comparing the observer-based MR linearised feedback with observer-based MR linearised sky-hook, MR linearised feedback control shows good performance for low control gains but after a certain level of the gain the MR linearised feedback reaches its maximum damping level. MR linearised feedback system has the crossover frequency around 5 Hz while crossover occurs for linearised sky-hook system at approximately 8.5 Hz.

The power spectral density of the random excitation is shown in Figure 6.5-(a), which illustrates that, the displacement signal used to excite the system has an almost constant power spectrum over the frequency range of 0-15 Hz. After the cut-off frequency of the filter (15 Hz), the power decays to the zero. At the same time, the Figure 6.5-(b) compares the mass acceleration spectral densities for the observer-based MR linearised feedback, and observer-based MR linearised sky-hook. This figure expresses almost same

characteristic with Figure 6.4, but it is much clearer to see the dynamics of control systems at the high frequency region. In general, the MR linearised sky-hook is much better, except for lower control gain, MR linearised feedback control shows better performance than the MR linearised sky-hook.

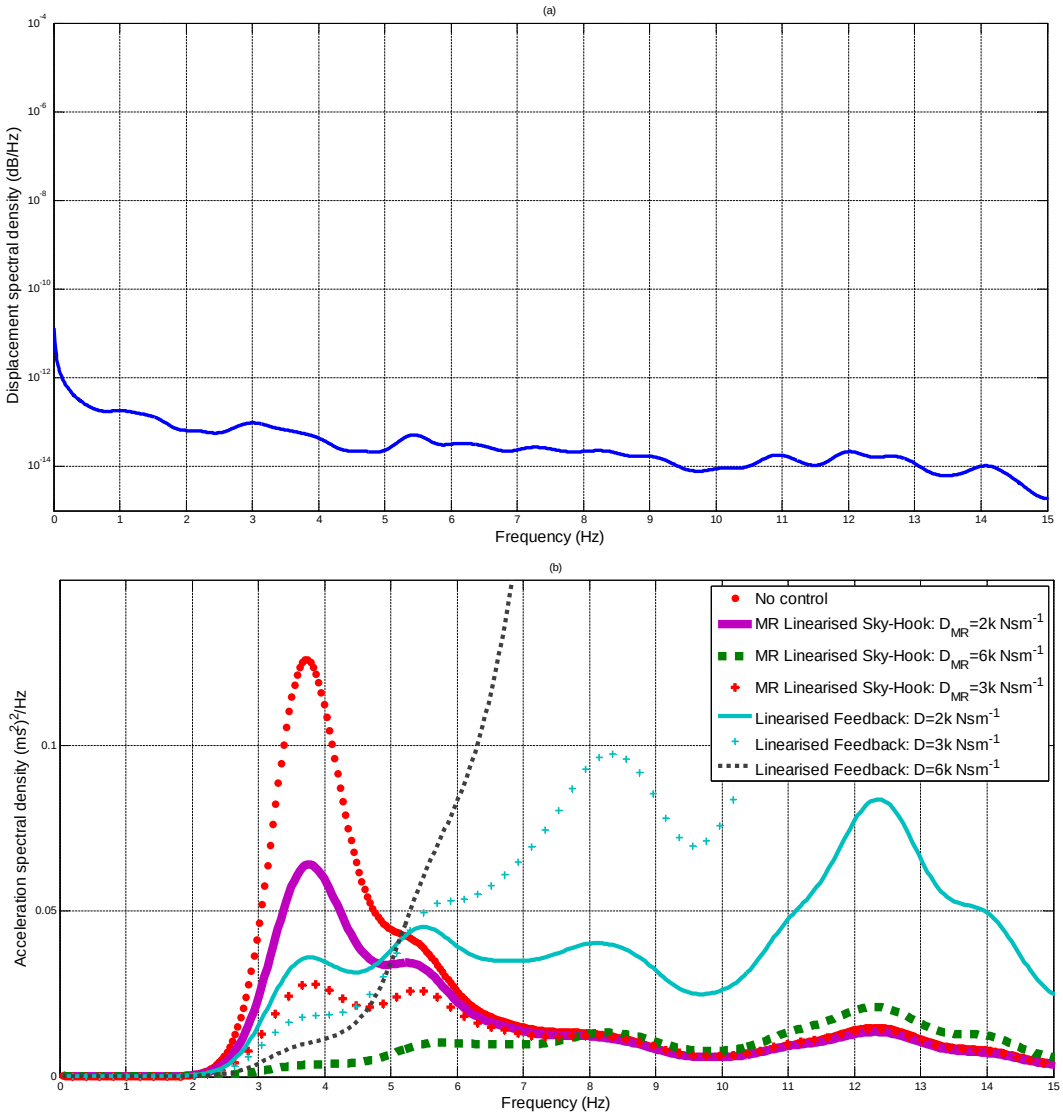

Figure 6.5: Power spectral density plots. (a) Spectral density of the base excitation, (b) mass acceleration spectral density comparison between MR linearised sky-hook and linearised system for different control gains.

Figure 6.6 compares the frequency response of observer-based MR linearised sky-hook, and the frequency response of observer-based MR linearised on-off sky-hook approaches. The plot indicates that observer-based MR linearised sky-hook system can be tuned to outperform the commonly used on-off sky-hook system throughout the frequency range (except the frequency range 2-3 Hz). Also, the observer-based on-off system has slightly lower crossover frequency around 7.8 Hz. The corresponding spectra of the mass accelerations are seen in Figure 6.7. There is a slight performance reduction for observer-based on-off sky-hook control after cross over frequency (7.8 Hz).

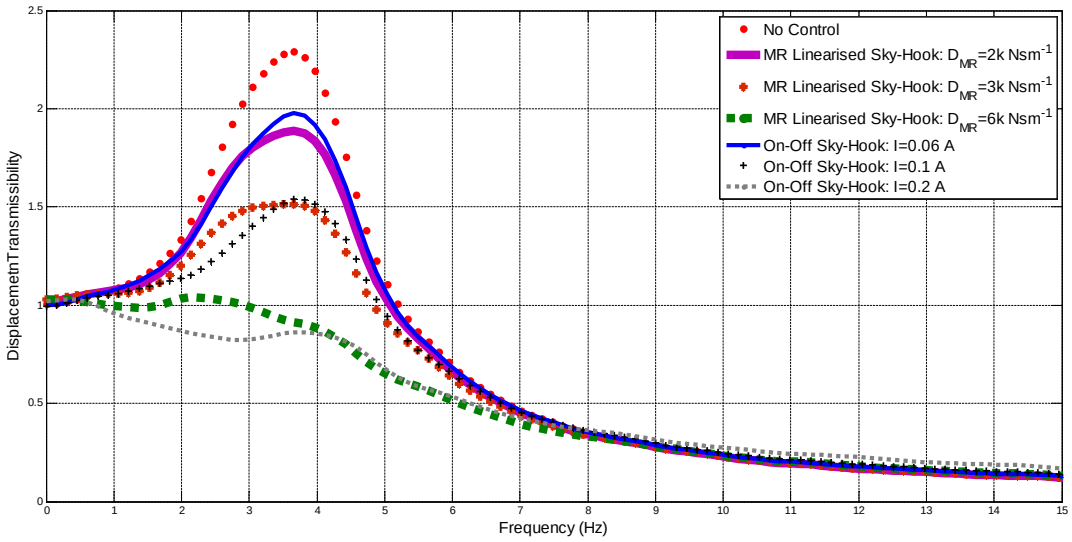

Figure 6.6: Transmissible comparison between MR linearised sky-hook and on-off sky-hook system for different control gains.

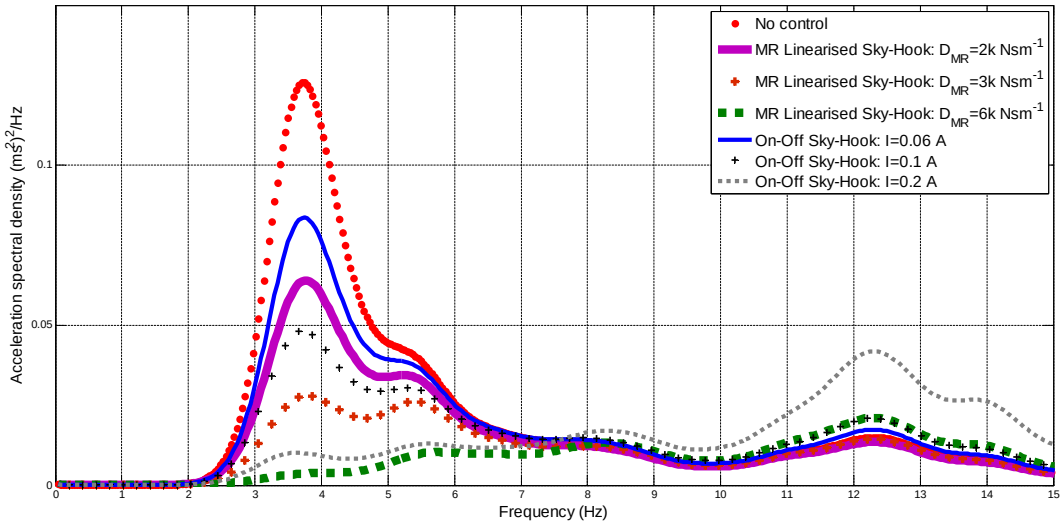

Figure 6.7: Mass acceleration spectral density comparison between MR linearised sky-hook and on-off sky-hook system for different control gains.

Figure 6.8 compares the relative performance of observer-based MR linearised sky-hook and observer-based MR linearised optimal systems. Almost the same transmissibility behaviour were observed for approximately equivalent control gains. The power spectral densities in Figure 6.9 indicate the same characteristic as well. Clearly these figures shows that the performance of linearised sky-hook was able to reach the performance of optimal systems.

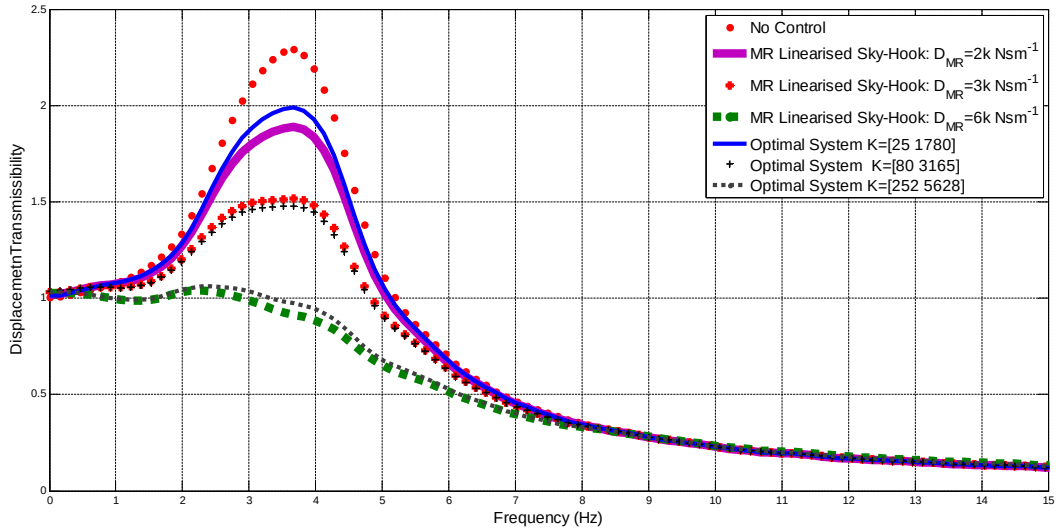

Figure 6.8: Transmissible comparison between MR linearised sky-hook and optimal system for different control gains.

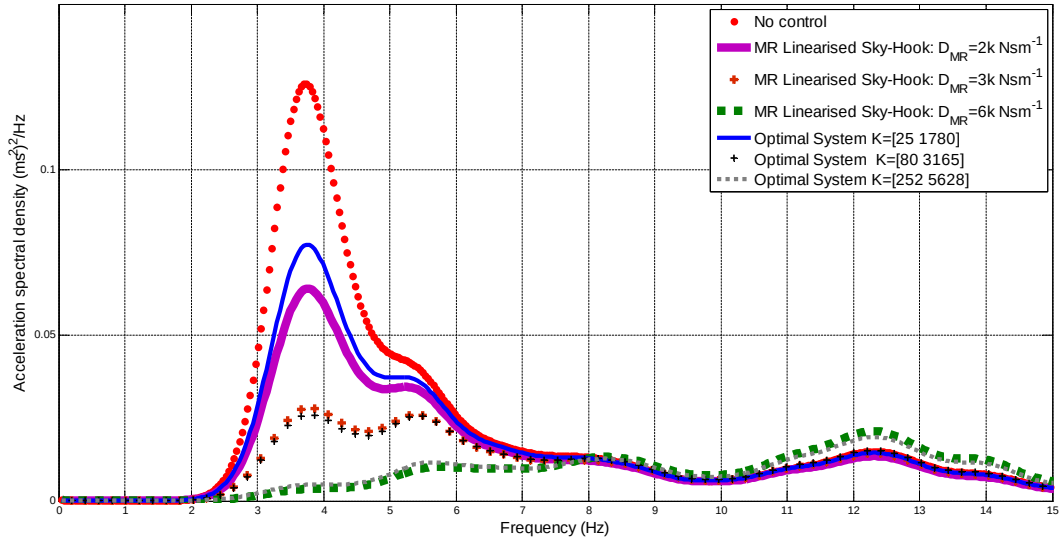

Figure 6.9: Mass acceleration spectral density comparison between MR linearised sky-hook and optimal system for different control gains.

It can be concluded that the proposed observer, consist of the unified MR damper model, the mass model, and spring model, is able to estimate the states, and the damping force of the experimental SDOF system by using the simple measurements of the base and the mass acceleration. This proposed observer model will overcome the complexity of the

linearised feedback implementation of semi-active control scenarios. Also extensive control testing showed good performance of the observer-based linearised feedback control strategies (sky-hook, and optimal).

6.5 Summary of Chapter 6

This chapter has presented the experimental investigation of semi-active SDOF mass isolation system. Here, SDOF mass isolation system consist of MR damper excited by a high response servo hydraulic actuator, while the observer and controller were implemented in a real time digital controller. For each study, the performance of observer based feedback linearisation was investigated by implementing sky-hook controllers, where comparisons were made with more simplistic on/off controllers, optimal controller, and the passive case. The results have validated the numerical performance of proposed system.

7 Case study: Tuned Mass Damping

7.1 Introduction

Having demonstrated the simulated and experimental performance of the observer based feedback linearisation strategy under the broadband excitation, now the approach will be used as part of a tuned mass damper (TMD) vibration absorber problem. The observer-based semi-active tuned mass damper system is analytically modelled and investigated in Simulink software and it is experimentally tested. The performance of the proposed semi-active control algorithms are compared with the equivalent optimal passive system.

The aim of this chapter is to investigate the performance of the proposed theory with the vibration absorber problem as a case study. It should be mentioned that the MR damper under investigation was not specifically designed for use in a tuned mass damper system. However, the intention here is not to fine-tune the actual device for a specific application but rather to demonstrate the performance potential of linearising an MR damper to implement observer based semi-active tuned mass control strategies. For this purpose, a simplified tuned mass damper scenario serves as a useful case study. The tuned mass damper (TMD) scenario is first described before presenting the simulated results. At this

point, a little attention is paid to the brief literature review of the vibration absorber problems.

Excessive vibration has been a common problem throughout engineering history which can result from a variety of sources; human body motions, rotating, oscillating and impacting machines, wind flows, earthquake induced vibration, road traffic, railway traffic, construction works etc. [160]. A massive example of excessive vibration on structures was observed recently at the opening ceremony of The London Millennium Footbridge on June 10, 2000 [161]. The bridge experienced pedestrian-induced lateral vibration up to 50 mm of lateral movement of the south span and 70 mm of the centre span and on June 12, 2000, the bridge was closed. Often the most effective and economic way to reduce vibration is to apply an additional dynamic system at a discrete point on the existing structure, to change the system dynamics in a desired way [6]. Simple mass-spring-damper systems attached to a selected point of the vibrating structure (as seen in Figure 7.1-(a)), are one example. They are called tuned mass dampers (TMD), tuned vibration absorbers [162], or vibration neutralisers [6]. In the history, the first time tuned mass dampers were used was to reduce the rolling motion of ships by Frahm in 1911 [163]. Later, TMDs were implemented to reduce the amplitude of the single degree of freedom systems by Ormondroyd and Den Hartog [164], and Brock [165]. Den Hartog developed closed form expressions of optimum damper parameters which are frequency ratio and damping ratio of the TMD [3]. These expressions are for only un-damped main systems with a single degree of freedom. Later, damping in the main system was included by several researchers [166, 6, 167, 168, 169]. To summarise, simple optimum solutions to excessive vibration problems using passive tuned mass damper have been widely investigated and implemented on real structures [170].

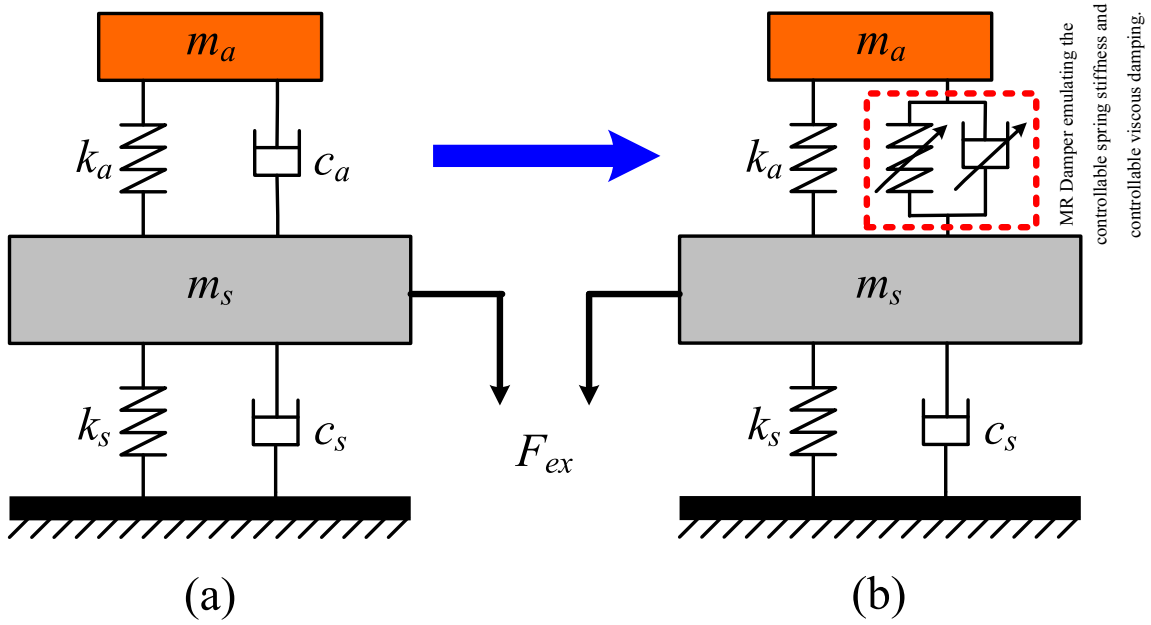

Figure 7.1: Lumped parameter model of tuned mass damper system. (a) Classical passive TMD, (b) adaptive TMD with an MR damper, modified from [130].

However, all these proposed tuning methods for optimal passive TMD system assumed that the natural frequency and structural mass are known and do not change. If the modal properties of the main structure are changed (e.g due to environmental effects) after the TMD has been installed, the performance can be significantly reduced [171, 172]. These environmental effects could be the time-varying pay loads, estimation errors or temperature changes. All these problems will result in the de-tuning of the pre-tuned mass damper. As a solution to this generic de-tuning problem, many adaptive TMD control concepts have been proposed to develop new designs and concepts by controlling the properties of the TMD in real time to match the changing properties of structure. Such concepts and their control were summarised by Fisco and Adeli [109, 173]. Due to high power requirements, expense and fail-safety problems of the active system, adaptive tuned mass damper systems are designed mostly based on semi-active approaches [174]. After seven decades of first passive TMD damper implementation, Hrovat et al. introduced the concept of a

semi-active TMD for wind-induced vibrations in a high rise building [18].

Semi-active dampers require simpler hardware and have lower power requirements thus reducing operational costs. These devices can provide variable damping and/or stiffness and have been used for vibration reduction of mechanical and civil engineering structures. Semi-active tune mass damper concept were designed with a tuned mass, a tuned passive spring and controlled semi-active damper. Variety of choices of semi-active damper were proposed, such as piezo stack [175], active smart materials (shape memory alloy) [176, 177], piezoelectric materials [178], controllable friction devices [179], and magnetorheological (MR) damper [180, 181, 182]. Weber et. al. presented a semi-active approach where a rotational MR damper was used to emulate both controllable damping and stiffness force under harmonic excitation [174]. In addition to this, the same authors extended this numerical work by experimental implementation of proposed theory on a laboratory footbridge, using accelerometers and a force transducer to implement force tracking control [130]. They were able to reduce the vibration amplitude between 38% to 63% relative to a passive TMD system, but they did not investigate the performance of proposed system under random or broadband excitation which is more-likely to be realistic case. In addition the use of a force transducer also increases the complexity of the system. In this study, these two drawbacks have been overcome by the proposed observer based linearised semi-active tuned mass damper system. The lumped parameters model of this system is shown in Figure 7.2.

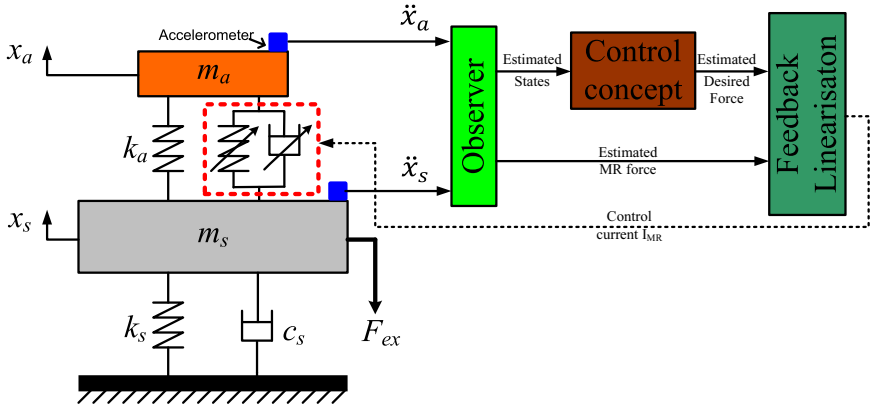

Figure 7.2: Observer base semi active tuned mass damper control scheme.

This chapter offers a description of the proposed observer base linearised control of semi-active tuned mass damper, along with a dynamic analysis of the optimal passive TMD that is based upon numerical simulations (optimal tuning). Before introducing the observer-based adaptive TMD, this chapter describes a classical passive tuned mass damper to help distinguish the two systems. Following the comparisons, this chapter discusses the controllers development for the proposed system, followed by the design of the non-linear two degree of freedom observer. The parameters of the structure system (mass, stiffness, and damping ratio) are optimally tuned using analytical optimization techniques described by Mead [6].

In this study, the inverse of this optimisation theory was first implemented so that the existing experimental system can be used as the vibration absorber. Finally, this chapter summarizes the dynamic performance of the observer base tuned systems and suggests the best control method for the proposed observer based semi-active system, based upon the numerical and experimental results.

7.2 Numerical modeling and optimal tuning

Figure 7.1-(a) shows a classical model of force-excited (F_{ex}) passive TMD configuration. The main structure is coupled with a classical passive vibration absorber, and the mass of the structure and absorber are defined by m_s and m_a, with their corresponding displacements as x_s and x_a, respectively. The absorber's spring (k_a) and damper (c_a) are mounted on the structure. The stiffness and damping of the structure are represented by k_s and c_s, respectively.

The equations of motion of the force-excited passive TMD in matrix form is;

$$\begin{bmatrix} m_s & 0 \\ 0 & m_a \end{bmatrix} \begin{bmatrix} \ddot{x}_\mathrm{s} \\ \ddot{x}_\mathrm{a} \end{bmatrix} + \begin{bmatrix} c_s + c_a & -c_a \\ -c_a & c_a \end{bmatrix} \begin{bmatrix} \dot{x}_s \\ \dot{x}_a \end{bmatrix} + \begin{bmatrix} k_s + k_a & -k_a \\ -k_a & k_a \end{bmatrix} \begin{bmatrix} x_s \\ x_a \end{bmatrix} = \begin{bmatrix} F_{ex} \\ 0 \end{bmatrix} \tag{7.1}$$

For the case of harmonic excitation, time domain solutions of the equation 7.1 are;

$$x_s(t) = X_\mathrm{s} \mathrm{e}^{st} \tag{7.2}$$

$$x_a(t) = X_\mathrm{a} \mathrm{e}^{st} \tag{7.3}$$

$$F_{ex}(t) = F_o \mathrm{e}^{st} \tag{7.4}$$

where $s = \mathrm{j}\omega$ and ω is the excitation frequency. Substituting equations 7.2-7.4 into equation 7.1 yields

$$\begin{bmatrix} m_s s^2 + (c_\mathrm{s} + c_a)s + k_\mathrm{s} + k_a & -c_a s - k_a \\ -c_a s - k_a & m_a s^2 + c_a s + k_a \end{bmatrix} \begin{bmatrix} X_s \\ X_a \end{bmatrix} = \begin{bmatrix} F_o \\ 0 \end{bmatrix} \tag{7.5}$$

By using the Cramer's Rule, the amplitude of X_s and X_a can be solved such that,

$$X_s = \frac{\begin{bmatrix} F_o & -c_a s - k_a \\ 0 & m_a s^2 + c_a s + k_a \end{bmatrix}}{\mathrm{detG}} = \frac{F_o(m_\mathrm{a}\mathrm{s}^2 + c_\mathrm{a}\mathrm{s} + k_\mathrm{a})}{\mathrm{detG}} \tag{7.6}$$

$$X_a = \frac{\begin{bmatrix} m_s s^2 + (c_s + c_a)s + k_s + k_\mathrm{a} & F_o \\ -c_a s - k_a & 0 \end{bmatrix}}{\mathrm{detG}} = \frac{F_o(c_a s + k_a)}{\mathrm{detG}} \tag{7.7}$$

where,

$$\mathrm{detG} = (m_s s^2 + (c_s + c_a)s + k_s + k_a)(m_a s^2 + c_a s + k_a) - (c_a \mathrm{s} + k_a)^2$$

the steady state solution of equation 7.1 can be obtained;

$$\frac{X_s}{\mathrm{F}_0} = \frac{(m_a s^2 + c_a s + k_a)}{(m_s s^2 + (c_s + c_a)s + k_s + k_a)(m_a s^2 + c_a s + k_a) - (c_a \mathrm{s} + k_a)^2} \tag{7.8}$$

$$\frac{X_a}{\mathrm{F}_0} = \frac{(c_a s + k_a)}{(m_s s^2 + (c_s + c_a)s + k_s + k_a)(m_a s^2 + c_a s + k_a) - (c_a \mathrm{s} + k_a)^2} \tag{7.9}$$

By defining the following parameters

$\mu = m_s/m_a$ = Mass ratio (Absorber mass/main mas)

$\delta_{st} = F_o/k_s$ = Static deflection of the system

$\omega_\mathrm{s} = (k_s/m_s)^{0.5}$ = Natural frequency of the main structure

$\omega_a = (k_a/m_a)^{0.5}$ = Natural frequency of the absorber (TM)

$\zeta_s = \mathrm{c_s}/(2m_s\omega_s)$ = Damping ratio of main structure

$\zeta_a = c_a/(2m_a\omega_a)$ = Damping ratio of absorber (TM)

$g = \omega_a/\omega_s$ = Ratio of natural frequencies

$r = \omega/\omega_s$ = Forced frequency ratio

$\eta_a = c_a/(m_a\omega_a)$ = Loss factor of absorber

$\eta_s = c_s/(m_s\omega_s)$ = Loss factor of main structure

the final transmissibility equations for the forced-excited system become;

$$\frac{X_s}{\delta_{st}} = \frac{(g^2 - r^2 + 2\zeta_a grj)}{(-r^2 + 2\zeta_s rj + 2\zeta_\mathrm{a}\mu grj + 1 + \mu g^2) + (-r^2 + 2\zeta_\mathrm{a} grj + g^2) - \mu(2\zeta_a grj + g^2)^2} \tag{7.10}$$

$$\frac{X_a}{\delta_{st}} = \frac{(g^2 + 2\zeta_\mathrm{a} grj)}{(-r^2 + 2\zeta_\mathrm{s} rj + 2\zeta_\mathrm{a}\mu grj + 1 + \mu g^2) + (-\mathrm{r}^2 + 2\zeta_\mathrm{a} grj + g^2) - \mu(2\zeta_a grj + g^2)^2} \tag{7.11}$$

The transmissibility equation 7.11 provide the means of tuning TMDs using Mead's [6] description. The target of the techniques is to minimize the maximum transmissibility.

As described in introduction of this chapter, the inverse optimisation of Mead theory was used to find out the optimal parameters of the main structure instead of tuning the absorber system. First step was to determining the mass ratio by using the optimal loss factor of the absorber. The optimal loss factor of absorber was defined as;

$$\eta_{a,opt} = \left[\frac{3\mu}{2(1+\mu)}\right]^{1/2} \tag{7.12}$$

Assuming the loss factor of the exist absorber was the optimal ($\eta_{a,opt} = c_a/(m_a\omega_a)$) , and than the mass of the main structure could be calculated from,

$$\mu_{opt} = \frac{\eta_a^{2\frac{2}{3}}}{(1-\eta_a^{2\frac{2}{3}})} \tag{7.13}$$

$$m_{s,opt} = m_a/\mu_{opt} \tag{7.14}$$

The main structure stiffness was calculated by using the optimal frequency ratio, which is

$$g_{opt} = \frac{1}{1+\mu_{opt}} \tag{7.15}$$

where, $g_{opt} = \omega_a/\omega_s$ and structural stiffness is;

$$k_s = \omega_a^2 m_s/g_{opt}^2 \tag{7.16}$$

Mead had not considered any optimisation for the main structural damping value but it is found that the level of the structural damping compared to the absorber damping ratio was quite low ($\eta_{a,opt} = 0.267$, and $\eta_s = 0.0072$). This identification is used to approximate the structural damping of the system. Where the structural damping is;

$$c_s = \eta_s(m_s\omega_s) \tag{7.17}$$

All the parameters of vibration absorber and structural system are given in table 7.1.

7.3 Semi-active TMD design

The proposed observer base semi-active tuned mass damper (TMD) model replaces a passive damping element with a controllable semi-active damper to emulate controllable stiffness and controllable damping, which distinguishes it from the classical passive system. Figure 7.1-(a) shows a conventional passive TMD model, and the proposed semi-active tuned mass damper model is shown in Figure 7.1-(b). A controllable damper, such as an MR damper, is the key element for the proposed system. It can provide a wide dynamic force range, can offer a real-time control environment at low power, and can be quite cost-effective. Incorporating this versatile damper into the proposed model will significantly enhance its performance, combining the benefits of both passive and active systems. The new system is anticipated to surpass the performance of classical passive TMD in reducing the maximum vibration levels of the primary structure and robustly adapt to the primary system's parameter changes.

Figure 7.3 was used to derive the dynamic equations of motion for the semi-active model. The equations of motion that describe this system were:

$$\begin{bmatrix} m_s & 0 \\ 0 & m_a \end{bmatrix} \begin{bmatrix} \ddot{x}_s \\ \ddot{x}_a \end{bmatrix} + \begin{bmatrix} c_s & 0 \\ 0 & 0 \end{bmatrix} \begin{bmatrix} \dot{x}_s \\ \dot{x}_a \end{bmatrix} + \begin{bmatrix} k_s + k_a & -k_a \\ -k_a & k_a \end{bmatrix} \begin{bmatrix} x_s \\ x_a \end{bmatrix} + \begin{bmatrix} 1 \\ -1 \end{bmatrix} F_{\text{MR}} = \begin{bmatrix} 1 \\ 0 \end{bmatrix} F_{ex} \tag{7.18}$$

where F_{MR} is the force produced by the semi active magnetorheological damper. Equation 7.18 will be used in the development of the numerical model of the semi-active TMD.

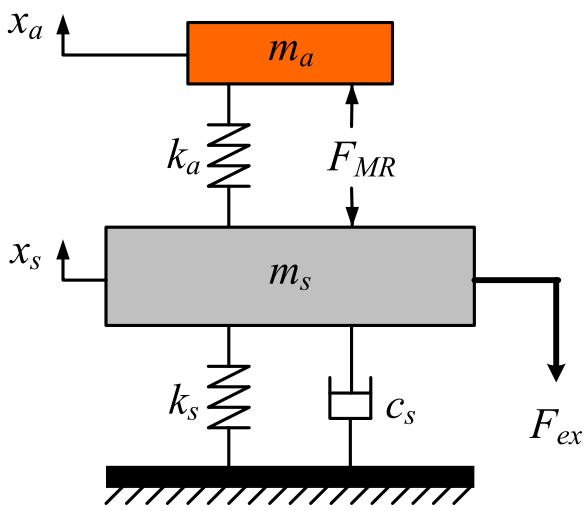

Figure 7.3: Lumped-parameter models of proposed semi-active tuned mass damper model, where semi-active element is the magnetorheological damper.

7.4 Observer design

The linear and non-linear observer designs are discussed in Chapter 3 and the same design theory will be used to develop a non-linear observer for semi-active tuned mass damper system. In this study the main focus was to evaluate the performance of the observer base feedback linearisation of the MR damper as a case study. Therefore, the purpose of

the observer was to be able to estimate the absolute velocities of the absorber mass and structural mass for the proposed control algorithms, and estimation of the MR damper force for feedback linearisation. Referring to Figure 7.3 the equation of motion 7.18 was used to design the basic state matrices such that;

$$\begin{bmatrix} m_s & 0 \\ 0 & m_a \end{bmatrix} \begin{bmatrix} \ddot{x}_s \\ \ddot{x}_a \end{bmatrix} + \begin{bmatrix} c_s & 0 \\ 0 & 0 \end{bmatrix} \begin{bmatrix} \dot{x}_s \\ \dot{x}_a \end{bmatrix} + \begin{bmatrix} k_s + k_a & -k_a \\ -k_a & k_a \end{bmatrix} \begin{bmatrix} x_s \\ x_a \end{bmatrix} + \begin{bmatrix} -1 \\ 1 \end{bmatrix} F_{\mathrm{MR}} = \begin{bmatrix} 1 \\ 0 \end{bmatrix} F_{ex}$$

where the state space model of the system is:

$$\begin{aligned} \dot{\underline{x}}(t) &= \mathrm{A}\underline{x}(t) + \mathrm{B}u + Gw(t) \\ y(t) &= \mathrm{C}\underline{x}(t) + \mathrm{D}u + Hw(t) \end{aligned} \tag{7.19}$$

the state vector is chosen $\underline{x} = [\ x_1 \quad x_2 \quad x_3 \quad x_4\ ]'$, where $x_1 = x_{\mathrm{a}} - x_s$, $x_2 = x_{\mathrm{s}}$, $x_3 = \dot{x}_{\mathrm{a}}$, and $x_4 = \dot{x}_{\mathrm{s}}$. Respectively y is the matrix of measured accelerations of absorber mass and structural mass, $y = [\ \ddot{x}_{\mathrm{a}} \quad \ddot{x}_{\mathrm{s}}\ ]'$, $w(\cdot) = F_{ex}(\cdot)$ is the system disturbance and system control input is $u = F_{MR}$. Thus the system state space representation is;

$$\begin{bmatrix} \dot{x}_1 \\ \dot{x}_2 \\ \dot{x}_3 \\ \dot{x}_4 \end{bmatrix} = \begin{bmatrix} 0 & 0 & 1 & -1 \\ 0 & 0 & 0 & 1 \\ -\frac{k_a}{m_a} & 0 & 0 & 0 \\ \frac{k_a}{m_{\mathrm{s}}} & -\frac{k_{\mathrm{s}}}{m_{\mathrm{s}}} & 0 & -\frac{c_s}{m_{\mathrm{s}}} \end{bmatrix} \begin{bmatrix} x_1 \\ x_2 \\ x_3 \\ x_4 \end{bmatrix} + \begin{bmatrix} 0 \\ 0 \\ -\frac{1}{m_{\mathrm{a}}} \\ \frac{1}{m_s} \end{bmatrix} u + \begin{bmatrix} 0 \\ 0 \\ 0 \\ \frac{1}{m_s} \end{bmatrix} w(t) \tag{7.20}$$

$$\begin{bmatrix} \dot{x}_3 \\ \dot{x}_4 \end{bmatrix} = \begin{bmatrix} -\frac{k_a}{m_a} & 0 & 0 & 0 \\ \frac{k_a}{m_s} & -\frac{k_s}{m_s} & 0 & -\frac{c_s}{m_s} \end{bmatrix} \begin{bmatrix} x_1 \\ x_2 \\ x_3 \\ x_4 \end{bmatrix} + \begin{bmatrix} -\frac{1}{m_a} \\ \frac{1}{m_s} \end{bmatrix} u + \begin{bmatrix} 0 \\ \frac{1}{m_s} \end{bmatrix} w(t) \quad (7.21)$$

where, $A = \begin{bmatrix} 0 & 0 & 1 & -1 \\ 0 & 0 & 0 & 1 \\ -\frac{k_a}{m_a} & 0 & 0 & 0 \\ \frac{k_a}{m_s} & -\frac{k_s}{m_s} & 0 & -\frac{c_s}{m_s} \end{bmatrix}$, $B = \begin{bmatrix} 0 \\ 0 \\ -\frac{1}{m_a} \\ \frac{1}{m_s} \end{bmatrix}$, $G = \begin{bmatrix} 0 \\ 0 \\ 0 \\ \frac{1}{m_s} \end{bmatrix}$,

$C = \begin{bmatrix} -\frac{k_a}{m_a} & 0 & 0 & 0 \\ \frac{k_a}{m_s} & -\frac{k_s}{m_s} & 0 & -\frac{c_s}{m_s} \end{bmatrix}$, $D = \begin{bmatrix} -\frac{1}{m_a} \\ \frac{1}{m_s} \end{bmatrix}$, and $H = \begin{bmatrix} 0 \\ \frac{1}{m_s} \end{bmatrix}$.

The following dynamical system 7.22 is considered as an observer.

$$\begin{aligned} \dot{\underline{\hat{x}}} &= A\underline{\hat{x}} + Bu + Lz + G\hat{F}_{ex} \\ \hat{y} &= C\hat{x} + Du + H\hat{F}_{ex} \end{aligned} \quad (7.22)$$

$$\hat{F}_{ex} = m_s\ddot{x}_s - \hat{F}_{MR} + k_s(\hat{x}_s) + k_a(\hat{x}_s - \hat{x}_a) + c_s(\dot{\hat{x}}_s) \quad (7.23)$$

where, $z = y - \hat{y}$, $\dot{\underline{\hat{x}}}$ is the observer state, $\hat{y}$ is the observer output, $\hat{F}_{ex}$ is the estimated disturbance force signal (Equation 7.23) and L is the observer gain matrix. The error between the actual state x and the observed state $\hat{x}$ is defined as

$$e = \underline{x} - \underline{\hat{x}} \tag{7.24}$$

where the dynamics of the state estimation error is then given by ;

$$\dot{e} = (A - LC)e + (G - LH)(F_{ex} - \hat{F}_{ex}) \tag{7.25}$$

here L is the 4x2 observer gain matrix. Several numerical and experimental test results showed that with a proper observer matrix the estimated disturbance force and the actual disturbance force matched each other. The pole placement method was used to evaluate the observer gain matrix [154].

$$L = \begin{bmatrix} l_1 & l_2 \\ l_3 & l_4 \\ l_5 & l_6 \\ l_7 & l_8 \end{bmatrix}$$

As explained for the non-linear SDOF observer (Section 5.2.3), the dynamics of the observer for adaptive TMD system were chosen to be 5 times slower than the actual system due to un-modelled friction inside the MR damper. The simulated model of the observer based adaptive TMD with an MR damper system is shown in Figure 7.4.

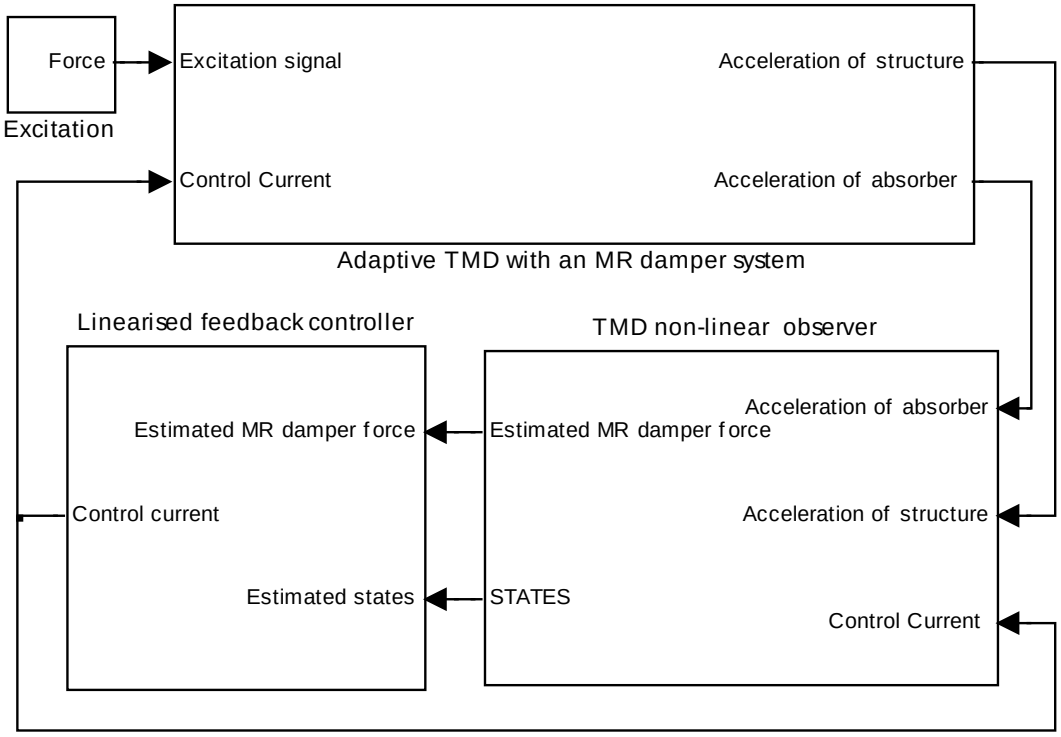

Figure 7.4: Simulated model of observer based linearised control of TMD with a controllable MR damper.

7.5 Main principle and control concepts

The proposed approach uses the same feedback linearisation control of an MR damper which has been investigated in the previous chapters. But the goal of this case study, is to emulate controllable viscous damping and/or controllable spring stiffness of the equivalent optimal passive system. As seen in Figure 7.2, this desired damper force is produced by control concept part, which uses the estimated states of the system. Two types of control concept are proposed, which are explained as;

Control concept 1

The first control concept is intended to simply linearise the non-linear dynamics of the MR damper, so it behaves as a linear viscous damper with varying linear damping. With reference to Figure 7.5 the estimated desired set-point force is;

$$\hat{F}_{desired} = c_a(\dot{\hat{x}}_s - \dot{\hat{x}}_a) \tag{7.26}$$

where $\hat{F}_{desired}$ is the estimated desired damper force, c_a is the optimal absorber damping, and $(\dot{\hat{x}}_s - \dot{\hat{x}}_a)$ is the relative piston velocity.

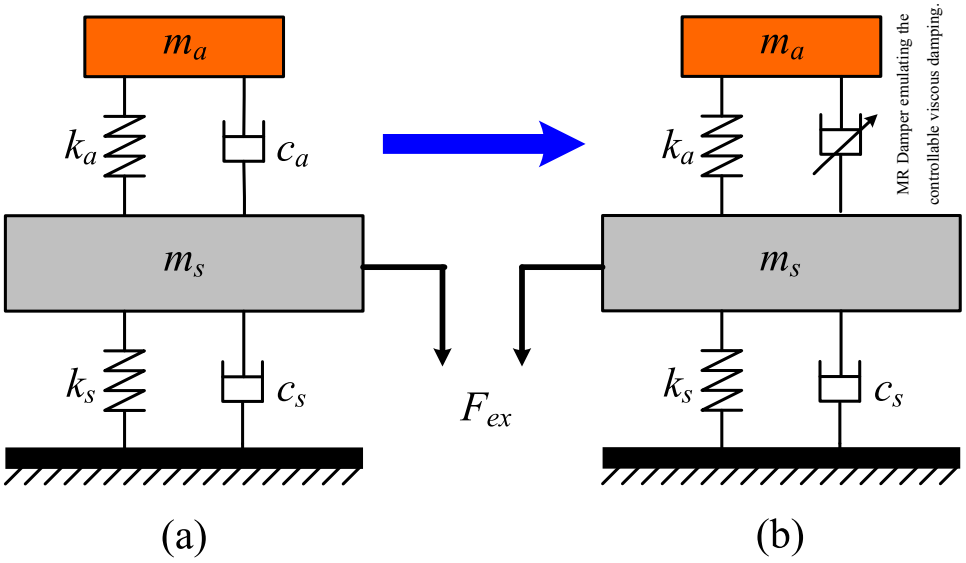

Figure 7.5: Lumped parameter models of tuned mass damper configurations. (a) passive tuned vibration absorber, (b) Semi-active MR based tuned vibration absorber (concept 1).

In this concept, the MR damper just emulates the optimal viscous damping of the passive tuned mass damper system.

Control concept 2

In the second control concept, the MR damper tries to emulate the optimal viscous damping and optimal spring stiffness of the passive tuned mass damper system. In this concept, optimal controllable spring stiffness is going to be the sum of the emulated controllable stiffness and passive spring stiffness of the proposed system (as seen in figure 7.1-(b)) due to parallel installation of the passive spring and controllable MR damper. This will enable frequency tuning of the TMD system by attempting to emulate the controllable positive or negative spring stiffness, and controllable damping force. Referring to Figure 7.1 -(b), the estimated desired set-point force is given by;

$$\hat{F}_{desired} = c_{a,opt}(\dot{\hat{x}}_s - \dot{\hat{x}}_a) + k_{added}(\hat{x}_s - \hat{x}_a) \tag{7.27}$$

where $(\hat{x}_s - \hat{x}_a)$ is the relative piston displacement, and k_{added} is the controllable stiffness which was assumed to be zero for control concept 1. But, for the control concept 2, $k_{added} = k_{a,opt} - k_a$.

These two control concepts are investigated by numerical and experimental testing. Tests are carried out in four steps with assumption that the absorber mass (m_a), absorber stiffness (k_a), structural spring stiffness (k_s) and structural damping (c_s) do not change at any step of testing. Then, $k_{a,opt}$ and $c_{a,opt}$ can be adjusted to the actual frequency of the main structure according to Mead's formulae without any constraints [6]. The testing step are:

- Step one: tuning of main structure. Optimal structural parameters are evaluated by using the inversed optimisation to the define lumped parameter system shown in Figure 7.5. By replacing the passive oil damper with an MR damper the proposed adaptive TMD is created, and the desired force is driven by the control concept 1,

Equation 7.28.

$$\hat{F}_{desired} = c_a(\dot{\hat{x}}_s - \dot{\hat{x}}_a) \tag{7.28}$$

- Step two is the de-tuning of the main structure. In this step, the service load of main structure is changed by adding or removing masses to/from main structure. The new structural mass becomes, $\bar{m}_s = m_s + m_d$, where m_d represents change of the service load (which could be positive or negative). Assuming the structural stiffness does not change, the system frequency ratio changes, and this leads to the detuned system as shown in Figure 7.6.

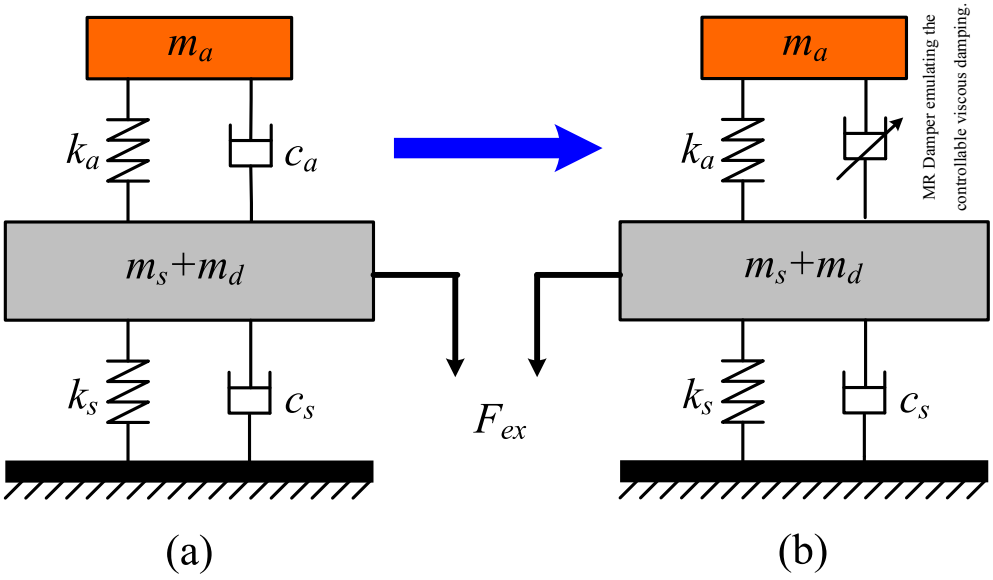

Figure 7.6: Detuned lumped parameter models of detuned mass damper configurations. (a) passive detuned vibration absorber, (b) Semi-active MR based detuned vibration absorber (step 2).

In this de-tuned case, the adaptive TMD with controllable MR damper is linearised to

emulate the pre-tuned viscous damping of the optimal passive pre-tuned damper system as in concept 1, Equation 7.28.

- Step three: retuning of damping. The analytical frequency retuning of the detuned absorber is done according to Mead's optimisation theory [6] by using the de-tuned structural mass ($\bar{m}_s$) and unchanged structural stiffness (k_s) as seen in Figure 7.7.

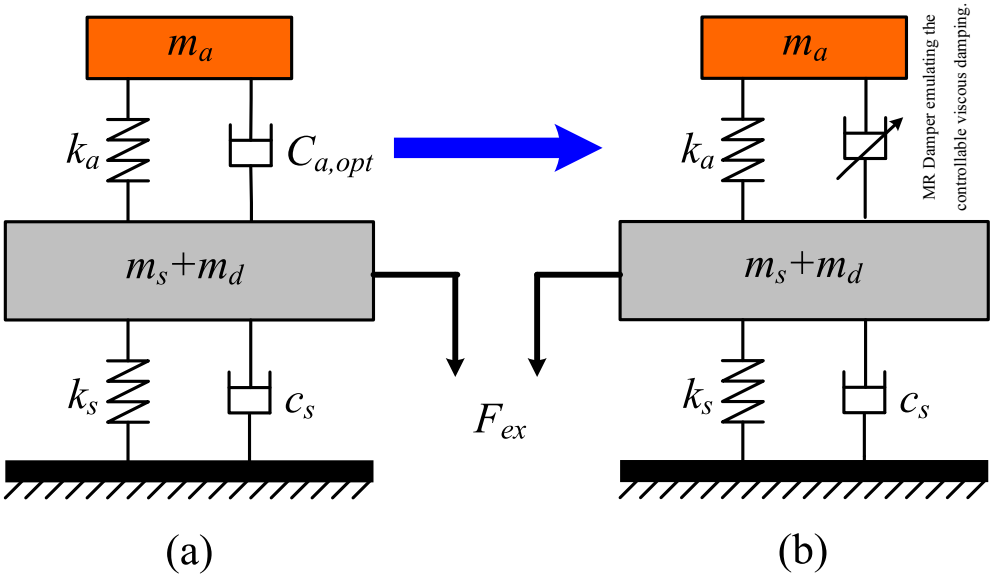

Figure 7.7: Detuned lumped parameter models of retuned mass damper configurations. (a) passive retuned vibration absorber, (b) Semi-active MR based retuned vibration absorber (step 3).

In this study, it is assumed that, structural mass of this new detuned could be estimated by empirical mode decomposition and Hilbert transform (EMD/HT) [183], or modified cross-correlation (MCC) method [172] in the real-time control process. So that, the frequency of the absorber system could be tuned to the actual frequency of the main structure by adjusting k_a to $k_{a,opt}$ and c_a to $c_{a,opt}$. This retuned passive TMD system is called as ideal adaptive TMD and expected to equalize the response peaks according to theory. In this step, just viscous damping was retuned so that MR damper only emulates the viscous

damping of the passive TMD and estimated desired force was chosen by control concept 1 as in Equation 7.29:

$$\hat{F}_{desired} = c_{a,opt}(\dot{\hat{x}}_s - \dot{\hat{x}}_a) \tag{7.29}$$

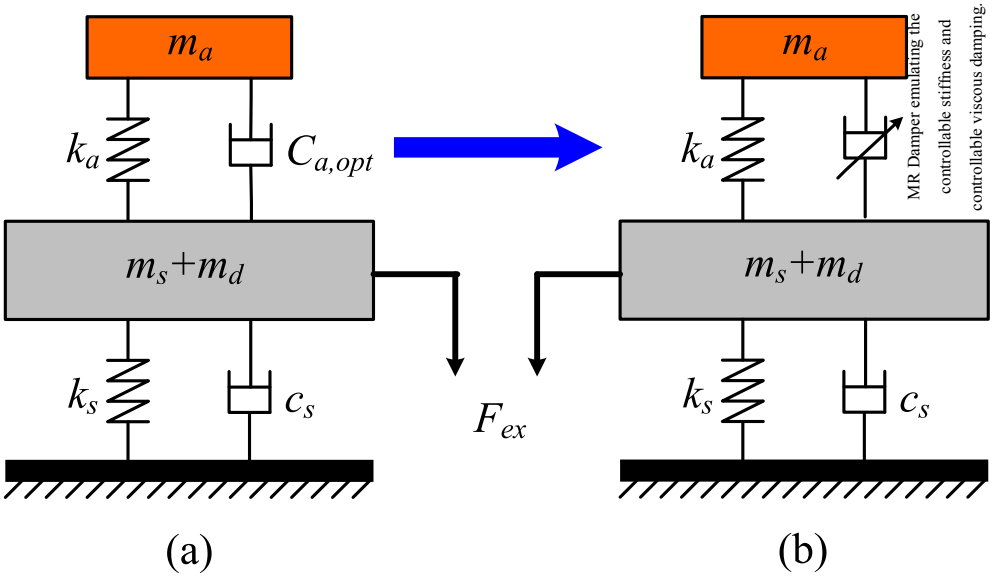

Figure 7.8: Detuned lumped parameter models of retuned mass damper configurations. (a) passive retuned vibration absorber, (b) Semi-active MR based retuned vibration absorber (step 4).

- Step four: retuning of damping and stiffness. In this step retuning of the stiffness element of the passive TMD was done according to theory. The estimated desired force was chosen by the control concept 2 so that the MR damper is forced to emulate the retuned viscous damping and retuned spring stiffness of the new retuned ideal adaptive TMD as seen in Figure 7.8 , as in equation 7.27.

7.6 Numerical testing

In this case study, the aim is to implement the proposed observer based linearised control of an MR damper system to the tuned mass damper problem, so that MR damper could emulate the controllable viscous and spring stiffness of the passive TMD. This section intends to numerically investigate this scenario with pre-chosen SDOF system parameters. Referring to the equations 7.12-7.17, the structural parameters are evaluated and listed in Table 7.1.

Parameter	Symbol	Unit	Value
Mass of absorber	m_a	kg	112
Mass of structure	m_s	kg	182.89
Absorber stiffness	k_a	Nm^{-1}	62690
Structural stiffness	k_s	Nm^{-1}	266140
Absorber damping	c_a	Nsm^{-1}	2000
Structural damping	c_s	Nsm^{-1}	50

Table 7.1: Optimal parameters of passive tuned mass damper.

These values implied that the optimal designable structure with pre-arbitrary chosen SDOF system has the mass ratio of 0.6124. However, according to [160], the optimal mass ratio (m_s/m_a) design approach for tuned mass damper may be chosen in the range of 1/15 to 1/50 for required vibration reduction. In other words, the coil spring stiffness and mass of the experimental absorber were too small to represent a realistic scenario. In order to catch this criteria, in the simulations the original SDOF parameters are modified such that natural frequency remains unchanged by four time increasing absorber mass and absorber spring stiffness. New modified optimal parameters are given in Table 7.2 with a mass ratio is equal to 0.0243 which lies in the realistic range [160]. The observer gain matrix is than evaluated by using pole placement method such as;

$$L = 10^{-3} \begin{bmatrix} -0.0009 & 0.0002 \\ 0.0003 & -0.0001 \\ 951.3691 & -25.3155 \\ 5.5240 & 969.9747 \end{bmatrix}$$

Parameter	Symbol	Unit	Value
Mass of absorber	m_a	kg	448
Mass of structure	m_s	kg	18425
Absorber stiffness	k_a	Nm^{-1}	250760
Structural stiffness	k_s	Nm^{-1}	10821000
Absorber damping	c_a	Nsm^{-1}	2000
Structural damping	c_s	Nsm^{-1}	50

Table 7.2: Modified parameters of passive tuned mass damper for numerical case study.

The main structure with optimal passive TMD and a observer based adaptive TMD with controllable MR damper is simulated for varied de-tuned structural masses $\widetilde{m}_s = 0.5m_s$, $0.6m_s$, ..., $1.5m_s$ and for each mass the structure is excited with high-pass filtered random white noise force signal with bandwidth of 0-15 Hz during 300 seconds, for each of the four steps. The first ten seconds of this excitation force signal is shown in Figure 7.9. The test results will indicate the damping potential of the proposed theory. The entire system is solved in MATLAB/Simulink using the ode4 (Runge Kutta) solver with fixed sampling frequency of 0.0002 Hz. The absorber viscous damper is replaced by the numerical unified model of MR damper (Chapter 5.2.1) where depending on the control concept, the MR damper will track the estimated desired force.

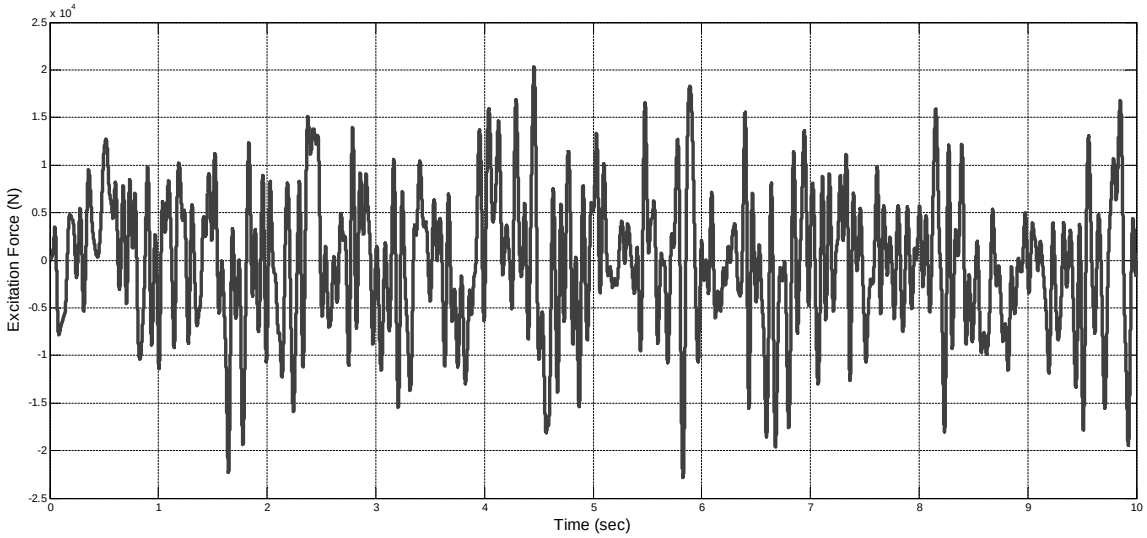

Figure 7.9: First ten seconds of the excitation force signal.

7.6.1 Numerical test results

Frequency response curves are used to analyse the performance of the each control concepts for numerical and experimental testing, which is evaluated by using tfestimate method of Simulink software.

A random force excitation signal, filtered with 15 Hz high pass filter, was used to excite set-up as seen in Figure 7.9.

The first frequency response plot indicates that the passive TMD is able to equalise the peaks at resonance amplitude, according the Mead's theory as seen in Figure 7.10 (solid line, step 1 tuning). But, the damping performance dramatically decreases with detuning of the system (dotted, dashed and dash-dotted lines, step 2). Also it is clear that from the Figure 7.10, if the detuning is done with increased structural mass, the host structure is over-damped with an almost un-damped absorber resonance frequency; whereas if the detuning process is done with decreased structural mass, the resonance frequency

amplitude of the absorber is over-damped and the structural resonance is un-damped. As expected, Figure 7.11 illustrates that the amplitude reduction of the ideal adaptive TMD (with retuned damping and stiffness), depends on the frequency of the main structure.

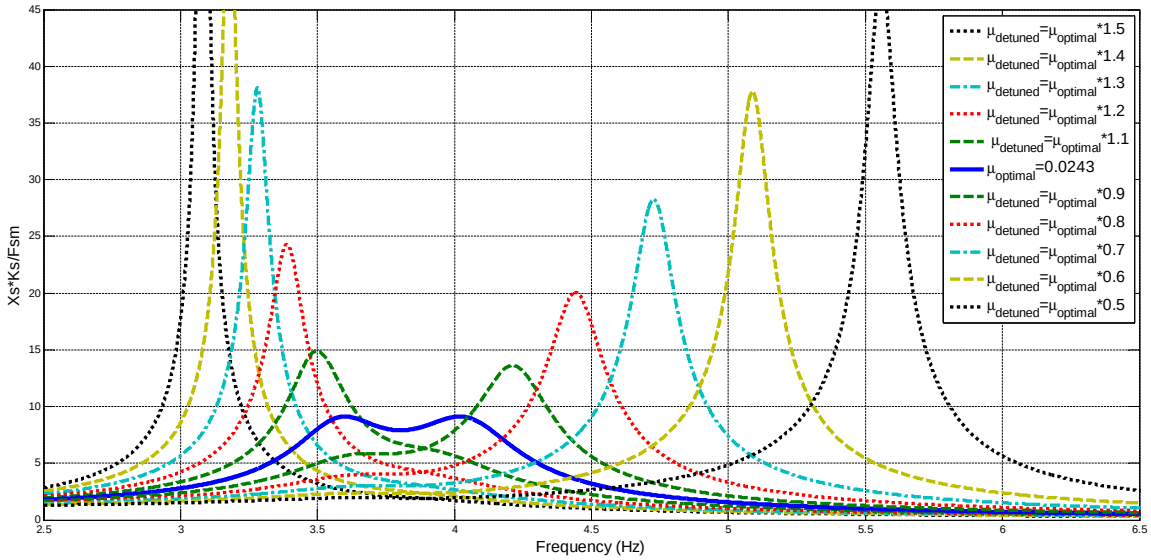

Figure 7.10: Frequency responses of the passive TMD, for optimally tuned case (step 1, solid line) and detuned cases (step 2, dotted, dashed and dash-dotted lines).

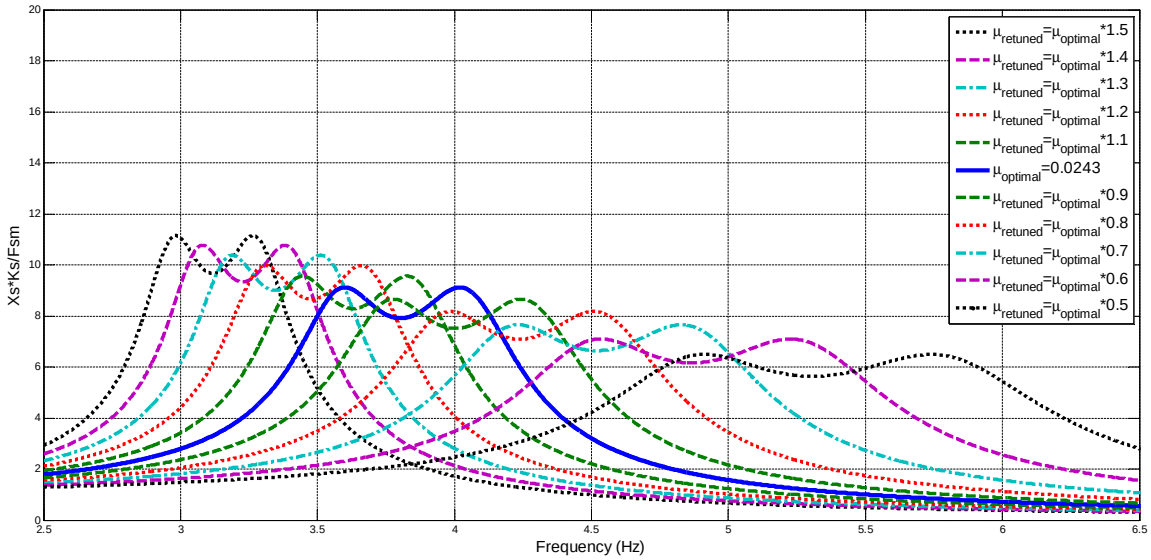

Figure 7.11: Frequency responses of the ideal adaptive TMD, for step 1 (solid line), and step 3 (dotted, dashed and dash-dotted lines).

The frequency response of the observer based adaptive TMD with linearised MR damper controlled according to concept 1 is shown in Figure 7.12. It is already been shown, that the observer based feedback linearisation is able to emulate a linear viscous damper (Chapter 6). So if the desired force gain is chosen as the viscous damping c_a of the passive tuned mass system, then it is expected to achieve the same amplitude reduction for tuned and detuned cases of passive TMD. Comparing Figure 7.10 and Figure 7.12 clearly proves that for the step 1, the observer based adaptive TMD with linearised MR damper is able to equalize the peak for tuned values (solid line). In addition, also for the step 2 (detuned case), it is also able to follow the performance of the passive TMD (dotted and dashed lines).

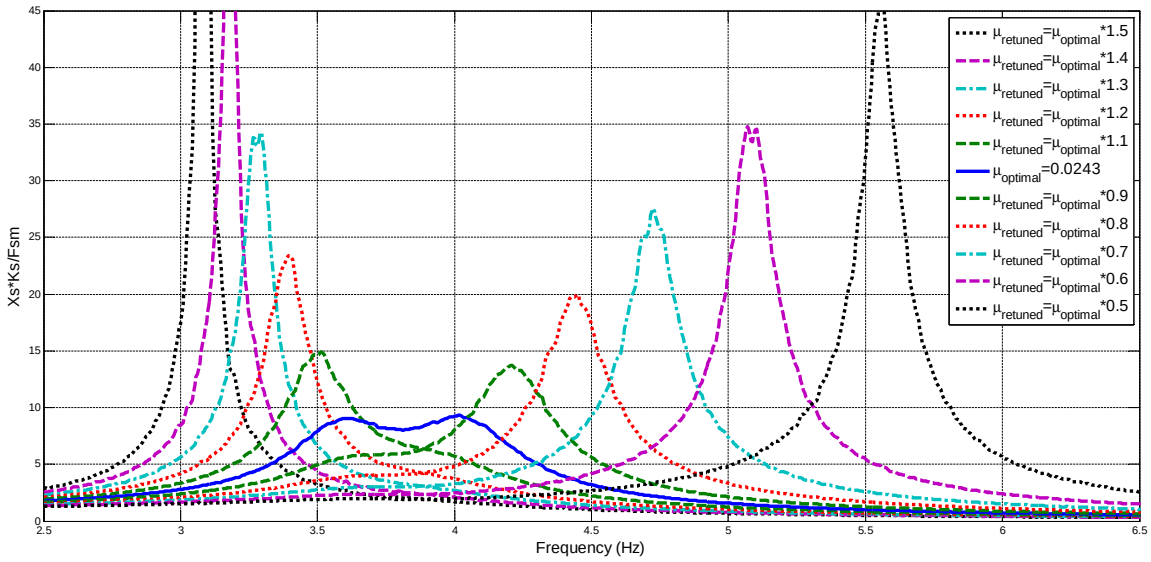

Figure 7.12: Frequency responses of the adaptive TMD with linearised MR damper, for optimally tuned case (step 1,solid line), and de-tuned cases (step 2, dotted, dashed and dash-dotted lines).

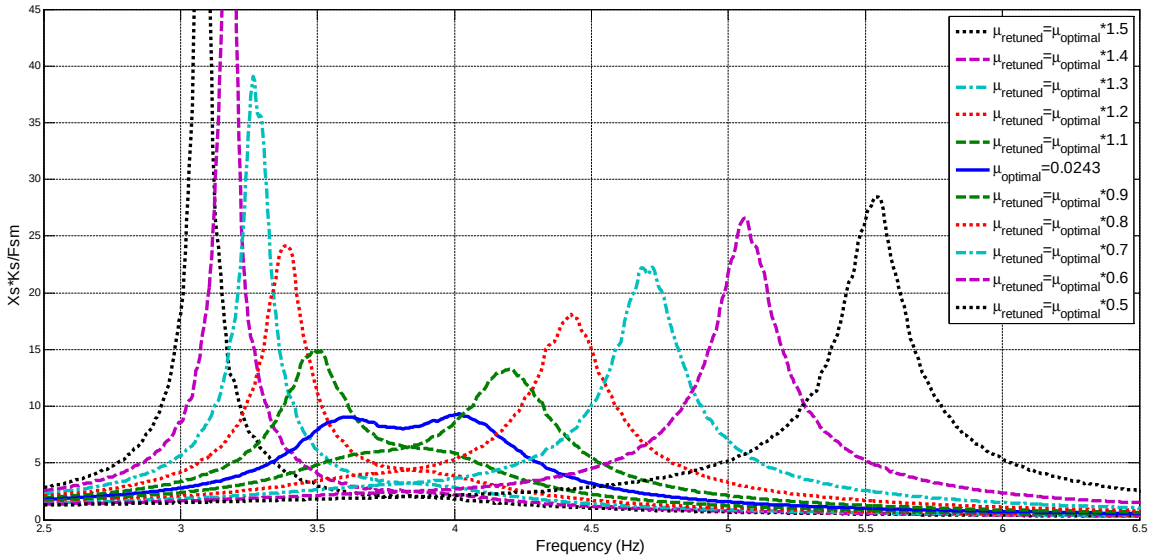

Figure 7.13: Frequency responses of the adaptive TMD with linearised MR damper, for optimally tuned case (step 1,solid line), and re-tuned cases (step 3, dotted, dashed and dash-dotted lines).

If the detuned system is retuned as in step 3 with control concept 1, then the observer based adaptive TMD with linearised MR damper improves the amplitude reduction compared to the passive TMD as seen in Figure 7.13. But, if the system is detuned with increased structural mass the frequency of the detuned structure get closer to the frequency of the absorber, which has greater effect on the system response. On the other hand, if the system is detuned with decreased mass, frequencies of host structure and the absorbers move away from each other.

However, the aim of this case study to investigate that whether the observer based linearised MR damper can emulate the controllable stiffness and viscous damping or not. To find this out, the last numerical tests step 4 and control concept 2 are implemented, where the linearised MR damper will emulate both damping and stiffness forces. The results are shown in Figure 7.14, where up to several 100% amplitude reduction is achieved for the observer based adaptive TMD with linearised MR damper.

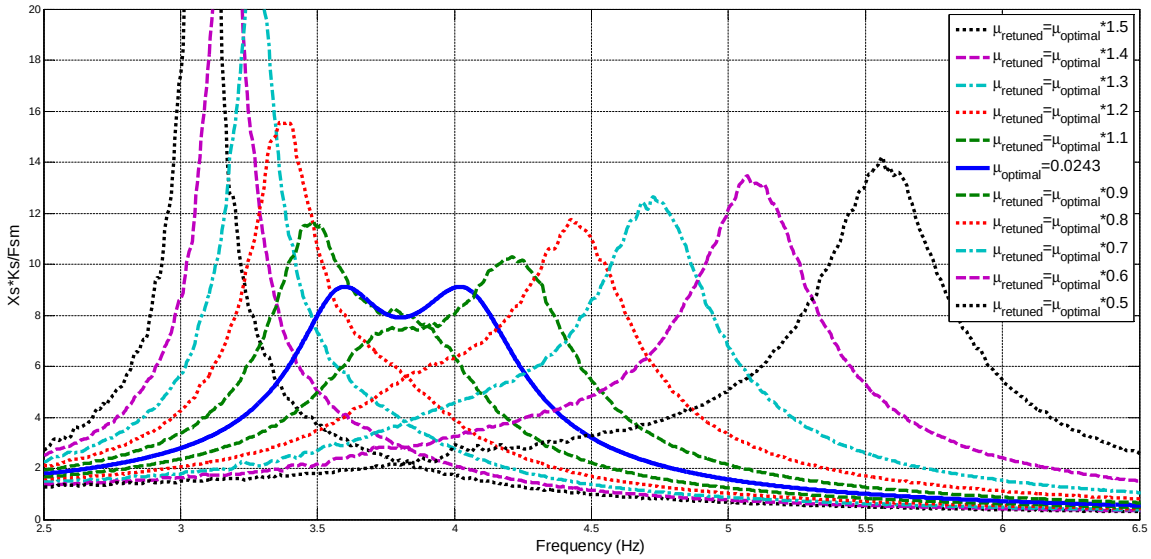

Figure 7.14: Frequency responses of the adaptive TMD with linearised MR damper, for optimally tuned case (step 1, solid line) and re-tuned with controllable viscous damping and controllable stiffness cases (step 4, dotted, dashed and dash-dotted lines).

To summarise, these numerical test results with a realistic mass ratio ($\mu_{opt} = 0.0243$) show that the observer based linearisation of an adaptive TMD is able to emulate the positive or negative stiffness in addition to providing energy dissipation in the TMD.

7.7 Experimental testing

In the previous section, numerical simulations were performed to show the effectiveness of using observer base feedback linearisation of an MR damper as a semi-active force generator, so that the MR damper can emulate the controllable spring stiffness and controllable viscous damping. The present section is aimed to build upon this work by performing experiments of an adaptive TMD system subject to the broadband force excitation. The Hardware-in-the-loop-simulation (HILS) method is used to perform the experiments, which is shown in Figure 7.15. Here, tuned mass damper system is physically tested,

whilst the real-time control software is used to simulate the non-physical elements of the system, which are the damping, stiffness and the mass of the host structure.

With reference to Figures 4.1 and 4.3, the damper test facility was configured for HILS testing as follows. Real time control software was used to develop the controllers, the non-linear observer, and the non-physical system of the host structure (mass, m_s, damping c_s, and stiffness k_s) on the host PC. These were downloaded onto the target PC, which performed the real-time simulation by transferring data to and from the hardware via the data acquisition card. Using D/A conversion, outputs from this simulation (structural displacement, x_s and control current, I_{MR}) are then used to excite MR damper based absorber using a servo-hydraulic actuator and current amplifier. Simultaneously, an A/D converter provides the simulation with structural and absorber accelerations data in order to estimate the states and damping force. These estimated states and damping force are used by controller to generate the desired control current and also they are used to generate the force transmitted to host structure from absorber, which is used for simulation of host structure. Here the experimental SDOF system (see Figure 4.5-(b)) with a controllable MR damper (Lord Corporation's RD-8040-1 [75]) is used to perform the HILS tests and described in Chapter 4.3. The experimental test model is shown in Figure 7.16. As seen in Figure 7.16, same scaling values were used to calibrate the load-cell, LVDT, current amplifier, and actuator as in Chapter 6.

In reality, the HILS system is proposed to use the physical force to excite simulated model of the structure, but instead the estimated force is used in this study. So, the unwanted noise captured by the force transducers was avoided, and the comparison of the actual and estimated force showed that the difference is negligible.

System parameters for experimental testing are shown in Table 7.1. It is accepted that there is no need to validate the numerical model with the experimental test rig, as this was already validated in Chapter 4. The experimental observer gain matrix is evaluated by using pole placement method such as;

$$L = 10^{-3} \begin{bmatrix} -0.0419 & -0.0168 \\ -0.0305 & -0.0173 \\ 860.3032 & -60.9661 \\ -72.9972 & 956.6894 \end{bmatrix}$$

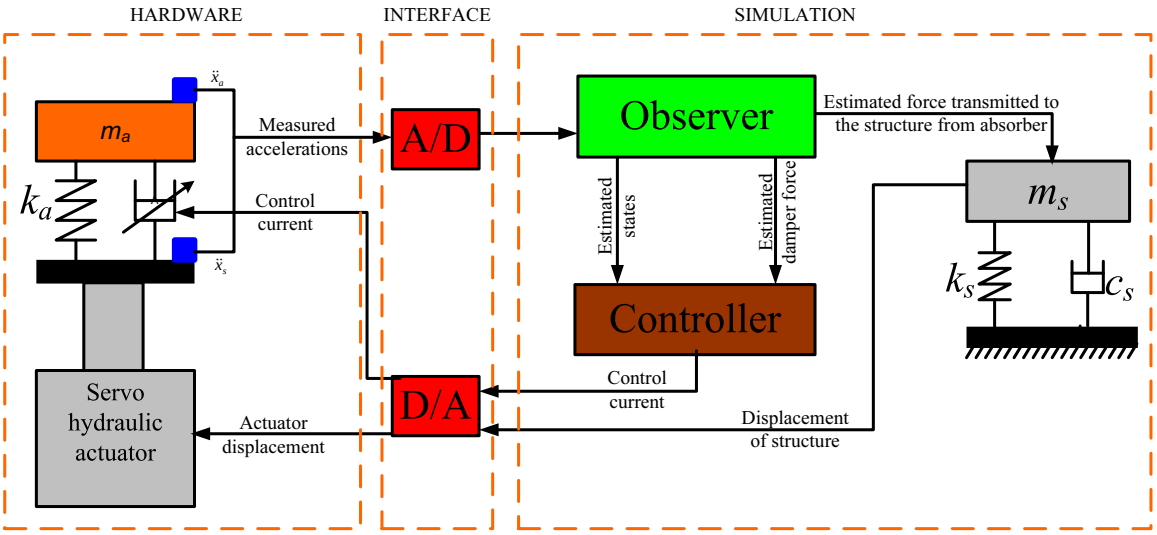

Figure 7.15: Schematic diagram of the HILS system.

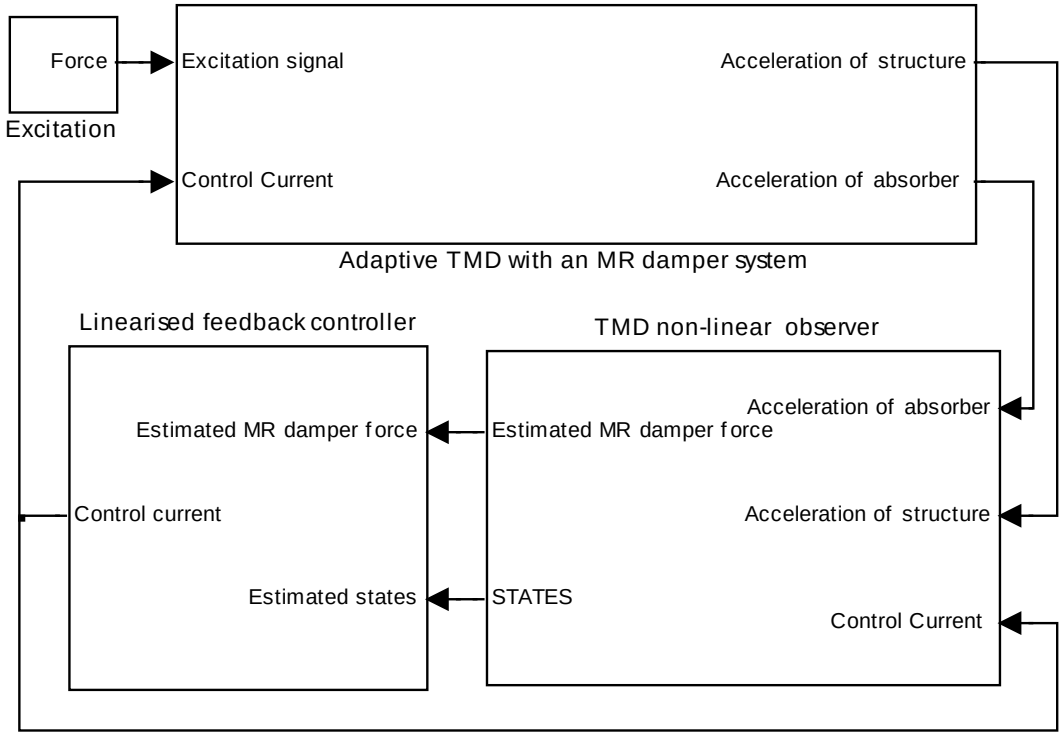

Figure 7.16: Experimental system for observer-based control of tuned mass damper system.

However, the implementation of the HILS system introduces the additional dynamics to the system, which affects the stability and the performance of the experimental testing. Batterbee investigated the accuracy of the servo-hydraulic system model, with the frequency response anlysis [184]. Where, the range of the excitation frequency (0-50 Hz) was chosen to be relatively higher than the bandwidth of the test facility (40 Hz), and good magnitude and phase response were predicted by the servo-hydraulic system. In addition, the author, described the dynamics characteristics of the two-stage electronic servo valves (38l/min Moog D765) and the Kepco BOB current amplifier (which is able to generate DC output in the range of ±36V and ±6A with bandwidth of 13kHz) [146]. In conclusion, the servo-hydraulic system have proper dynamic characteristic to minimise the phase delay

and improve the control performance [184]. For this study, under these specification, it is assumed that the servo-hydraulic test facility with the MR damper current amplifier is suitable for HILS testing.

7.8 Results and Discussion

The testing steps were now re-implemented with the HILS system. First the transfer function was estimated according to step 1 and control concept 1 which was followed by step 2, detuning and applying control concept 1. Retuning process of detuned system was evaluated (step 3) and control concept 1 was applied. Last tests were carried out with step 4 and control concept 2. The difference from the numerical testing was the different optimal parameters of the system were used, shown in Table 7.1 with an optimal mass ratio of $\mu_{opt} = 0.6124$. Four detuned cases were investigated, which were established by 20%, and 50% increased and decreased structural mass.

Estimated transfer function of the all these experimental tests are shown in Figures 7.17-7.20. Solid lines represent the observer based optimal adaptive TMD with linearised MR damper for step 1 and control concept 1, these solid lines also follows the optimal passive TMD behaviour, dashed lines illustrate the step 2, detuned cases with control concept 1, these dashed lines also follows the detuned passive TMD behaviour, dotted lines exhibit step 3 with control concept 1 where the detuned system was retuned again and last frequency response plotted with dash-dotted lines for step 4 of control concept 2 in these figures. These estimated frequency responses show that the proposed observer based adaptive TMD with linearised MR damper outperforms the the passive TMD in all tested cases relatively also they exhibit same characteristic as the numerical results.

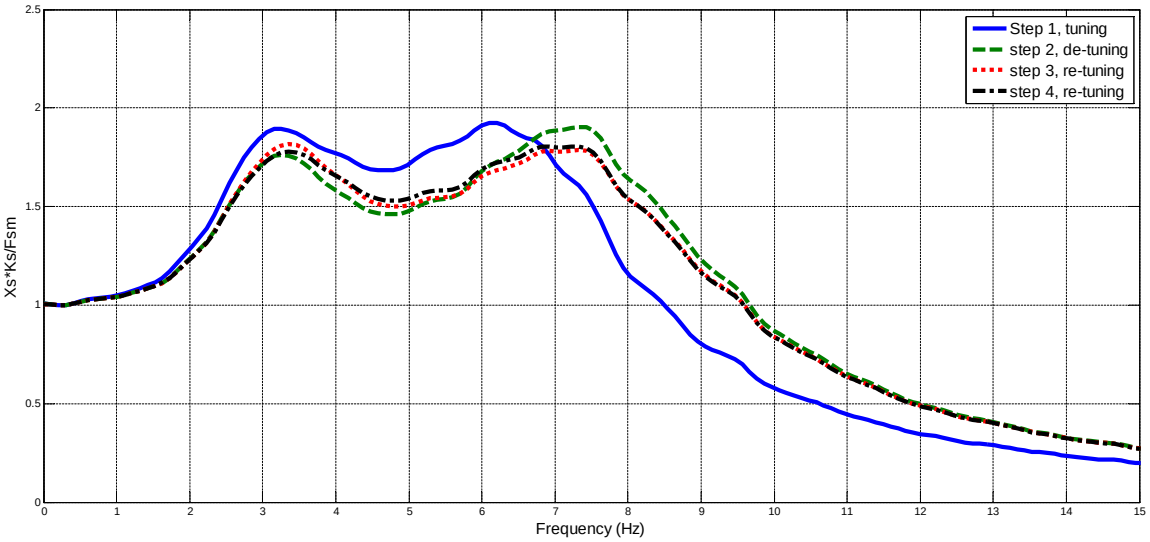

Figure 7.17: Experimental test results for adaptive TMD with linearised MR damper when de-tuned by 20 percent reduced structural mass.

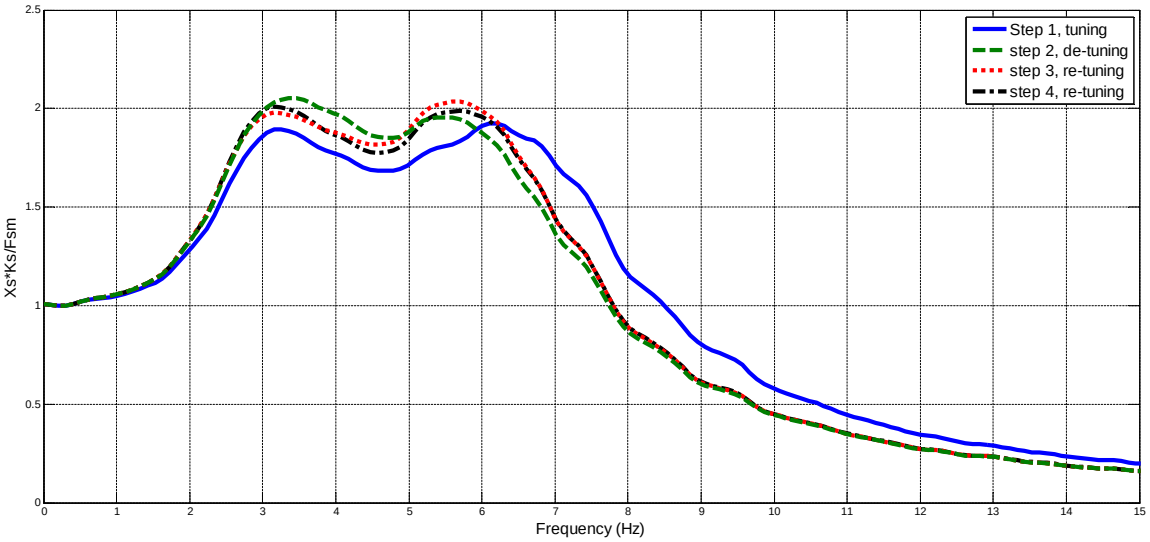

Figure 7.18: Experimental frequency response of adaptive TMD with linearised MR damper with 20 percent detuned by increased structural mass.

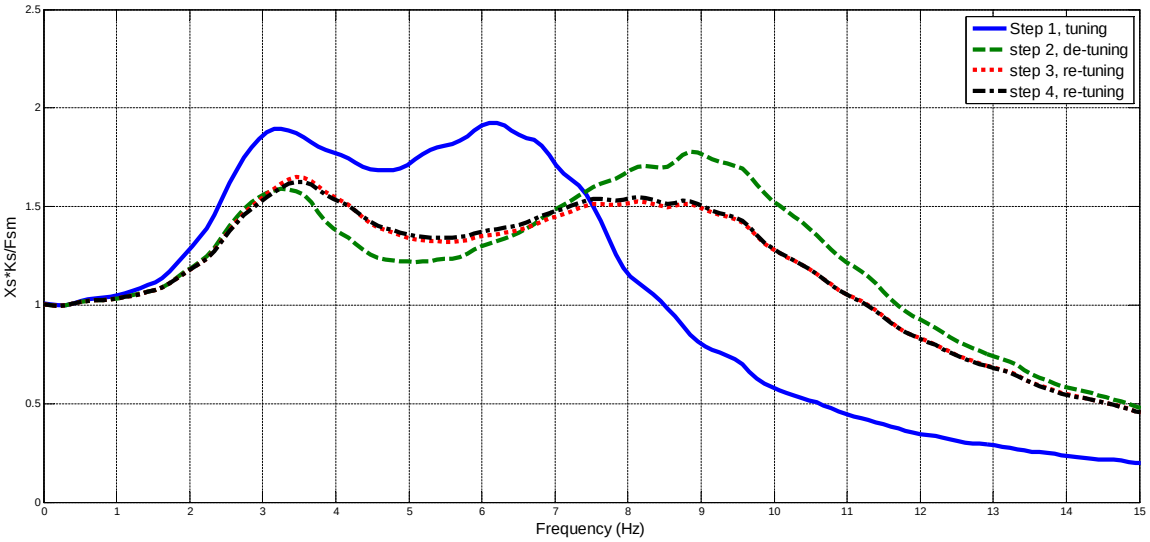

Figure 7.19: Experimental frequency response of adaptive TMD with linearised MR damper with 50 percent detuned by reduced structural mass.

In conclusion, both the numerical and experimental results clearly indicate that, it is possible to emulate the controllable viscous damping and negative or positive controllable spring stiffness, so as to match classical vibration absorber theory [6].

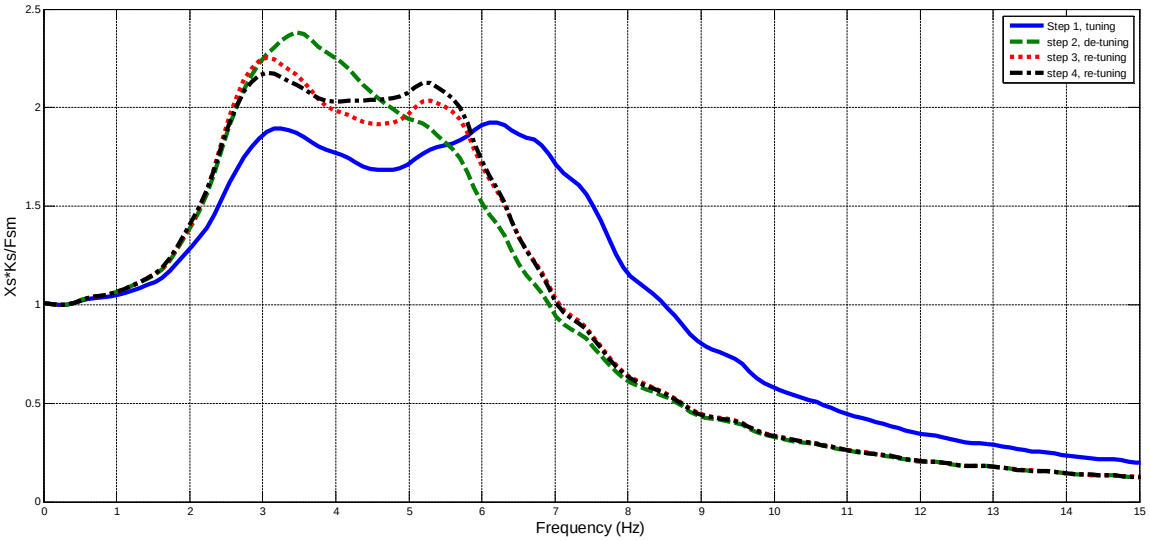

Figure 7.20: Experimental frequency response of adaptive TMD with linearised MR damper with 50 percent detuned by increased structural mass.

7.9 Summary of Chapter 7

This chapter has described numerical and HILS experimental investigations of an observer based adaptive tuned mass magnetorheological damper that attempts to mitigate random vibrations of the main structure. Here, the hardware-in-the-loop simulation (HILS) method was adopted, which enabled the complex behaviour of the TMD (with a controllable MR damper) to be physically tested, whilst the remainder of the system dynamics were simulated in real-time. Numerical models were also evaluated.

Two control concepts have been presented representing different approaches to retuning or adopting the system. Control concept 1, simply converted the non-linear MR to the linear viscous device with varying damping rates. Control concept 2 was the goal of the chapter; this was used to control the MR damper to emulate positive or negative stiffness in addition to providing the energy dissipation in the TMD. The positive or negative stiffness decreases or increases the stiffness of the passive TMD spring and thereby adjusts the TMD to the actual frequency of the main structure according to classical theory. The performance of these control concepts has been tested by varying the structural mass $\bar{m}_s$, over a wide range. The numerical model of system uses the modified parameters (Table 7.2) of the passive TMD to exhibit more realistic dynamics of the problem while the optimal parameters (Table 7.1) were used for experimental testing due to the pre-determined test rig parameters.

The frequency response results have been compared to the damping performances of the passive TMD and an ideal adaptive TMD where ideal adaptive TMD has been determined as a benchmark for this study. Simulated and experimental results have demonstrated that the damping performance of the observer based adaptive TMD with a linearised MR damper exceeds that of a passive TMD significantly, depending on the parameters

changed in the main structural mass.

8 Conclusions and further work

This research has focused on the observer-based feedback linearised control of an MR damper under the harmonic and broadband mechanical excitations. To conclude the thesis, a summary of each chapter is provided, which is followed by conclusions and the discussion of the key contributions to knowledge.

8.1 Summary

The introduction of this thesis gave the description of the relative merits of passive, active, and semi-active vibration control methods, and suggested that semi-active schemes can offer an attractive compromise between the low cost and simplicity of passive systems, and the high performance of active systems, which are heavier, more complex, and have significant power requirements. This was followed by history of the smart fluids and semi-active vibration control, as a literature review for this research. In particular, MR dampers were identified as one of the most promising means to implement semi-active vibration control.

The proposed theory of observer based feedback linearisation of an MR damper was explained in Chapter 3. A single-degree-of freedom structure was chosen as the basis for this study. One way to convert the highly non-linear smart device (MR damper) into a variable semi-active force generator was discussed by using estimated states and estim-

ated damping force, instead of measured values which increase the complexity of the system. In particular, the proposed linearisation method uses force feedback to linearise the force/velocity response of the MR damper, but this relies on knowledge of the actual damper force.

In Chapter 4, the experimental test facility used for this research was described in detail, and some preliminary test results were used to validate the open loop and closed loop responses of the MR damper device under sinusoidal and random excitations. The experimental results show considerable agreement with the predicted model, which makes further numerical modelling feasible.

The aim of Chapters 5 and 6 was to investigate observer based control strategies for broadband excited MR vibration systems. Numerical studies of observer based single-degree-of-freedom (SDOF) MR vibration systems was performed in Chapter 5. Three types of MR damper model were investigated; basic, complex and unified model. In order to validate the performance of the proposed non-linear observer, each of these MR models are used to implement the SDOF system with a feedback linearised controller. The numerical results have showed that the non-linear observer is able to estimate states with small error even, the modelling of friction inside the observer has been mismatched with the real value. Also, using observer-based sky-hook based control laws, feedback linearisation was been shown to outperform more simplistic observer-based on/off controllers and equivalent passive systems, whilst approaching that of observer-based ideal semi-active and fully active schemes.

In Chapter 6, the results from this numerical study were further validated by the experimental investigations of observer based SDOF MR vibration system. Here, a high

response servo hydraulic actuator was used to excite the observer based SDOF mass isolation system. The non-linear observer and controller were implemented in a real time digital system. The performance of observer based feedback linearisation was investigated by implementing sky-hook based controllers, where comparisons were made with more simplistic on/off controllers, optimal controllers, and the passive case. The results have validated the numerical performance of the proposed system.

The last chapter aimed to investigate the performance of the proposed theory for the real structural vibration problem, where a tuned mass damper system was chosen as case study for this research. Numerical and hardware-in-the-loop simulation (HILS) experimental testing was carried out. The HILS method enabled the complex behaviour of the adaptive semi-active TMD with a controlled MR damper to be physically tested, whilst the remainder of the system dynamics were simulated in real-time. The simulated and experimental results have demonstrated that the damping performance of the observer based adaptive TMD with a linearised MR damper exceeds that of a passive TMD significantly, depending on the change in the main structural mass.

8.2 Key conclusions and contributions

The key contribution of this thesis is that by proposing an observer-based controller, the complexity of the feedback linearisation theory is solved. The force transducers (damping force) and LVDT (system state) sensors are replaced with simple, commercially available, low-cost accelerometers.

The design of the Luenberger gain plays key role in the performance of the proposed non-linear observer. The Luenberger gain is designed by using the pole placement method based on the linear state matrix of the system, where the passive damping level of the MR

damper is used. Referring to [154], for acceptable estimation of the states, the dynamics of the observer is chosen to be relatively faster than the dynamics of the controller.

To the author's knowledge, the approach has not been previously applied within the context of MR dampers.

The advantages and effectiveness of passive tuned mass dampers (a simple, inexpensive and reliable means to suppress the undesired vibrations of systems) have been studied by many researchers. However, the performance of TMD is very sensitive to tuning frequency ratio because of its fixed parameters, even when optimally designed. The TMD loses its optimal performance if the host structures frequency changes due to environmental effects, i.e varying pay load. As an promising alternative solution to this problem is a adaptive tuned mass damper system with linearised MR damper. Using the semi-active variable damping device. It has been shown that, this system is able to continuously retune its frequency in real time which makes it robust to changes in building stiffness and damping.

To conclude, it has been shown that, the observer-based theory is a useful approach to implement the feedback linearisation technique by using a simple accelerometer instead of a complex force transducer. However, the usefulness of the observer-based system is only validated with a single degree of freedom sliding mass configuration.

In addition, it can concluded that, the observer-based approach is able to estimate the damping force and the system states by using accelerometers, for tuned mass damper control. To the author's knowledge, the approach has not been previously applied within the context of tuned mass damper system.

8.3 Further work

In this section, the potential areas for further research are discussed. The present thesis has made a significant contribution towards to development of effective observer based controller for MR vibration systems. In particular, using numerical and experimental methods, observer based feedback linearisation was shown to provide superior performance over more simplistic observer based on/off strategies. As a further extension to this thesis, it would be interesting to investigate the performance comparison of the non-linear Kalman or reduced order Luenberger observers to the present non-linear state observer model under the practical conditions.

Another research topic would be to formally investigate the sensor-less (no sensor) implementation of semi-active control algorithms, by using the conductivity property of the smart fluid. If the relationship between the damper displacement and voltage/current across the smart fluid can be discovered, then this phenomenon could be used to develop senseless semi-active force generators.

As an extension to this thesis, an additional study could be the investigation of the temperature effects on the performance of observer based control system. The viscosity of the MR fluid will vary with the change in temperature, which will obviously effect the system performance. In practice, it is difficult the control the temperature of fluid. However, the analytical method could be used to investigate this phenomena, for example, using uncertainty propagation techniques [185].

Lastly, the smart fluid actuators could be the another extension of this research. It would be interesting to find out whether similar observer base feedback control strategies could be applied to actuators for position or force control.

Bibliography

[1] C. Beards, *Engineering vibration analysis with application to control systems*. Butterworth-Heinemann, London, 1995.

[2] S. Timoshenko, D. H. Young, and W. Weaver, *Vibration problems in engineering*. Wiley, New York, 1974.

[3] J. D. Hartog, *Mechanical vibrations*. McGraw-Hill, New York, 1947.

[4] R. Sharp and S. Hassan, "The relative performance capabilities of passive, active and semi-active car suspension systems," *ARCHIVE: Proceedings of the Institution of Mechanical Engineers, Part D: Transport Engineering 1984-1988 (vols 198-202)*, vol. 200, no. 34, pp. 219–228, 1986.

[5] N. Sims, R. Stanway, and A. Johnson, "Vibration control using smart fluids: a state-of-the-art review," *The Shock and vibration digest*, vol. 31, no. 3, pp. 195–203, 1999.

[6] D. Mead, *Passive Vibration Control*. John Wiley and Sons, New York, 1999.

[7] M. D. Symans and M. C. Constantinou, "Semi-active control systems for seismic protection of structures: a state-of-the-art review," *Engineering structures*, vol. 21, no. 6, pp. 469–487, 1999.

[8] T. T. Soong and M. C. Costantinou, *Passive and active structural vibration control in civil engineering*. Springer-Verlag, New York, 1994.

[9] M. C. Constantinou, T. T. Soong, and G. F. Dargush, *Passive energy dissipation systems for structural design and retrofit*. Multidisciplinary Center for Earthquake Engineering Research Buffalo, New York, 1998.

[10] T. Kakimoto, "Fluid-filled engine mount device," Mar. 20 1984, US Patent 4,437,653.

[11] D. Karnopp, "Active and semi-active vibration isolation," *Journal of Mechanical Design*, vol. 117, p. 177, 1995.

[12] D. Crolla, "Vehicle dynamics-theory into practice," *Proceedings of the Institution of Mechanical Engineers, Part D: Journal of Automobile Engineering*, vol. 210, no. 2, pp. 83–94, 1996.

[13] T. Soong, A. Reinhorn, Y. Wang, and R. Lin, "Full-scale implementation of active control i: Design and simulation," *Journal of Structural Engineering*, vol. 117, no. 11, pp. 3516–3536, 1991.

[14] W. Krüger, "Design and simulation of semi-active landing gears for transport aircraft," *Mechanics of structures and machines*, vol. 30, no. 4, pp. 493–526, 2002.

[15] N. Sims and R. Stanway, "Semi-active vehicle suspension using smart fluid dampers: a modelling and control study," *International journal of vehicle design*, vol. 33, no. 1, pp. 76–102, 2003.

[16] D. Karnopp, M. Crosby, and R. Harwood, "Vibration control using semi-active force generators," *ASME Journal of Engineering for Industry*, vol. 96, no. 2, pp. 619–626, 1974.

[17] E. K. Bender, D. C. Karnopp, and I. Paul, "On the optimization of vehicle suspension using random process theory," *Proceedings of the Institution of Mechanical Engineers, Part D: Journal of Automobile Engineering*, vol. 210, no. 67-Trans-12, 1967.

[18] D. Hrovat, P. Barak, and M. Rabins, "Semi-active versus passive or active tuned mass dampers for structural control," *Journal of Engineering Mechanics*, vol. 109, no. 3, pp. 691–705, 1983.

[19] D. Cebon, F. Besinger, and D. Cole, "Control strategies for semi-active lorry suspensions," *Proceedings of the Institution of Mechanical Engineers, Part D: Journal of Automobile Engineering*, vol. 210, no. 2, pp. 161–178, 1996.

[20] Delphi MagneRide, "Materials Division ,406 Gregson Drive, Cary, NC 27511, USA," `http://am.delphi.com/products/parts/shock-absorber-index-/shock-absorbers/`.

[21] J. Carlson, D. Catanzarite, and K. Clair, "Commercial magnetorheological fluid devices," *International Journal of Modern Physics B*, vol. 10, no. 23, pp. 2857–2866, 1996.

[22] J. Ouellette, "Smart fluids move into the marketplace," *Industrial Physicist*, vol. 9, no. 6, pp. 14–17, 2004.

[23] D. A. Brookes, "Electro-rheological devices," *Chartered Mechanical Engineer*, vol. 29, pp. 91–93, 1982.

[24] J. E. Stangroom, "Viscous shear clutch," Apr. 24 1984, US Patent 4,444,298.

[25] J. Stangroom, "Electro-rheological transducer," Jan. 15 1985, US Patent 4,493,615.

[26] J. D. Carlson, "Mr fluids and devices in the real world," *International Journal of Modern Physics B*, vol. 19, no. 07n09, pp. 1463–1470, 2005.

[27] Lord Corporation, "Magneto-rheological-(MR) Automotive Suspensions, 5725 Delphi Drive, Troy, Michigan 48098-2815,USA," `http://www.lord.com/products-and-solutions/magneto-rheological-(mr)/automotive-suspensions.xml`.

[28] Y. Ma, Y. Zhang, and K. Lu, "Frequency and temperature dependence of complex strontium titanate electrorheological fluids under an alternating electric field," *Journal of applied physics*, vol. 83, no. 10, pp. 5522–5524, 1998.

[29] W. M. Winslow, "Induced fibration of suspensions," *Journal of applied physics*, vol. 20, no. 12, pp. 1137–1140, 1949.

[30] W. M. Wlnslow, "Method and means for translating electrical impulses into mechanical forces," 1947, US Patent 2,417,850.

[31] J. E. Stangroom, "Electrorheological fluids," *Physics in Technology*, vol. 14, no. 6, p. 290, 1983.

[32] J. Rabinow, "The magnetic fluid clutch," *Electrical Engineering*, vol. 67, no. 12, pp. 1167–1167, 1948.

[33] ——, "Magnetic fluid torque and force transmitting device," 1951, US Patent 2,575,360.

[34] ——, "High-speed magnetic fluid clutch," Dec. 23 1952, US Patent 2,622,713.

[35] ——, "Radial flux diagnetic fluid clutch," Feb. 24 1953, US Patent 2,629,471.

[36] ——, "Magnetic fluid shock absorber," 1954, US Patent 2,667,237.

[37] E. M. Shtarkman, "Fluid responsive to a magnetic field," Feb. 12 1991, US Patent 4,992,190.

[38] Lord Corporation, Materials Division, "406 Gregson Drive, Cary, NC 27511, USA," `http://www.lord.com`.

[39] J. D. Carlson, "Mmagnetorheological fluids - engineering applications today and tomorrow," *2nd ECCOMAS Thematic Conference on Smart Structures and Materials*, 2005.

[40] General motors , " 2500 East Grand Boulevard Detroit, MI 48211, USA," `http://www.gm.com`.

[41] A. J. Bombard and J. de Vicente, "Boundary lubrication of magnetorheological fluids in ptfe/steel point contacts," *Wear*, vol. 296, no. 1, pp. 484–490, 2012.

[42] A. Lind, "Semi-active suspension systems using magneto-rheological fluids," 2008.

[43] M. Lorite Gutiérrez, "Estudio del comportamiento dinámico de un vehículo automóvil equipado con amortiguación magneto-reológica," Ph.D. dissertation, Universidad Carlos III De Madrid Escuela Politécnica Superior Departamento De Ingenieria Mecánica, 2011.

[44] P. Grad, "Against the flow-smart fluids that can change their viscosity in real time," *Engineering & Technology*, vol. 1, no. 9, pp. 34–37, 2006.

[45] E. Guglielmino, *Semi-active suspension control: improved vehicle ride and road friendliness*. Springer, London, 2008.

[46] S. F. Wiesbaden, "Range rover evoque-versatile technology, pure art," *Auto Tech Review*, vol. 1, no. 8, pp. 58–63, 2012.

[47] T. Butz and O. Von Stryk, "Modelling and simulation of electro-and magnetorheological fluid dampers," *ZAMM-Journal of Applied Mathematics and Mechanics/Zeitschrift für Angewandte Mathematik und Mechanik*, vol. 82, no. 1, pp. 3–20, 2002.

[48] W. M. Winslow, "Field controlled hydraulic device," 1953, US Patent 2,661,596.

[49] N. D. Sims, R. Stanway, A. R. Johnson, D. J. Peel, and W. A. Bullough, "Smart fluid damping: shaping the force/velocity response through feedback control," *Journal of intelligent material systems and structures*, vol. 11, no. 12, pp. 945–958, 2000.

[50] W. Kordonsky, "Magnetorheological effect as a base of new devices and technologies," *Journal of Magnetism and Magnetic Materials*, vol. 122, no. 1, pp. 395–398, 1993.

[51] ——, "Elements and devices based on magnetorheological effect*," *Journal of Intelligent Material Systems and Structures*, vol. 4, no. 1, pp. 65–69, 1993.

[52] J. D. Carlson, "Electrophoretic fluid differential," Feb. 25 1992, US Patent 5,090,531.

[53] S. B. Gentry, J. F. Mazur, and B. K. Blackburn, "Muscle training and physical rehabilitation machine using electro-rheological magnetic fluid," Oct. 24 1995, uS Patent 5,460,585.

[54] J. D. Carlson and M. R. Jolly, "Mr fluid, foam and elastomer devices," *Mechatronics*, vol. 10, no. 4, pp. 555–569, 2000.

[55] Y. Park and B. Jung, "Force-feedback device using magneto-rheological fluid: Mr clutch," *New actuators; Actuator*, pp. 456–459, 2000.

[56] J. T. Russo, J. V. Schiralli, P. E. Brodzik, and J. S. Pioquinto, "Semi-active clutch assembly," Jul. 1 2003, US Patent 6,585,252.

[57] J. L. Kincad, B. A. Mattila, and T. V. Ignatius, "Semi-active anti-roll system," Aug. 6 2002, US Patent 6,428,019.

[58] N. R. Harland, B. Mace, and R. Jones, "Adaptive-passive control of vibration transmission in beams using electro/magnetorheological fluid filled inserts," *Control Systems Technology, IEEE Transactions on*, vol. 9, no. 2, pp. 209–220, 2001.

[59] B. Spencer, S. Dyke, M. Sain, and J. Carlson, "Phenomenological model for magnetorheological dampers," *Journal of engineering mechanics*, vol. 123, no. 3, pp. 230–238, 1997.

[60] V. A. Neelakantan and G. N. Washington, "Modeling and reduction of centrifuging in magnetorheological (mr) transmission clutches for automotive applications," *Journal of intelligent material systems and structures*, vol. 16, no. 9, pp. 703–711, 2005.

[61] E. C. McIntyre, *Compression of smart materials: Squeeze flow of electrorheological and magnetorheological fluids*. ProQuest, Michigan, 2008.

[62] Y. Yu, N. G. Naganathan, and R. V. Dukkipati, "A literature review of automotive vehicle engine mounting systems," *Mechanism and machine theory*, vol. 36, no. 1, pp. 123–142, 2001.

[63] J. Wang, G. Meng, N. Feng, and E. Hahn, "Dynamic performance and control of squeeze mode mr fluid damper–rotor system," *Smart materials and structures*, vol. 14, no. 4, p. 529, 2005.

[64] S. Mazlan, N. Ekreem, and A. Olabi, "The performance of magnetorheological

fluid in squeeze mode," *Smart materials and structures*, vol. 16, no. 5, p. 1678, 2007.

[65] G. Monkman, "The electrorheological effect under compressive stress," *Journal Of Physics D: Applied Physics*, vol. 28, no. 3, p. 588, 1995.

[66] A. Lukkarinen and K. Kaski, "Simulation studies of electrorheological fluids under shear, compression, and elongation loading," *Journal of applied physics*, vol. 83, no. 3, pp. 1717–1725, 1998.

[67] C. Carmignani, P. Forte, and E. Rustighi, "Design of a novel magneto-rheological squeeze-film damper," *Smart materials and structures*, vol. 15, no. 1, p. 164, 2006.

[68] G. M. Kamath, M. K. Hurt, and N. M. Wereley, "Analysis and testing of bingham plastic behavior in semi-active electrorheological fluid dampers," *Smart Materials and Structures*, vol. 5, no. 5, p. 576, 1996.

[69] G. A. Dimock, J. Yoo, and N. M. Wereley, "Quasi-steady bingham biplastic analysis of electrorheological and magnetorheological dampers," *Journal of intelligent material systems and structures*, vol. 13, no. 9, pp. 549–559, 2002.

[70] D. Lee and N. M. Wereley, "Analysis of electro-and magneto-rheological flow mode dampers using herschel-bulkley model," in *SPIE's 7th Annual International Symposium on Smart Structures and Materials*. International Society for Optics and Photonics, 2000, pp. 244–255.

[71] D. Lee, Y. Choi, and N. M. Wereley, "Performance analysis of er/mr impact damper systems using herschel-bulkley model," *Journal of intelligent material systems and structures*, vol. 13, no. 7-8, pp. 525–531, 2002.

[72] X. Wang and F. Gordaninejad, "Flow analysis of field-controllable, electro-and

magneto-rheological fluids using herschel-bulkley model," *Journal of intelligent material systems and structures*, vol. 10, no. 8, pp. 601–608, 1999.

[73] N. M. Wereley, "Nondimensional herschel-bulkley analysis of magnetorheological and electrorheological dampers," *Journal of Intelligent Material Systems and Structures*, vol. 19, no. 3, pp. 257–268, 2008.

[74] D. Peel and W. Bullough, "Prediction of electro-rheological valve performance in steady flow," *Proceedings of the Institution of Mechanical Engineers, Part C: Journal of Mechanical Engineering Science*, vol. 208, no. 4, pp. 253–266, 1994.

[75] Lord Corporation, "RD-8040-1 MR Damper (Short Stroke), 5725 Delphi Drive, Troy, Michigan 48098-2815,USA ," `http://www.lord.com/products-and-solutions/magneto-rheological-(mr)/product.xml/1651`.

[76] N. Sims, D. Peel, R. Stanway, A. Johnson, and W. Bullough, "The electrorheological long-stroke damper: A new modelling technique with experimental validation," *Journal of sound and vibration*, vol. 229, no. 2, pp. 207–227, 2000.

[77] R. Stanway, J. Sproston, and N. Stevens, "Non-linear modelling of an electro-rheological vibration damper," *Journal of Electrostatics*, vol. 20, no. 2, pp. 167–184, 1987.

[78] D. Gamota and F. Filisko, "Dynamic mechanical studies of electrorheological materials: moderate frequencies," *Journal of Rheology*, vol. 35, p. 399, 1991.

[79] A. Dominguez, R. Sedaghati, and I. Stiharu, "Modelling the hysteresis phenomenon of magnetorheological dampers," *Smart materials and structures*, vol. 13, no. 6, p. 1351, 2004.

[80] M. Giuclea, T. Sireteanu, D. Stancioiu, and C. W. Stammers, "Model parameter identification for vehicle vibration control with magnetorheological dampers using computational intelligence methods," *Proceedings of the Institution of Mechanical Engineers, Part I: Journal of Systems and Control Engineering*, vol. 218, no. 7, pp. 569–581, 2004.

[81] N. Kwok, Q. Ha, M. Nguyen, J. Li, and B. Samali, "Bouc–wen model parameter identification for a mr fluid damper using computationally efficient ga," *ISA transactions*, vol. 46, no. 2, pp. 167–179, 2007.

[82] M. Boada, J. Calvo, B. Boada, and V. Diaz, "Modeling of a magnetorheological damper by recursive lazy learning," *International Journal of Non-Linear Mechanics*, vol. 46, no. 3, pp. 479–485, 2011.

[83] M. Giuclea, T. Sireteanu, and A. Mitu, "Use of genetic algorithms for fitting the bouc-wen model to experimental hysteretic curves," *Rev Roumaine Sci Tech-Serie Mec Appl. v54 i1*, vol. 54, no. 1, pp. 3–10, 2009.

[84] S. Talatahari, A. Kaveh, and N. M. Rahbari, "Parameter identification of bouc-wen model for mr fluid dampers using adaptive charged system search optimization," *Journal of mechanical science and technology*, vol. 26, no. 8, pp. 2523–2534, 2012.

[85] N. Sims, N. Holmes, and R. Stanway, "A unified modelling and model updating procedure for electrorheological and magnetorheological vibration dampers," *Smart materials and structures*, vol. 13, pp. 100–121, 2004.

[86] G. M. Kamath and N. M. Wereley, "A nonlinear viscoelastic-plastic model for electrorheological fluids," *Smart Materials and Structures*, vol. 6, no. 3, pp. 351–359, 1997.

[87] H. Gavin, R. Hanson, and F. Filisko, "Electrorheological dampers, part ii: testing and modeling," *Journal of applied mechanics*, vol. 63, no. 3, pp. 676–682, 1996.

[88] S. B. Choi, S. K. Lee, and Y. P. Park, "A hysteresis model for the field-dependent damping force of a magnetorheological damper," *Journal of Sound Vibration*, vol. 245, pp. 375–383, Aug. 2001.

[89] C.-C. Chang and P. Roschke, "Neural network modeling of a magnetorheological damper," *Journal of Intelligent Material Systems and Structures*, vol. 9, no. 9, pp. 755–764, 1998.

[90] S. Dyke, B. Spencer Jr, M. Sain, and J. Carlson, "Modeling and control of magnetorheological dampers for seismic response reduction," *Smart Materials and Structures*, vol. 5, no. 5, p. 565, 1996.

[91] S. J. Dyke, B. F. Spencer Jr, M. K. Sain, and J. D. Carlson, "Experimental verification of semi-active structural control strategies using acceleration feedback," in *Proc. of the 3rd Intl. Conf. on Motion and Vibr. Control*, vol. 3, 1996, pp. 291–296.

[92] X. Wang and F. Gordaninejad, "Lyapunov-based control of a bridge using magnetorheological fluid dampers," *Journal of Intelligent Material Systems and Structures*, vol. 13, no. 7-8, pp. 415–419, 2002.

[93] L. M. Jansen and S. J. Dyke, "Semiactive control strategies for mr dampers: comparative study," *Journal of Engineering Mechanics*, vol. 126, no. 8, pp. 795–803, 2000.

[94] F. Yi, S. J. Dyke, J. M. Caicedo, and J. D. Carlson, "Experimental verification of multiinput seismic control strategies for smart dampers," *Journal of Engineering Mechanics*, vol. 127, no. 11, pp. 1152–1164, 2001.

[95] O. Yoshida and S. J. Dyke, "Seismic control of a nonlinear benchmark building using smart dampers," *Journal of engineering mechanics*, vol. 130, no. 4, pp. 386–392, 2004.

[96] Z.-D. Xu, Y.-P. Shen, and Y.-Q. Guo, "Semi-active control of structures incorporated with magnetorheological dampers using neural networks," *Smart materials and structures*, vol. 12, no. 1, p. 80, 2003.

[97] Z. Q. Gu and S. O. Oyadiji, "Application of mr damper in structural control using anfis method," *Computers & structures*, vol. 86, no. 3, pp. 427–436, 2008.

[98] A. Karamodin, H. Haji Kazemi, A. Rowhanimanesh, and M. R. Akbarzadeh Totonchi, "Semi-active control of structures using a neuro-inverse model of mr dampers," *Scientia Iranica*, vol. 16, no. 3, pp. 256–263, 2009.

[99] S. D. Nguyen and S. Choi, "A new neuro-fuzzy training algorithm for identifying dynamic characteristics of smart dampers," *Smart Materials and Structures*, vol. 21, no. 8, p. 085021, 2012.

[100] W. Pawlus and H. R. Karimi, "Neural network-based models for a vibration suppression system equipped with mr brake," in *Intelligent Systems (IS), 2012 6th IEEE International Conference*. IEEE, 2012, pp. 330–335.

[101] L. Zong, X. Gong, C. Guo, and S. Xuan, "Inverse neuro-fuzzy mr damper model and its application in vibration control of vehicle suspension system," *Vehicle System Dynamics*, vol. 50, no. 7, pp. 1025–1041, 2012.

[102] M. Zapateiro, N. Luo, H. Karimi, and J. Vehí, "Vibration control of a class of semiactive suspension system using neural network and backstepping techniques," *Mechanical Systems and Signal Processing*, vol. 23, no. 6, pp. 1946–1953, 2009.

[103] P. W. Nugroho, H. Du, W. H. Li, and G. Alici, "A new adaptive fuzzy-hybrid control strategy of semi-active suspension with magneto-rheological damper," in *4th International Conference on Computational Methods (ICCM2012)*, Gold Coast, Australia, 2012, pp. 1–9.

[104] M. Yu, C. R. Liao, W. M. Chen, and S. L. Huang, "Study on mr semi-active suspension system and its road testing," *Journal of intelligent material systems and structures*, vol. 17, no. 8-9, pp. 801–806, 2006.

[105] D. Das, T. K. Datta, and A. Madan, "Semiactive fuzzy control of the seismic response of building frames with mr dampers," *Earthquake Engineering & Structural Dynamics*, vol. 41, no. 1, pp. 99–118, 2012.

[106] D. A. Shook, P. N. Roschke, P. Lin, and C. H. Loh, "Ga-optimized fuzzy logic control of a large-scale building for seismic loads," *Engineering structures*, vol. 30, no. 2, pp. 436–449, 2008.

[107] M. Zapateiro, H. R. Karimi, N. Luo, and B. F. Spencer Jr, "Frequency domain control based on quantitative feedback theory for vibration suppression in structures equipped with magnetorheological dampers," *Smart Materials and Structures*, vol. 18, no. 9, p. 095041, 2009.

[108] H. Du, K. Yim Sze, and J. Lam, "Semi-active h infinity control of vehicle suspension with magneto-rheological dampers," *Journal of Sound and Vibration*, vol. 283, no. 3, pp. 981–996, 2005.

[109] N. Fisco and H. Adeli, "Smart structures: part ii-hybrid control systems and control strategies," *Scientia Iranica*, vol. 18, no. 3, pp. 285–295, 2011.

[110] S. Morishita and T. Ura, "Er fluid applications to vibration control devices and an

adaptive neural-net controller," *Journal of intelligent material systems and structures*, vol. 4, no. 3, pp. 366–372, 1993.

[111] Y. Choi and N. M. Wereley, "Vibration control of a landing gear system featuring electrorheological/magnetorheological fluids," *Journal of Aircraft*, vol. 40, no. 3, pp. 432–439, 2003.

[112] A. H. F. Lam and W. H. Liao, "Semi-active control of automotive suspension systems with magneto-rheological dampers," *International Journal of Vehicle Design*, vol. 33, no. 1, pp. 50–75, 2003.

[113] J. Shaw, R. Pan, and Y. C. Chang, "Fuzzy sliding mode control of an mr mount for vibration attenuation," *Journal of the Chinese Society of Mechanical Engineers*, pp. 330–335, 2012.

[114] J. Yao, W. Shi, J. Zheng, and H. Zhou, "Development of a sliding mode controller for semi-active vehicle suspensions," *Journal of Vibration and Control*, vol. 19, no. 8, pp. 1152–1160, 2013.

[115] N. Yagiz, Y. Hacioglu, and Y. Taskin, "Sliding mode control of a vehicle with nonlinearities," in *6th EUROMECH Nonlinear Dynamics Conference (ENOC 2008)*. ENOC, Saint Petersburg, Russia, 2008.

[116] S. A. Royel, Z. Movassaghi, N. Kwok, and Q. Ha, "Smart structures using mr dampers with second order sliding mode control," in *Control, Automation and Information Sciences (ICCAIS), 2012 International Conference on*. IEEE, 2012, pp. 170–175.

[117] Y. Kim, K. Wang, and H. Lee, "Feedback control of er-fluid-based structures for vibration suppression," *Smart materials and structures*, vol. 1, no. 2, p. 139, 1992.

[118] S. H. Choi, Y. T. Choi, S. B. Choi, and C. C. Cheong, "Performance analysis of an engine mount featuring er fluids and piezoactuators," *International Journal of Modern Physics B*, vol. 10, no. 23n24, pp. 3143–3157, 1996.

[119] R. Pan, J. Shaw, W. Kuo, and G. Lin, "Design and control of mr mount for vibration isolation," in *SICE Annual Conference 2010, Proceedings of.* IEEE, 2010, pp. 990–995.

[120] D. Ledezma-Ramirez, N. Ferguson, and M. Brennan, "Shock performance of different semiactive damping strategies," *Journal of applied research and technology*, vol. 8, no. 2, pp. 249–257, 2010.

[121] Y. Liu, H. Matsuhisa, and H. Utsuno, "Semi-active vibration isolation system with variable stiffness and damping control," *Journal of sound and vibration*, vol. 313, no. 1, pp. 16–28, 2008.

[122] B. Kim and P. Roschke, "Linearization of magnetorheological behaviour using a neural network," in *American Control Conference, 1999. Proceedings of the 1999*, vol. 6. IEEE, 1999, pp. 4501–4505.

[123] C. C. Chang and L. Zhou, "Neural network emulation of inverse dynamics for a magnetorheological damper," *Journal of Structural Engineering*, vol. 128, no. 2, pp. 231–239, 2002.

[124] D. H. Wang and W. H. Liao, "Modeling and control of magnetorheological fluid dampers using neural networks," *Smart Materials and Structures*, vol. 14, no. 1, p. 111, 2005.

[125] N. Sims, R. Stanway, D. Peel, W. Bullough, and A. Johnson, "Controllable viscous damping: an experimental study of an electrorheological long-stroke damper under

proportional feedback control," *Smart materials and structures*, vol. 8, pp. 601–615, 1999.

[126] N. Sims, R. Stanway, and S. Beck, "Proportional feedback control of an electro-rheological vibration damper," *Journal of intelligent material systems and structures*, vol. 8, no. 5, pp. 426–433, 1997.

[127] D. Batterbee and N. Sims, "Vibration isolation with smart fluid dampers: a benchmarking study," *Smart Structures and Systems*, vol. 1, no. 3, pp. 235–256, 2005.

[128] ——, "Hardware-in-the-loop-simulation of magnetorheological dampers for vehicle suspension systems," *Proceedings of the Institution of Mechanical Engineers, Part I: Journal of Systems and Control Engineering*, vol. 221, pp. 265–278, 2006.

[129] V. Sankaranarayanan, M. E. Emekli, B. Gilvenc, L. Guvenc, E. Ozturk, E. Ersolmaz, I. E. Eyol, and M. Sinal, "Semiactive suspension control of a light commercial vehicle," *Mechatronics, IEEE/ASME Transactions on*, vol. 13, no. 5, pp. 598–604, 2008.

[130] F. Weber and M. Maślanka, "Frequency and damping adaptation of a tmd with controlled mr damper," *Smart Materials and Structures*, vol. 21, no. 5, p. 055011, 2012.

[131] A. Giua, M. Melas, C. Seatzu, and G. Usai, "Design of a predictive semiactive suspension system," *Vehicle System Dynamics*, vol. 41, no. 4, pp. 277–300, 2004.

[132] R. K. Dixit and G. D. Buckner, "Sliding mode observation and control for semi-active vehicle suspensions," *Vehicle System Dynamics*, vol. 43, no. 2, pp. 83–105, 2005.

[133] R. Rajamani and J. K. Hedrick, "Adaptive observers for active automotive suspensions: theory and experiment," *Control Systems Technology, IEEE Transactions on*, vol. 3, no. 1, pp. 86–93, 1995.

[134] J. Hedrick, R. Rajamani, and K. Yi, "Observer design for electronic suspension applications*," *Vehicle System Dynamics*, vol. 23, no. 1, pp. 413–440, 1994.

[135] H. Nakai, S. Oosaku, and Y. Motozono, "Application of practical observer to semi-active suspensions," *Journal of dynamic systems, measurement, and control*, vol. 122, no. 2, pp. 284–289, 2000.

[136] K. Yi and B. Suk Song, "Observer design for semi-active suspension control," *Vehicle System Dynamics*, vol. 32, no. 2-3, pp. 129–148, 1999.

[137] L. Li, G. Song, and J. Ou, "Nonlinear structural vibration suppression using dynamic neural network observer and adaptive fuzzy sliding mode control," *Journal of Vibration and Control*, vol. 16, no. 10, pp. 1503–1526, 2010.

[138] D. Luenberger, "Observing the state of a linear system," *Military Electronics, IEEE Transactions on*, vol. 8, no. 2, pp. 74–80, 1964.

[139] S. Aubouet, L. Dugard, and O. Sename, "Hinf/lpv observer for an industrial semi-active suspension," in *Control Applications, 2009 IEEE/Intelligent Control,(ISIC)*. IEEE, 2009, pp. 756–763.

[140] V. Sankaranarayanan, M. E. Emekli, B. Giivenc, L. Giivenc, E. Oztiirk, S. Ersolmaz, I. E. Eyol, and M. Sinai, "Observer based semi-active suspension control applied to a light commercial vehicle," in *Advanced intelligent mechatronics, 2007 IEEE/ASME international conference on*. IEEE, 2007, pp. 1–7.

[141] A. W. Smyth, S. F. Masri, E. B. Kosmatopoulos, A. G. Chassiakos, and T. K. Caughey, "Development of adaptive modeling techniques for non-linear hysteretic

systems," *International Journal of Non-Linear Mechanics*, vol. 37, no. 8, pp. 1435–1451, 2002.

[142] Lord Corporation, "RD-1005-3 MR Damper (Short Stroke), 5725 Delphi Drive, Troy, Michigan 48098-2815,USA ," `http://www.lord.com`.

[143] C. W. John, *Analytical Techniques for Non-linear Control Systems*. English Universities Press, London, 1960.

[144] Instron Structural Testing, "825 University Ave.,Norwood, MA 020622643, USA," `http://www.instron.com`.

[145] Moog Inc., "Jamison Road, East Aurora, New York 14052, USA," `http://www.moog.co.uk`.

[146] Kepco Inc., "131-138 Sandford Avenue, Flushing, NY 11352, USA," `http://www.kepcopower.com/bop.htm`.

[147] xPC Target, "The Mathworks, Inc., 3 Apple Hill drive, Natick, MA,2002," `http://www.mathworks.com/products/xpctarget/` .

[148] National Instument, "11500 N Mopac Expwy Austin, TX 78759-3504, USA," `http://www.ni.com` .

[149] PCB Piezotronics, Inc., "3425 Walden Avenue, Depew, New York 14043-2495, USA," `http://www.pcb.com`.

[150] RS Components Ltd., " Birchington Road, Corby, Northants, NN17 9RS, UK," `http://uk.rs-online.com/web/c/automation-control-gear/sensors-transducers/thermocouples/`.

[151] Valley Spring Carporation., "Carporation,"Round Wire Compression BS 1726-1",Pottery Lane East, Chesterfield, Derbyshire, S41 9BH, United Kingdom ," `http://www.valleyspring.com/`.

[152] M. A. Eroglu and N. D. Sims, "Observer based linearisation of mr dampers," in *EuroMech Colloquium 530: Structural Control and Energy Harvesting*, Bristol, United Kingdom, 25th-27th July 2011.

[153] M. Eroglu and N. Sims, "Observer based optimal control of mr damper," in *10th World Congress on Computational Mechanics*, Sao Paulo, Brazil, 8th-13rd July 2012.

[154] K. Ogata and Y. Yang, *Modern control engineering*. Prentice-Hall Englewood Cliffs, New Jersey, 1970.

[155] B. Spencer Jr, J. Suhardjo, and M. Sain, "Frequency domain optimal control strategies for aseismic protection," *Journal of Engineering Mechanics*, vol. 120, no. 1, pp. 135–158, 1994.

[156] S. Dyke, B. Spencer Jr, P. Quast, M. Sain, D. Kaspari Jr, and T. Soong, *Experimental verification of acceleration feedback control strategies for an active tendon system*. National Center for Earthquake Engineering Research, 1994.

[157] S. Dyke, B. Spencer, P. Quast, D. Kaspari, and M. Sain, "Implementation of an active mass driver using acceleration feedback control," *Computer-Aided Civil and Infrastructure Engineering*, vol. 11, no. 5, pp. 305–323, 1996.

[158] D. Simon and M. Ahmadian, "Vehicle evaluation of the performance of magneto rheological dampers for heavy truck suspensions," *Journal of vibration and acoustics*, vol. 123, no. 3, pp. 365–375, 2001.

[159] A. V. Oppenheim, R. W. Schafer, J. R. Buck *et al.*, *Discrete-time signal processing*. Prentice Hall Upper Saddle River, 1999, vol. 5.

[160] H. Bachmann, W. J. Ammann, F. Deischl, J. Eisenmann, I. Floegl, G. H. Hirsch, G. K. Klein, G. J. Lande, O. Mahrenholtz, H. G. Natke *et al.*, *Vibration problems in structures: Practical guidelines*. Birkhäuser Basel, 1994.

[161] P. Dallard, T. Fitzpatrick, A. Flint, A. Low, R. R. Smith, M. Willford, and M. Roche, "London millennium bridge: pedestrian-induced lateral vibration," *Journal of Bridge Engineering*, vol. 6, no. 6, pp. 412–417, 2001.

[162] J. Koo and M. Ahmadian, "A qualitative analysis of groundhook tuned vibration absorbers for controlling structural vibrations," *Proceedings of the Institution of Mechanical Engineers, Part K: Journal of Multi-body Dynamics*, vol. 216, no. 4, pp. 351–359, 2002.

[163] H. Frahm, "Device for damping vibrations of bodies," Oct. 30 1909, uS Patent 989958.

[164] D. H. J. Ormondroyd J, "The theory of the dynamic vibration absorber," *Transactions of the ASME*, vol. APM-50-7, no. 3, pp. 9–22, 1928.

[165] J. Brock, "A note on the damped vibration absorber," *Journal of Applied Mechanics*, vol. 13, pp. A–284, 1946.

[166] G. Warburton and E. Ayorinde, "Optimum absorber parameters for simple systems," *Earthquake Engineering & Structural Dynamics*, vol. 8, no. 3, pp. 197–217, 1980.

[167] T. Ioi and K. Ikeda, "On the dynamic vibration damped absorber of the vibration system," *Bulletin of JSME*, vol. 21, no. 151, pp. 64–71, 1978.

[168] K. Falcon, B. Stone, W. Simcock, and C. Andrew, "Optimization of vibration absorbers: a graphical method for use on idealized systems with restricted damping," *Journal of Mechanical Engineering Science*, vol. 9, no. 5, pp. 374–381, 1967.

[169] J. Snowdon, "Steady-state behavior of the dynamic absorber," *The Journal of the Acoustical Society of America*, vol. 31, p. 1096, 1959.

[170] N. Hoang, Y. Fujino, and P. Warnitchai, "Optimal tuned mass damper for seismic applications and practical design formulas," *Engineering Structures*, vol. 30, no. 3, pp. 707–715, 2008.

[171] A. Occhiuzzi, M. Spizzuoco, and F. Ricciardelli, "Loading models and response control of footbridges excited by running pedestrians," *Structural Control and Health Monitoring*, vol. 15, no. 3, pp. 349–368, 2008.

[172] B. Hazra, A. Sadhu, R. Lourenco, and S. Narasimhan, "Re-tuning tuned mass dampers using ambient vibration measurements," *Smart Materials and Structures*, vol. 19, no. 11, p. 115002, 2010.

[173] N. Fisco and H. Adeli, "Smart structures: part iihybrid control systems and control strategies," *Scientia Iranica*, vol. 18, no. 3, pp. 285–295, 2011.

[174] F. Weber, C. Boston, and M. Maślanka, "An adaptive tuned mass damper based on the emulation of positive and negative stiffness with an mr damper," *Smart Materials and Structures*, vol. 20, no. 1, p. 015012, 2011.

[175] D. Gsell, G. Feltrin, and M. Motavalli, "Adaptive tuned mass damper based on prestressable leaf-springs," *Journal of Intelligent Material Systems and Structures*, vol. 18, no. 8, pp. 845–851, 2007.

[176] K. Williams, G. Chiu, and R. Bernhard, "Dynamic modelling of a shape memory

alloy adaptive tuned vibration absorber," *Journal of sound and vibration*, vol. 280, no. 1, pp. 211–234, 2005.

[177] W. Sun and Q. Li, "Tmd semi-active control with shape memory alloy," *Journal of Harbin Institute of Technology*, vol. 6, p. 038, 2009.

[178] G. Jiang and L. M. Hanagan, "Semi-active tmd with piezoelectric friction dampers in floor vibration control," in *Smart Structures and Materials*. International Society for Optics and Photonics, San Diego, CA, 2006.

[179] C. Lin, G. Lin, and J. Wang, "Protection of seismic structures using semi-active friction tmd," *Earthquake Engineering & Structural Dynamics*, vol. 39, no. 6, pp. 635–659, 2010.

[180] J.-H. Koo, M. Ahmadian, and M. Setareh, "Experimental evaluation of magnet-orheological dampers for semi-active tuned vibration absorbers," in *Smart Structures and Materials*. International Society for Optics and Photonics, 2003, pp. 83–91.

[181] J. Kang, H.-S. Kim, and D.-G. Lee, "Mitigation of wind response of a tall building using semi-active tuned mass dampers," *The Structural Design of Tall and Special Buildings*, vol. 20, no. 5, pp. 552–565, 2011.

[182] J.-H. Koo, M. Ahmadian, and M. Setareh, "Experimental robustness analysis of magneto-rheological tuned vibration absorbers subject to mass off-tuning," *Journal of vibration and acoustics*, vol. 128, no. 1, pp. 126–131, 2006.

[183] N. Varadarajan and S. Nagarajaiah, "Wind response control of building with variable stiffness tuned mass damper using empirical mode decomposition/hilbert transform," *Journal of engineering mechanics*, vol. 130, no. 4, pp. 451–458, 2004.

[184] D. C. Batterbee, "Magnetorheological shock absorbers: Modelling, design, and control," Ph.D. dissertation, The University of Sheffield, Department of Mechanical Engineering, 2006.

[185] K. Worden, G. Manson, T. Lord, and M. Friswell, "Some observations on uncertainty propagation through a simple nonlinear system," *Journal of sound and vibration*, vol. 288, no. 3, pp. 601–621, 2005.

Appendix A: Abstract of published work

Observer based linearisation of MR dampers

Mehmet Eroglu * and Neil Sims

Department of Mechanical Engineering, The University of Sheffield, UK

* email: M.Eroglu@sheffield.ac.uk

Extended abstract

Magnetorheological, or MR, dampers are one of the most promising semi-active control devices for protecting civil engineering structures, vehicles, ships, or aircraft from the damaging effects of dynamic loading. They have many advantages over alternative technologies, such as low power requirement, reliability, and low cost. A wide range of control schemes have been considered for MR dampers, with no general consensus on the most appropriate approach. Research at the University of Sheffield has focussed on feedback linearisation, but this requires measurement of the damping force which increases the complexity of the system.

The present study aims to overcome this problem by investigating the application of ob-

server based control to the feedback linearisation of an MR damper. A single-degree-of freedom structure is chosen as the basis for study. The aim is to perform force-feedback linearisation of the MR damper (so that it can perform as an arbitrary semi-active force generator) using an observation of the feedback force, rather than a measured value. The present abstract considers a simplified modelling approach to this problem, although corresponding experiments are planned for the near future.

Appendix B: Abstract of published work

OBSERVER BASED OPTIMAL CONTROL OF MR DAMPERS

Mehmet A. Eroglu*, Neil D. Sims

Department of Mechanical Engineering, The University of Sheffield, U.K.

*(M.eroglu@sheffield.ac.uk)

Abstract. Magneto-rheological, or MR, dampers are one of the most promising semi-active control devices for protecting civil engineering structures, vehicles, ships, or aircraft from the damaging effects of dynamic loading. They have many advantages over alternative technologies, such as low power requirement, reliability, and low cost. A wide range of control schemes have been considered for MR dampers, with no general consensus on the most appropriate approach. Research at the University of Sheffield has focused on feedback linearisation, but this requires measurement of the damping force which increases the complexity of the system. This study aims to overcome this problem and improve the vibration absorbability of the system by investigating the application of observer based optimal control to the force-feedback linearisation of an MR damper. The proposed force-feedback linearisation chose the set point force as proportional to the piston velocity. But in this study, in order improve the performance of the system, the desired set point force is chosen to be the optimal control force. The implementation of the optimal control theory requires the measurement of the system states (displacement and velocity of the mass), are provided by the observer as well. Due to passivity limitation of the MR damper the set point force is diverted to the zero at the active region to satisfy the passivity theory of Karnopp. The results of this study is compared to observer based force-feedback linearisation algorithm and it is concluded that the proposed control system is able to reduce the displacement transmissibility of the damped system better then the compared one.

Keywords: Smart Fluids, Optimal Control, Observer, Force-feedback linearisation